Shell-Isolated Nanoparticle-Enhanced Raman Spectroscopy for Heterogeneous Catalysis

Verbeterde Raman Spectroscopie door Schil-Geïsoleerde Nanodeeltjes voor Heterogene Katalyse

(*met een samenvatting in het Nederlands*)

Proefschrift

ter verkrijging van de graad van doctor aan de Universiteit Utrecht op gezag van de rector magnificus, prof. dr. H.R.B.M. Kummeling, ingevolge het besluit van het college voor promoties in het openbaar te verdedigen op maandag 15 april 2019 des middags te 4.15 uur

door

Thomas Hartman
geboren op 11 mei 1991 te Woerden

Promotor: Prof. dr. ir. B. M. Weckhuysen

Dit proefschrift werd mede mogelijk gemaakt met financiële steun van Shell Global Solutions en de Nederlandse Organisatie voor Wetenschappelijk Onderzoek (NWO) in het kader van *Chemical Industrial Partnership Programme* (CHIPP 731.013.301).

Shell-Isolated Nanoparticle-Enhanced Raman Spectroscopy for Heterogeneous Catalysis

Author: Hartman, T.
Title: Shell-Isolated Nanoparticle-Enhanced Raman Spectroscopy for Heterogeneous Catalysis
ISBN: 978-94-6375-334-0
Printed By: Ridderprint - The Netherlands
Cover Design: Vassily Kandinsky - Several Circles

Table of Contents

1

Introduction: SERS and TERS in Catalysis

Surface- and tip-enhanced Raman spectroscopy (SERS and TERS) techniques exhibit highly localized chemical sensitivity, making them ideal to study chemical reactions, including processes at catalytic surfaces. Catalyst structures, adsorbates and reaction intermediates can be observed in low quantities at hot spots where electromagnetic fields are the strongest, providing ample opportunities to elucidate reaction mechanisms. Moreover, under ideal measurement conditions it can even be used to trigger chemical reactions. However, factors, such as substrate instability and insufficient signal enhancement still limit the applicability of SERS and TERS in the field of heterogeneous catalysis. By the use of sophisticated colloidal synthesis methods and advanced techniques, like shell-isolated nanoparticle-enhanced Raman spectroscopy (SHINERS), these challenges could be overcome. In this chapter, the reader is introduced to the concepts of SERS, TERS and catalysis and we will end with a brief scope of this thesis.

1.1 Catalysis and Spectroscopy

Catalysis is essential in the field of sustainable chemistry since it allows chemical reactions to take place faster, more efficiently and safer.[1–3] By lowering the activation energy of reactions (Figure 1.1a), the applied temperature and pressures can be lowered while improving the selectivity towards the desired products. To improve these chemical processes even more, it is crucial to know how catalysts operate and how, why and when they cease to work. Understanding the mechanism of all involved surface reactions in the case of heterogeneous catalysts is the key to designing the best possible catalytic materials. For this purpose, researchers use a wide variety of techniques, such as spectroscopy, (electron) microscopy and many more. These methods were mostly applied before and after reactions. Although these methods have greatly enhanced our understanding of catalysts, knowledge of actual *operating* catalysts still remains incomplete. Understanding working catalysts requires the use of techniques that are able to identify when and where reactions take place, ultimately linking this information to the catalytic performance of these materials.[4]

Valuable techniques for elucidating molecular structures under operating conditions are vibrational spectroscopy methods, including various forms of infrared (IR)[5–7] and Raman spectroscopy (Figure 1.1b).[8–11] Raman and IR spectroscopy provide information about molecular compositions and structures within a sample, by studying the interaction of light with a sample. These spectroscopic techniques probe the vibrational energy levels of molecules and solid lattices. Because the vibrational energy levels are different for every combination of atoms, these methods can give conclusive details about the molecular structure.[12]

For IR spectroscopy, molecular vibrations are excited when the frequency of the incident electromagnetic wave matches that of the vibration, resulting in the absorption of light. For Raman spectroscopy, the vibrations are excited when the sample inelastically scatters light of any energy, ranging from IR to UV. Typically, IR and Raman spectroscopy both probe molecular vibrations in the same energy range, but do not always observe the same kind of vibrations. The selection rules dictate that IR spectroscopy only observes vibrations when a change in electronic dipole moment occurs during the vibrational motion. Raman scattering, on the other hand, is only active when the vibrational motion leads to a change in polarizability. The techniques are therefore complementary and this sometimes results in 'mutual exclusion': for molecules with a center of symmetry, no normal vibrational mode can both be Raman and IR active.[13]

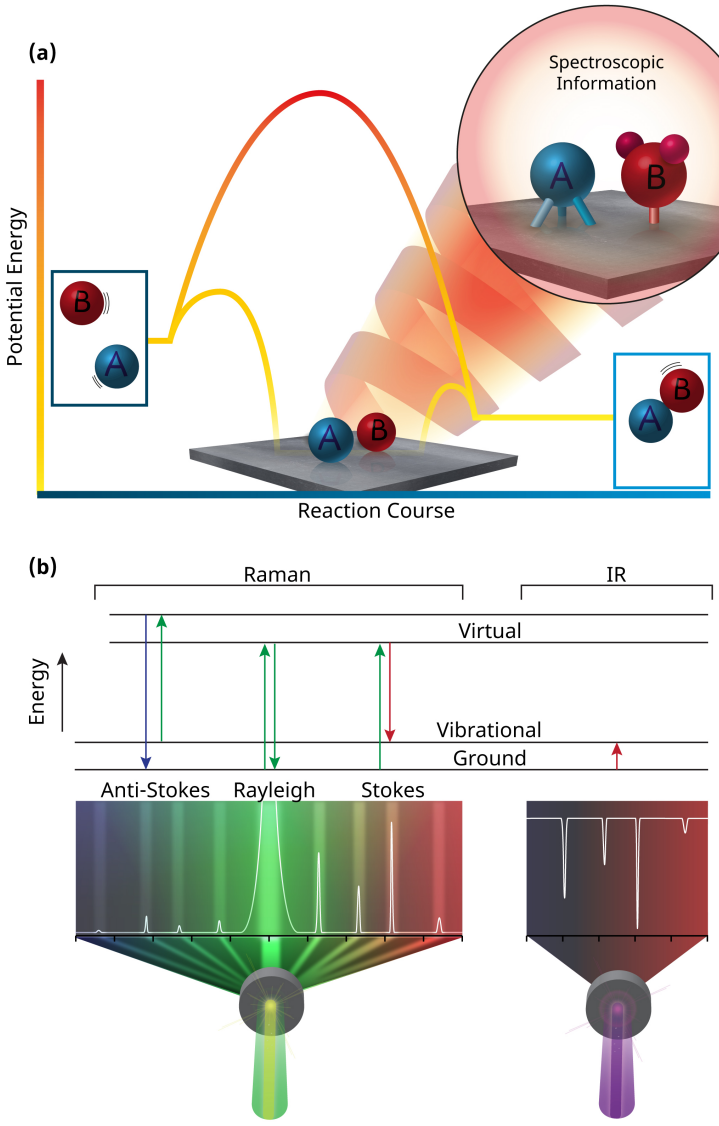

Figure 1.1. *In situ* spectroscopy for the understanding of heterogeneous catalysis. (a) The activation energy required for a reaction to occur between two compounds A and B can be significantly reduced by the presence of a catalytic surface. Vibrational spectroscopy can give information on the structural conformation of the reactants and the catalyst. **(b)** Raman spectroscopy probes the inelastic scattering of light and requires a change in the polarizability of the molecule. The loss (Stokes) and gain (anti-Stokes) in energy are related to the vibrational energies of the bonds. IR spectroscopy measures the direct absorption of IR light when the vibrational motion results in a change of the dipole moment in the molecule.

Raman gives an advantage over IR: it can be easily applied to probe lower energetic vibrations in the range 100-1000 cm^{-1}, which are related to the vibration of heavier atoms. It can therefore be used to observe direct interactions between catalysts and reactants. Furthermore, operative under many different conditions, Raman spectroscopy has greatly improved the knowledge of both the syntheses[8,9] and operation[10,11] of catalytic solids. However, it lacks sensitivity due to the inherent low Raman scattering cross-section of molecules.[14]

The sensitivity of Raman spectroscopy can be enhanced by implementing specialized techniques, of which resonance Raman,[14–17] coherent anti-Stokes Raman spectroscopy (CARS)[18] and surface-enhanced Raman spectroscopy (SERS) are the three most popular choices.[13] All of these techniques have their own strengths and weaknesses, but compared to others, SERS exhibits a strong feature for catalysis: highly localized sensitivity. This local sensitivity can be exploited to sense surface species and adsorbates.[19–21] Multiple techniques, such as CARS and SERS, can be combined to obtain even stronger Raman signal intensities.[22]

SERS is not the only surface-sensitive vibrational spectroscopic technique to be used in the field of catalysis. For example, other characterization techniques to study surface adsorbates include polarization modulation infrared reflection absorption spectroscopy (PM-IRRAS)[23,24] and sum frequency generation (SFG).[25–27] The latter approach has been pioneered by the group of Somorjai and was used to investigate the hydrogenation of benzene over platinum single crystals with a combined high-pressure scanning tunneling microscope (HP-STM) and SFG.[28] On the other hand, SERS enables the observation and characterization of the structure of surface species and adsorbates with greater sensitivity up to the level of detecting single molecules. When combined with scanning probe microscopy (SPM) methods, tip-enhanced Raman spectroscopy (TERS) can even reach nanoscale spatial resolution.[29] Furthermore, the SERS substrates can be triggered to start a reaction due to the formation of the strong electric field, hot electrons and the involved heat generation.[30,31] With increased control over these SERS substrates, improved Raman signals are obtained with shorter acquisition times, allowing the observation of possible reaction intermediates or even transition states.[32,33]

SERS and TERS can possibly become a routine analytical tool for catalysis, although a number of hurdles need to be overcome. In what follows, we briefly introduce the capabilities and challenges of SERS and TERS and present several examples of past work and future perspectives to enthuse the reader to start working with and expand the knowledge of these powerful analytical tools for the study of catalytic reactions. Although this PhD thesis is mostly aimed at heterogeneous catalysis, it is important to realize that the strengths of SERS are not necessarily limited to this field of research and can also be applied to the field of homogeneous catalysis.[34,35] Furthermore, SERS is promising to become one of the characterization tools of choice for monitoring the dynamics of biological

macromolecules in biomedical applications and is useful for the characterization of biocatalysts, although its current main use is in diagnostics.[36,37]

1.2 Surface-Enhanced Raman Spectroscopy

SERS and TERS are both plasmon-enhanced Raman spectroscopic (PERS) techniques.[38] The strong Raman signal enhancement in PERS arises from the excitation of localized surface plasmons in metallic nanostructures by an external oscillating electric field that matches the resonant frequency of the plasmon (Figure 1.2). Metal NPs are polarized by the electric field and the induced dipole will resonate with the frequency of the incident light. This phenomenon is known as a "localized surface plasmon resonance" (LSPR) and creates a strong localized electromagnetic field, which strongly enhances the Raman signal from analyte molecules in close vicinity of the metallic nanoparticles (NPs, Figure 1.2b). The strength of SERS signals dissipates by r^{-10} to r^{-12}, depending on the substrate and analyte.[19–21,39,40] Effectively, plasmonic NPs can be seen as nano-antennas, focusing the incident light into the nanometer scale.[38] This distance dependency makes the technique an ideal surface specific characterization technique.

SERS substrates are often fabricated from gold and silver NPs. Depending on their size, shape, aggregation state and the properties of the excitation laser, the Raman signal can be enhanced by over a factor of 10^6.[19–21,33,41] Ag NPs can provide stronger SERS signals than Au NPs, however, Au NPs are often preferred due to their higher stability.[42] They are easier to handle and store. Additionally, Au NPs are more likely to retain their SERS activity during experiments requiring elevated temperatures and/or pressures. Ag NPs exhibit a stronger LSPR below 600 nm, and therefore they provide stronger signal enhancement since Raman scattering intensity is proportional to λ^{-4}.[13]

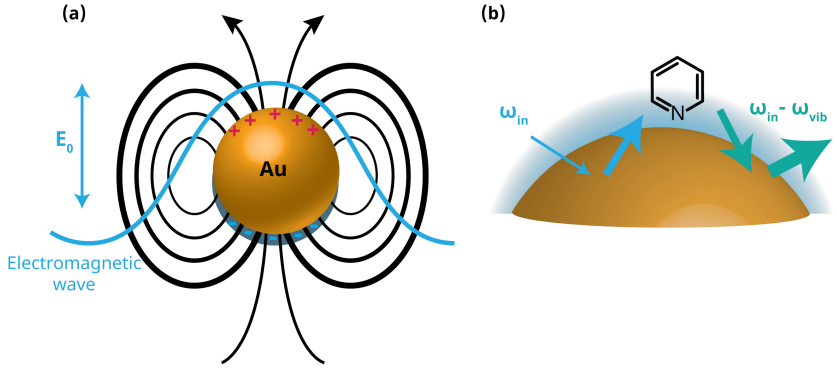

Figure 1.2. A single Au nanoparticle (NP) acting as a nano-antenna. (a) Excitation of a localized surface plasmon resonance (LSPR) of a single Au NP. **(b)** The elastic scattering of the plasmonic Au NP enhances both the incoming (ω_{inc}) and the outgoing ($\omega_{out}=\omega_{inc}-\omega_{vib}$) radiation.[19] Adapted from reference 19.

The strongest signal enhancements in SERS substrates are obtained from so-called "hot spots", sites that have the strongest LSPR. For example, at the junction between two NPs, or a bulk metal surface, the surface plasmons can overlap to form gap-mode plasmons (Figure 1.3a - b). Depending on the distance between the particles, these gap-mode plasmons tremendously enhance the signal intensity in comparison to single particles. The hot spots lose intensity quickly when the distance between the NPs increase (Figure 1.3c-e).[43,44] This knowledge of hot spots illustrates the difficulty of applying SERS to other catalysts besides silver, gold and copper. Because the highest Raman signal enhancements arise at the junction of multiple plasmonic particles, one of the largest challenges is to observe surface species and adsorbates on other relevant catalytic materials.

The magnitude of the SERS enhancement is often described by the term "enhancement factor" (EF). It is a theoretical number that can be calculated with multiple methods. Each giving certain advantages over another. Two examples of the methods to calculate EFs are the substrate enhancement factor (EF) and the analytical enhancement factor (AEF). They are calculated as follows:

$$EF = \frac{I_{SERS}/N_{Sur}}{I_{RS}/N_{Vol}} \tag{1.1}$$

$$AEF = \frac{I_{SERS}/c_{SERS}}{I_{RS}/c_{RS}} \tag{1.2}$$

Where I_{SERS} is the intensity of the signal under SERS conditions; N_{sur} is the amount of molecules adsorbed on the substrates surface in the spot size of the incident laser; I_{RS} is the average intensity of the signal during normal Raman spectroscopy; N_{vol} is the average number of molecules in the volume probed by normal Raman spectroscopy; c_{SERS} is the concentration of analyte under SERS conditions. For more details we refer to the pioneering work of Felidj and co-workers.[45]

1.3 Micro and Nanostructured SERS Surfaces

Nanoparticle-based SERS offers advantages in terms of their ease of preparation and control of chemistry, but have limited reproducibility due to surface inhomogeneity, varying dimer orientation and ill-defined dimer spacing. For over a decade, efforts have been made to create SERS surfaces with well-defined and homogeneously distributed hot spots using a variety of methods, such as nanoimprinting, e-beam lithography, focused ion beam (FIB) milling, laser interference lithography (LIL) and template-based technologies.[46,47] Of these methods, photolithography holds great promise because of its exact geometric

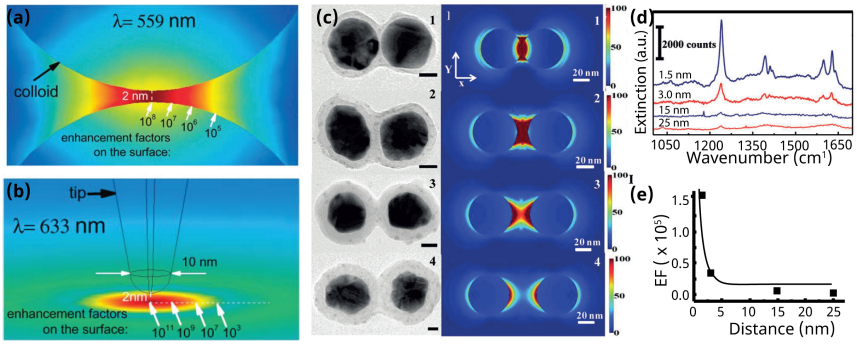

Figure 1.3. Local sensitivity in SERS and TERS. The strongest enhancement factors (EFs) arise from hot spots, which are produced by gap-mode plasmons that emerge between closely spaced plasmonic particles or tip-surface interactions where the plasmons overlap. **(a)** The EF can reach theoretical values of 10^8 for dimer gold NPs under 559 nm laser irradiance and **(b)** 10^{11} for a sharp Au tip - Au surface interaction under 633 nm laser irradiance as calculated by finite-element modeling.[43] Reproduced from reference 43. **(c)** The electric field is at its strongest when the particles touch and rapidly reduces to a negligible value when the particles are more than 15 nm away from each other. **(d)** This can be observed in the SERS spectra of adsorbed ammonium salt of pyrene on Ag@SiO_2 spheres. **(e)** Plot of SERS EF versus distance between the particles.[44] Adapted from reference 44.

control and availability of an extensive technological toolbox. With photolithography, structures such as nanogroove-, nanopyramid- and nanogap/nanowire-arrays have been recently realized with tunable gap spacing and high spatially averaged AEF,[45] as shown in Figure 1.4a - c.[48,49] Since in the first two of these approaches LIL is used in combination with anisotropic <100> silicon etching to create nanometer pitches and spacing, no mask is needed and the method is therefore relatively cheap. However, a disadvantage of these anisotropically etched structures is that the SERS hotspots with high signal enhancement only occur at a very small percentage of the surface area, since the groove width and spacing between the pyramid sidewalls vary strongly.

The third structure, the nanogap/nanowire, is particularly interesting for two reasons. First, the gap size remains constant (< 20 nm) as opposed to the groove and pyramid structures, while a large percentage of the surface gives high AEFs. The latter fact is due to the extremely high nanogap density of ~1000 $m \cdot cm^{-2}$.[48] In Figure 1.4d it is shown that practically all of the 2500 spots measured (at 1068 cm^{-1}) exhibit AEF values between 1×10^7 and 2×10^7 with an average value of 1.5×10^7.[48] The second advantage of the nanowire/nanogap structure is that it offers the opportunity of combining electrochemical reactions with *in situ* SERS analysis. Such a spectro-electrochemical technique gives the opportunity to study redox reactions and electron driven processes *in situ*, and has great importance for the study of catalytic reactions. It has also been shown to be of great value to study and analyze adsorbates, chemisorbed species and reaction intermediates.[50]

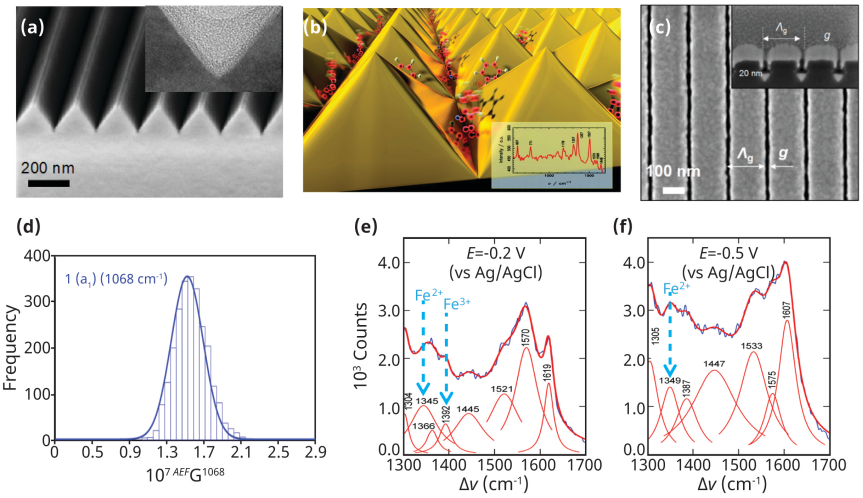

Figure 1.4. Examples of micro- and nanostructured SERS surfaces. (a) Nano v-grooves;[49] **(b)** Artist's impression of nanopyramids;[49] **(c)** nanowires/nanogaps with cross-section in inset;[48] **(d)** histogram of analytical enhancement factor (AEF) on a nanowires/nanogaps substrate;[48] **(e)** -0.2 V and **(f)** -0.5 V spectro-electrogram of MPY/hemin modified gold nanowire electrodes with Fe^{2+} and Fe^{3+} bands indicated in blue.[51]

The nanowires can be contacted electrically in an interdigitated way under potentiostatic control, and finally the nanostructured surface can be integrated in a microfluidic system. For example, such a setup can be utilized to measure the spectral shift of iron bands upon using a Ag/AgCl reference electrode and a platinum counter electrode. It was found that when the redox state of the hemin group of the mercaptopyridine (MPy)/hemin modified gold nanowires was changed by shuttling the voltage between -0.2 V (Figure 1.4e) and -0.5 V (Figure 1.4f) versus Ag/AgCl a corresponding change in the SERS spectra was observed.[51] This demonstrates that a combination of orthogonal analytical techniques combined with dynamic control of environmental conditions using microfluidics clearly holds great promise for *in situ* studies of catalytic reactions.

1.4 Combining SERS and Catalysis

Gold and silver metal NPs show catalytic behavior in a variety of reactions, implying that they can simultaneously act as sensor as well as catalyst.[52,53] Gold and silver catalysts can generally be used in three different types of surface reactions: heterogeneous catalysis,[54] electrochemical reactions[50] and photocatalytic (plasmon-driven) reactions.[55–57]

Valuable industrial reactions, such as NO_x reduction,[58] epoxidation reactions[53,59] and methanol synthesis,[60] can be carried out over copper and silver metals. However, because of their lower stability in air, they are less implemented

for SERS in comparison to gold NPs. Alloys made from silver/gold or copper/gold often have higher stability than pure materials. Gold-silver alloys can be fabricated for example by a simple co-reduction of $HAuCl_4$ and $AgNO_3$ using trisodium citrate.[61] Star-shaped copper/gold alloys have been prepared as well by a co-reduction using glucose as reductant, which have interesting catalytic and plasmonic properties.[62] The introduction of other metals during the synthesis to prepare alloyed NPs is not only interesting to increase the stability, but will affect the position of the LSPR as well as catalytic activity.[63]

A recent study by Marimuthu *et al.* showed that the oxidation state of surface atoms in copper NPs can be tuned by light during the epoxidation of propylene.[59] When the LSPR of the metallic core of the particles is excited, the subsequent increased electric field or hot electrons can reduce the copper oxide shell. The threshold light intensity to reduce the copper oxide surface was found to be 550 mW/cm^2, meaning that Raman lasers can easily be used to reduce the oxide surface. A plasmonic material that can reduce its oxidized surface by using Raman lasers sounds like the ideal SERS substrates. Although the threshold intensity is far below the laser intensity used in SERS, we are skeptical if this can be applied for SERS experiments since this mechanism has not been mentioned anywhere else in literature.

When SERS activity and catalytic activity do not go hand in hand, innovative materials have to be applied. For example, gold NPs become most catalytically active for sizes of approximately 5 nm,[64,65] whereas particles smaller than roughly 20 nm do not give a significant Raman signal enhancement.[66] Several research groups have devised methods to combine the catalytic activity of small gold NPs with bigger SERS particles. By varying the synthesis conditions of a seeded growth method slightly, 125 nm gold particles were prepared with porous surfaces. These porous surfaces behaved in a similar fashion as sub-5 nm gold NPs, whereas the overall particle provided the plasmonic enhancement for SERS.[67] Other methods describe the use of particles with different exposed facets,[68] adsorbing small gold NPs to gelatin covered SERS particles[69] or by adsorption of smaller gold particles to an oxide-coated plasmonic particle.[70]

1.5 Model Reactions

One of the most investigated reactions in recent SERS studies is the reduction of 4-nitrothiophenol (4-NTP) to 4-aminothiophenol (4-ATP).[71] Thiol functionalized molecules, such as 4-NTP and 4-ATP, exhibit high affinity for metal surfaces, guaranteeing their close contact with the SERS substrate. The Raman scattering cross-section of these types of molecules, containing nitro- and amino-functionalized groups in combination with aromatic rings, is relatively large and at certain excitation wavelengths this can lead to resonance Raman scattering. Furthermore, the use of thiols in catalysis gives the possibility to study the kinetics

of surface reactions with only minor interference of diffusion, adsorption and desorption mechanisms since they are fixed on the surface. The combination of these properties makes 4-ATP and 4-NTP ideal model molecules for SERS experiments. The reduction of 4-NTP by $NaBH_4$ requires the presence of a metal catalyst and can be performed at ambient conditions. Consequently, gold and silver NPs meet the requirements for both catalysis and SERS substrate. Various research papers and review articles have already been published concerning the reactions of 4-ATP and 4-NTP.[57,71–76] Model studies using 4-ATP and 4-NTP molecules can be used to increase our understanding of SERS in catalysis and to gain more insight into the interpretation of SERS spectra.

Catalyst structure-performance relations can be studied with the model studies using well-defined particles with controlled morphologies and different facets. However, it should be kept in mind that SERS activity is strongly dependent on a particle's size and shape. Since the electric field enhancement is highly local, it is inherent that the probing area of SERS only measures a fraction of the catalytically active surface. For example, Zhang *et al.* used gold NPs with different geometries to study their facet-dependent catalytic activity for the reduction of 4-ATP to 4-NTP with SERS.[68] As expected, high-index facetted particles were the most active according to the data obtained by SERS. However, the more anisotropic particles required a much shorter acquisition time for sufficient SERS signal in order to observe clear bands in the spectra, indicating that these particles exhibit intrinsic hot spots. Drawing conclusions about the overall catalytic activity of a particle is therefore difficult based solely on SERS data, since the Raman signal intensity at hot spots is several orders of magnitude stronger than at the rest of the particle and therefore dominates the overall spectrum. Additional studies, such as UV-Vis measurements, should then be performed for comparison.

1.6 Plasmon-driven Reactions

Plasmonic NPs are not inert and SERS therefore cannot be seen as a non-invasive characterization technique; the plasmons can interfere with the reaction of interest in multiple ways.[30,55,72,77–79] First, the massive electromagnetic field near the surface can weaken certain bonds in the analyte, initiating reactions.[30] Second, the heat generated as a result of the absorbed light will change the reaction conditions: affecting both temperature[80] and subsequently analyte concentrations.[76,81] Third, the plasmonic particles can generate new and alternative reaction pathways by the formation and injection of hot electrons (Figure 1.5).

Hot electrons can be generated at hot spots, where electrons are excited from below the Fermi level to an occupied state below the vacuum level. When an electron-acceptor is close to the surface, these "hot electrons" can be injected into the lowest unoccupied molecular orbital (LUMO) of this molecule. Simultaneously,

the hole can also accept electrons from the highest occupied molecular orbital (HOMO) of a nearby molecule (Figure 1.5a).[82]

The three alternative pathways are not isolated, they can take place simultaneously and can affect each other. These side-effects do not mean that SERS is useless for catalysis, however, it does mean that one has to make sure that what is measured is definitely the reaction of interest, and not a SERS artifact. Additionally, the three side effects can be advantageously used to initiate chemical reactions, for example by extreme heating of the sample by applying pulsed lasers.

The use of plasmonic materials as catalysts has recently become a growing field within photo-catalysis since it can produce chemicals with alternative pathways at ambient temperatures. Because both the reaction and the SERS signal are the strongest at hot spots, SERS seems to be an ideal method to study plasmon-driven reactions.[74] Photo-catalysts are useful as wastewater treatment and as sustainable energy-supplier for the future[83] and plasmon-driven catalysis is an exciting field in its own right. Interested readers are therefore directed to the recent literature.[30,57,72,79]

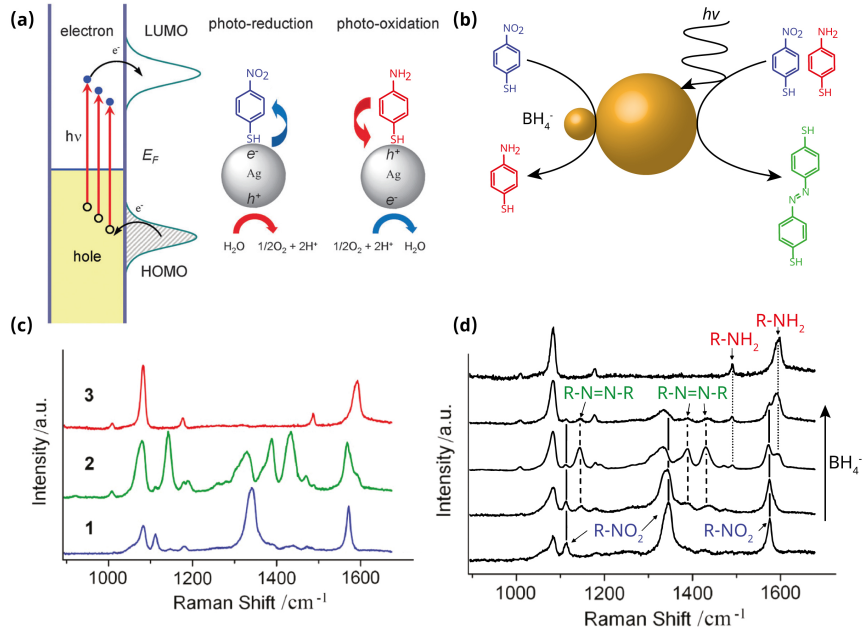

Figure 1.5. Alternative reaction pathways over plasmonic NPs. (a) Schematic diagram of the formation of hot electrons and holes in silver NPs, which are able to catalyze both oxidative and reductive reactions.[84] adapted from reference 83; **(b)** Possible reactions occurring during the chemical reduction of 4-NTP by $NaBH_4$ over gold NPs; **(c)** NMF-calculated SERS spectra of the three pure components including their assignment to the three molecular species 4-NTP (blue), 4,4'-DMAB (green) and 4-ATP (red)[85]; **(d)** Raw SERS spectra of the reduction of 4-NTP to 4-ATP over Au/Pt/Au catalysts, including DMAB-associated peaks for intermediate volumes of $NaBH_4$ added, corresponding to the calculated spectra from (c).[85] Adapted from reference 84.

To study the more conventional solid catalysts, one has to assure that the characterization technique does not interfere with the reaction of interest. Decreasing laser energy, power and changing the polarization are known to affect the catalytic power of the plasmons, although the signal enhancing effects of the plasmonic particles are thereby sacrificed.[31,75,86]

1.7 Borrowing SERS Activity

Since SERS is limited to a few materials,[87–89] SERS activity has to be 'borrowed' from existing substrates when the catalysts itself is not SERS active.[90] Catalytically active NPs can be directly assembled on a SERS substrate. Joseph *et al.*, for example, reported a novel method to study the reduction of 4-NTP to 4-ATP over platinum catalysts.[35] They compared two systems, one were 2 nm platinum NPs were anchored to a SERS substrate consisting of gold NPs, the other system involved a colloidal solution of the catalytic NPs. The SERS signal of 4-NTP was used to obtain kinetic data of the reaction in solution. The reaction kinetics of immobilized particles did not significantly differ from the colloidal catalyst, indicating that the involved reaction mechanism is the same. The immobilization method can thus be applied to other chemical reactions as well.[35] However, this method does not give information exclusive to the platinum catalyzed reaction, since the gold particles are not entirely inert nor are they isolated.

Post-synthesis mixing of separately prepared Au and Pt NPs can result in a heterogeneous distribution of different particles throughout the sample. To guarantee close contact between sensor and catalyst, thin overlayers of catalytically active metal can be sputtered over existing SERS substrates. For example, Heck *et al.*[91] prepared gold nanoshells with sub-monolayer coverages of palladium and observed improved activity for the aqueous-phase hydrodechlorination of dichloroethylene. These nanostructures allowed for the detection of the dechlorination of 1,1-DCE to ethane. Although the signal intensity of the probe molecule 4-ATP was reduced after palladium was grown on the gold nanoshells, the signal intensities of adsorbed 1,1-DCE increased as a result of the stronger interaction of 1,1-DCE to palladium. The dechlorination at the surface was observed by the appearance of peaks associated with Cl-M and C-M bonds. Additionally, a range of intermediate structures from 1,1-DCE to ethane were detected.[91]

Core-shell NPs can be fabricated by colloidal synthesis as well.[90] Using this method, any direct interaction with the plasmonic particle can be prevented when a uniform coating is applied. A crucial side effect can take place when thin metal layers are deposited over other metals. Due to the formation of alloys or by electron transfer from the core to the shell, the electronic structure of the catalyst may change, influencing its activity.[92] It has been reported that it is necessary to keep the metal coatings at least 5 monolayers thick so that it behaves as a 'pure' material.[93] Attard *et al.* have used a colloidal method to produce platinum-coated

SERS particles for studying the effect of surface poisoning on the alkyne adsorption on platinum catalysts.[94]

In order to apply SERS substrates for studying homogeneous catalysis, the materials will have to be cleverly designed, since SERS substrates are heterogeneous by definition. To increase the signal of low concentrated catalysts, reactants and products, the materials can be simply mixed in solution.[35] However, when these materials show a negative affinity to the SERS substrates, insufficient signal will be obtained and no conclusive Raman spectrum is observed. Additionally, some molecules in the solution have a higher affinity to gold or silver (also depending on the facets), increasing the chance to observe them and simultaneously decreasing the chance to observe other molecules. Similar to heterogeneous catalysis, the catalysts are preferred to be fixed to the surface of a well-defined SERS substrate, so that we know what we are looking at. Other methods are to fix the catalysts to a self-assembled monolayer (SAM) to a gold substrate, or to induce aggregation between the NPs by introducing the catalyst.[36,39,43]

1.8 SHINERS, Stable and Non-invasive Characterization

A promising method to minimize plasmonic side-reactions is by isolating the noble metal NPs using thin dielectric oxide coatings. Coatings of silica have been proposed to make plasmonic particles inert.[95] The technique, quite aptly named "shell-isolated nanoparticle-enhanced Raman spectroscopy" (SHINERS), has been successfully applied, amongst others to study catalysts.[70,95–97] Coating NPs with oxides enhances their stability in demanding conditions and increases their shelf life. Al_2O_3 shells of less than 1 nm thick can enhance the stability of Ag NPs to withstand temperatures of up to 400 °C under nitrogen for a few hours (Figure 1.6c - d).[98] The improved stability makes SHINERS a highly promising technique to study a wide variety of heterogeneous catalysts. SHINs can be used to expand SERS activity to other materials, since the oxide coating reduces plasmon-driven reactions (Figure 1.6a) and increases the stability of the plasmonic particle (Figure 1.6c - d).

An effective method to implement SHINERS in catalysis, is to prepare a physical mixture of bulk catalyst material with shell-isolated NPs (SHINs). Such a strategy was used by Li *et al.* to study nickel-based solid oxide fuel cell (SOFC) anodes. Spherical silver NPs were coated with 10 nm thick silica layers to increase their thermal stability, enabling them to withstand temperatures of up to 500 °C. However, due to the thickness of the coating the Raman signal was only enhanced by a factor of 150. Even with this low EF, the authors were able to observe surface species in ceria (CeO_2) at elevated temperatures and detect small quantities of coke that lay beneath the sensitivity limit of conventional Raman spectroscopy. Li *et al.* state that this technique can be readily applied to other catalytic and electrochemical

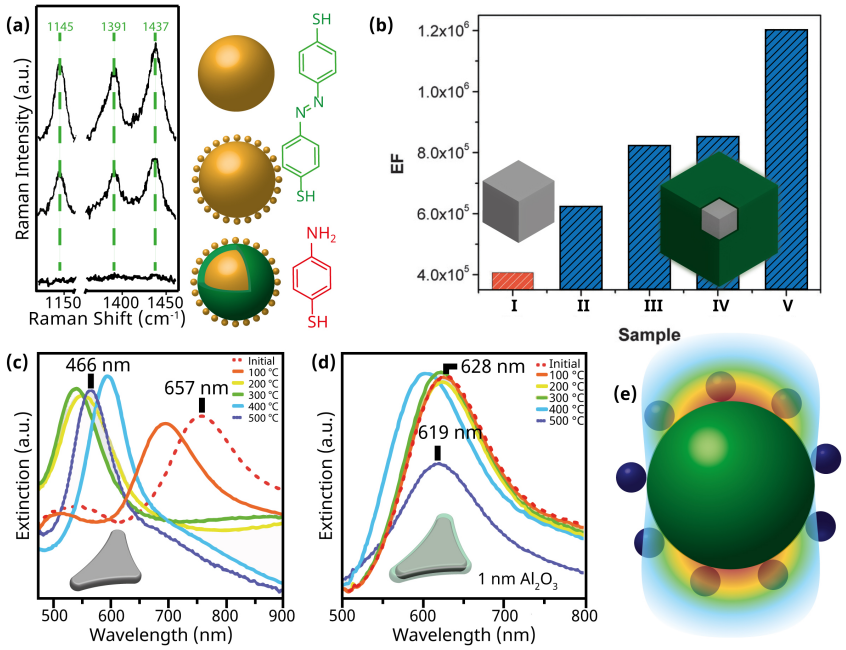

Figure 1.6. The advantages of shell-isolated NPs (SHINs). (a) SHINs prevent plasmon-driven reactions. SERS spectra collected from 4-ATP adsorbed on: 80 nm gold particles, 80 nm gold NPs covered with 5 nm gold particles and 80 nm SHINs covered with 5 nm gold particles. DMAB is not observed when SHINs are implemented.[70] Adapted from reference 70; **(b)** SERS EF calculated for a variety of silver nanocubes: bare (I, red) and SiO_2 coated cubes using different methods (II-V, blue). All SiO_2 coated nanocubes show increased EFs compared to bare silver nanocubes.[99] Adapted from reference 99; **(c)** UV-Vis absorption spectra of Ag NPs at elevated temperatures indicate that their LSPR shifts above temperatures of 100 °C;[98] **(d)** UV-Vis absorption spectra of Ag NPs coated with 1 nm Al_2O_3 at elevated temperatures indicate that stability is maintained up to 400 °C;[98] Adapted from reference 98. **(e)** SHINs (green) could potentially serve as a support for many other catalysts (purple spheres). Since the electric field is stronger (red) at the surface of the SHIN, it is expected that the catalyst-support interface can be characterized.

systems, and we feel similarly. This method is highly suitable for the detection of surface species and adsorbates and could show even greater potential when more stable and/or thinner coatings can be produced.[96,97]

The oxide layer can furthermore serve as a support material for NPs (Figure 1.6e), facilitating close contact between the SERS-active particle and the catalyst.[70,100,101] Similarly to other studies concerning the reduction of 4-NTP to 4-ATP,[67,68,85] Xie *et al.* observed DMAB as intermediate when the large plasmonic particles were not coated with silica.[70] However, when the large particle was isolated by an ultrathin (~ 1.5 nm), but nonporous silica coating, the bands associated with DMAB were no longer observed and only the reduction of 4-NTP to 4-ATP was detected (Figure 1.6a). Gold catalysts of 5 and 10 nm were used to show that smaller particles were indeed more effective catalysts.

A similar approach was applied by Attard *et al.* where they used silica-coated gold NPs on single crystal platinum surfaces to observe adsorbates with SHINERS, and

more recently during the hydrogenation of ethyl pyruvate (EP) to (R)-ethyl lactate (EL) over modified and unmodified Pt{hkl} electrodes (Figure 1.7).[94,102] SHINERS deposited on different platinum surfaces proved to non-invasively enhance the signal of EP adsorbed to the surface. An intermediate structure of the ethyl pyruvate, more specifically a half-hydrogenation state (HHS), formed by addition of a hydrogen atom to the keto carbonyl group, as well as a new species identified as intact chemisorbed EP bound in a μ_2(C,O) configuration, as illustrated in Figure 1.7 with a series of SHINERS spectra, as well as for the calculated structures of Pt-chemisorbed EP and HHS.[102] The relative ratio of both species was sensitive to the Pt surface structure. More specifically, the μ_2(C,O) EP surface species was dominant at pristine Pt{111} and Pt{100} surfaces, whereas the HHS was only observed at surfaces with defects and kinks, such as Pt (110) and

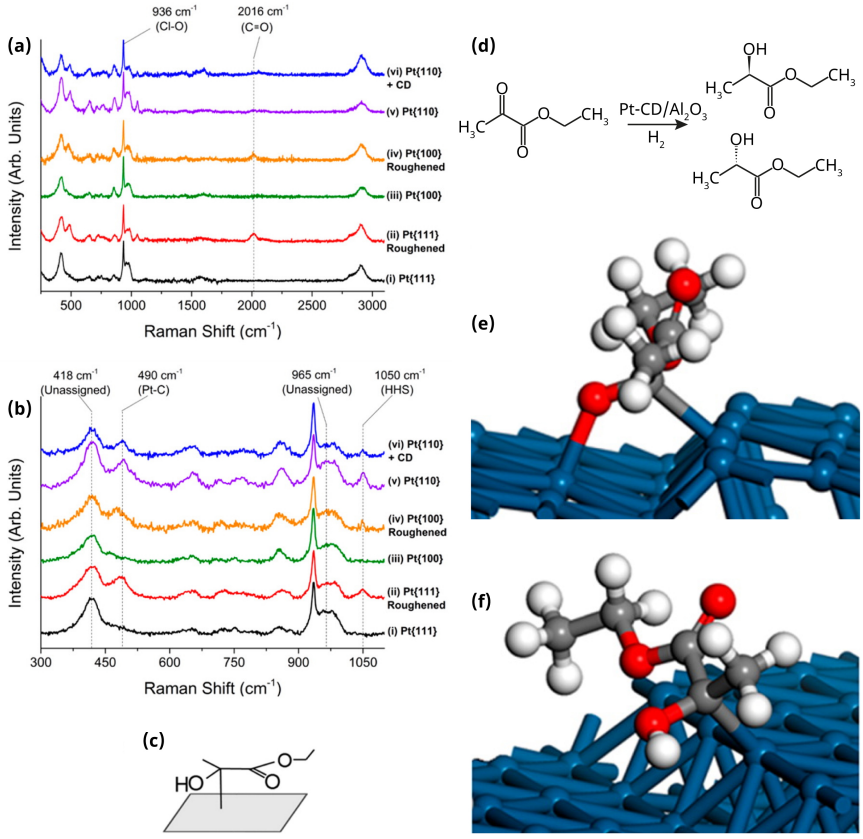

Figure 1.7. SHINERS investigation of the structure-sensitive hydrogenation ethyl pyruvate (EP) over Pt single crystals. (a-b) SHINERS spectra of Pt{hkl} single crystals immersed in 0.1 M EP/0.1M $HClO_4$ recorded under hydrogen evolution conditions (-0.1 V); **(c)** Schematic depiction of the half-hydrogenated state (HHS) intermediate; **(d)** Reaction mechanism of the hydrogenation of EP to E; **(e)** Calculated structure of (a) EP adsorbed in the μ_2(C,O) configuration; and **(f)** Calculated structure of HHS at a Pt{221} surface. Reproduced from reference 102.

roughened Pt electrodes.

In our lab, the dimerization of 4-ATP over pinhole-free SHINs was observed, contradicting the previously mentioned experiments.[73] This indicates that in the research conducted by Xie *et al.* the rate of plasmon-driven reaction is most likely slowed down significantly by the SiO_2 coating in comparison to the reduction by $NaBH_4$, making the observation of DMAB impossible.[70] In many publications, side effects are reported to be related to hot electrons injected into nearby molecules, but the extremely strong electric field at hot spots should not be neglected as they can facilitate photosensitive reactions as well.[30] Although the SERS signal intensity can increase for some coated particles,[99] increasing thickness of oxide coatings will usually result in a decrease of the signal enhancing effect and prevent side reactions caused by hot electrons or a strong electric field.

Any catalyst can potentially be assembled on the surface of SHINs, allowing the observation of Raman active surface species on these catalysts. These particles can then be tuned in size, shape and structure to characterize the effect on the reaction, similar to the method described by Xie *et al.*[70] One could also make use of different oxide[95,103,104] or carbon[105] coatings to mimic the support material, although some combinations of materials are effective photo-catalysts, such as titania-coated gold NPs.[77,103] A coating of several nanometers separates the catalyst particle and the plasmonic particle, meaning that for increasing catalyst size, the signal intensity decreases dramatically for the far side of the particle (Figure 1.6e). The strongest signals are produced at the metal-support interface in comparison to the far side of the particle. This effect can be exploited by attaching larger catalysts to the surface, making it more likely to observe chemical reactions or catalyst structures at the support-catalyst interface.[106]

1.9 Tip-enhanced Raman Spectroscopy

SERS exhibits the sensitivity to measure low concentrated species in the single-molecule regime. In order to use this tool to directly relate catalytic activity with the morphology of catalysts, we need to include a nanoscale topological map and monitor the catalytic activity on a single catalyst particle. SERS should then be combined with other techniques that have nanoscale spatial resolutions.[107] A more direct method to correlate catalyst structure to activity is by combining high chemical sensitivity of SERS with the nanoscale spatial resolution of SPM. To showcase the possibilities of the AFM-Raman methodology, the catalytic activity of silver nanocubes in rhodamine 6G degradation was linked to their distribution.[108] However, the diffraction-limited spatial resolution of Raman spectroscopy (typically 200-300 nm) is not overcome by combining SERS and AFM.

The spatial resolution can be significantly improved when a metal-coated tip is implemented in SPM, this technique is referred to as TERS.[109] Compared to SERS where hot spots are randomly distributed over the substrate, the electromagnetic

enhancement in TERS occurs only at a single point of the TERS tip-apex, which can be scanned over a surface using sensitive SPM feedback to make a nanoscale map of surface chemistry and catalytic activity simultaneously with the topography. TERS surpasses the diffraction-limited spatial resolution of confocal Raman spectroscopy to the nanoscale, with a recent breakthrough reaching the sub-nanometer regime with STM-based TERS, demonstrating the capability of TERS to map even single molecules.[29]

The potential of TERS for *in situ* catalysis research was first demonstrated by Domke and Pettinger[110] who studied the organometallic catalyst cobalt *meso*-tetraphenylporphyrin (CoTPP) on Au (111) substrate using STM-TERS with a Au tip. With TERS, the authors could spectroscopically discriminate between axially complexed and ligand-free CoTPP regions on the Ag substrate and identify chemical species complexed with CoTPP. TERS spectra from well-ordered CoTPP regions identified in the STM topography images showed vibrational bands characteristic of linker-modified CoTPP sandwiched between two Au layers. Whereas TERS spectra from the disordered region showed vibrational features of CoTPP axially complexed with CO and NO formed by catalytic reduction of CO_2 and NO_2 from ambient air. This study demonstrated that TERS could be successfully used to correlate structure with catalytic activity in heterogeneous catalysis, while the observation of such complexes indicates possible applications in homogeneous catalysis.

1.10 Studying Light-triggered Reactions with TERS

TERS studies of the plasmon-driven photo-catalytic reaction of 4-NTP to DMAB was carried out for the first time in a collaborative effort by Weckhuysen and Deckert *et al.*[31] The reaction was triggered using a 532 nm laser and was unobtrusively monitored using a 633 nm laser. It was found that a complete self-assembled monolayer (SAM) is necessary to obtain a stable starting signal as the molecules in an incomplete monolayer can change their orientation or move in and out of the sampling area more easily.[31] Since TERS measures only a small number of molecules and spectra are not averaged out over an ensemble, signal intensities are highly influenced by small fluctuations of analyte molecules in the measured area.[111] Time-series Raman spectra measured before and after the reaction at the tip-apex clearly showed the Raman bands associated with 4-NTP decrease and DMAB increase in intensity over time. This demonstrated the potential of TERS to monitor reactions on single catalytic particles over time.[31] Almost simultaneously, Xu *et al.*[112] performed a similar experiment using high-vacuum (HV) STM-TERS to demonstrate that this photo-catalytic reaction is driven by hot electrons produced during surface plasmon resonance. The authors showed that the reaction can be controlled by the plasmon intensity, which depends on laser power or the tip-substrate distance. In an additional report it was shown using HV

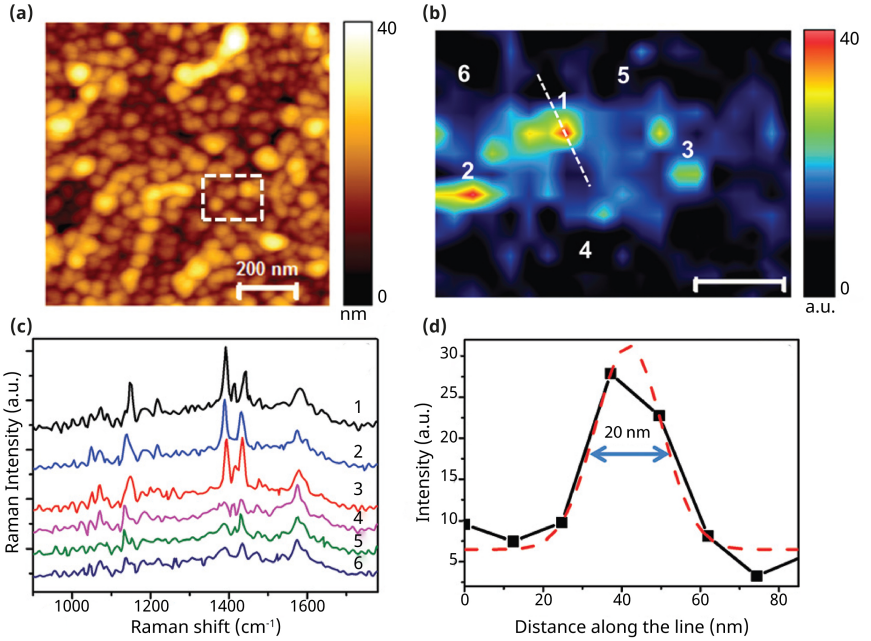

Figure 1.8. Relating catalyst structure to activity using TERS. (a) AFM topography image of the Ag catalyst substrate. **(b)** TERS map of the area marked by dashed rectangle in (a) showing signal intensities of a DMAB-associated band at 1142 cm^{-1}. **(c)** Near field spectra measured at the positions marked in (b). **(d)** Intensity profile along the dotted line marked in (b) showing the spatial resolution of the TERS map using a fitted Gaussian curve (Red) to be 20 nm.[113] Reproduced from reference 114.

STM-TERS that the reaction was indeed the result of the plasmon resonance in the nanogap between a Au tip and a Ag substrate; thermal effects could be neglected.[114]

Very recently, the potential of TERS to actually relate catalyst structure to activity was realized by Kumar *et al.* with AFM-based TERS.[113] The activity of silver NPs was studied using the plasmon-driven photocatalytic dimerization of 4-ATP to DMAB. The authors first mapped the reaction at a single point of contact of the Ag-coated TERS tip with a reactant substrate. Since both the silver particles and the silver-coated tip were catalytically active in the reaction 4-ATP to DMAB, the tip was made inert using a 3-5 nm thick Al_2O_3 coating while preserving its plasmonic enhancement. Using the alumina-protected TERS tip, the authors were able to map catalytically active sites on the Ag substrate with 20 nm spatial resolution as shown in Figure 1.8.[113]

We believe that coating TERS tips is a good strategy in order to obtain reliable and stable data during measurements, similarly to the application of SHINERS. It is known that the tips can be contaminated by surface species, causing additional bands in the spectrum or worse, losing their signal enhancing properties.[115] Dielectric coatings, such as oxides, can prevent the adsorption of contaminants or irreversible tip damage from oxidative reactions thereby enhancing their stability.

However, since the decay length of TERS near-field is only a few nm,[116] a dielectric coating may significantly decrease the plasmonic enhancement of the TERS tip.[40] Therefore, the thickness of the protective dielectric coating should not be more than a few nm (ideally 1-2 nm) and should be pinhole-free for TERS tips to provide Raman signal enhancements. Alternatively, aluminum tips have been used in TERS in combination with a 363.8 nm ultraviolet laser.[117] Since aluminum is known to form a thin native oxide layer of approximately 3 nm, such tips are expected to be chemically more stable although higher energy lasers are required that may cause degradation of chemical species.[87]

The sensitivity of TERS measurements can be significantly enhanced by utilizing the plasmonic coupling of a metal or metal-coated tip with a metal substrate. Using this so-called "gap-mode" TERS, extremely high EFs can be reached. For example, gold-coated tips close to metallic substrates can produce Raman signals that are a factor of 10^3 stronger than tips close to dielectric substrates, such as SiO_2.[118]

So far, TERS has been mainly used for the study of plasmon-driven photocatalytic reactions where reactants and the products have a rather large Raman cross-section. However, the reactants and products employed in more industrially relevant catalytic reactions usually have a much lower Raman cross-section. Furthermore, such reactions are carried out at temperatures and pressures much higher than the ambient. Therefore, TERS probes with a high plasmonic enhancement, stability and lifetime are required to make TERS a powerful tool for the study of catalytic reactions under operating conditions.

1.11 Towards the Observation of Single Molecules

Spectral fluctuations can arise in TERS and SERS experiments due to the highly localized sensitivity. These fluctuations are not necessarily undesired, but can be a topic of interest as well; shifts in the band position can give clues about the mechanism of a chemical reaction. Not only orientational effects become more visible when the homogeneous broadening is reduced by measuring smaller ensembles, but other interesting events can be observed as well. For example, one can distinguish between isotopes, since vibrational energy levels are related to the reduced mass of the participating atoms.[119]

Additionally, the chance to find short-lived species such as intermediates should increase when approaching single-molecule experiments. Knowing which and how many intermediates are present during the reaction is crucial to optimally tune the catalyst as it will tell us the amount of rate-limiting steps and how to possibly improve the reaction kinetics. Combining single-particle and single-molecule kinetic studies have been performed in fluorescence microscopy experiments, revealing intermediates and inter-particle heterogeneities, such as size-dependent activity.[120] However, fluorescence microscopy experiments do not enable the observation of structures of the reactants and requires the use of fluorescent

reactants or products, thereby limiting its use. SERS, on the other hand, can supply us with structural information of both the reactant and catalyst and can be applied to a wider range of molecules, allowing a larger versatility.

To approach the single-molecule regime in SERS experiments, the analytes can be diluted. However, dilution of the reactants cannot always be applied to obtain reaction mechanisms. Reaction conditions will often change upon dilution and this can lead to different reaction pathways. For example, dimerization reactions cannot proceed with single molecules. It was expected that the plasmonic conversion of highly diluted 4-NTP monolayers would therefore be inhibited. However, Zhang *et al.* found that a plasmon-driven reaction of 4-NTP can still take place, although resulting in a different product[75] When there is no nearby molecule, the nitro-group is split from the substrate and thiophene (TP) is obtained as the product. Hot electrons generated at the hot spots were proposed to have sufficient energy to excite 4-NTP to a transient negative ion. The negative ion "travels" to the excited state of TP and returns to the ground state of TP, returning the electron to the gold surface.[78]

Single or several molecules can dominate the spectrum over larger ensembles in SERS, because the electric field is significantly stronger for the few molecules residing at hot spots than for molecules positioned outside the hot spots. If a reaction takes place while the molecule is situated at the hot spot, we should be able to observe the reaction. Plasmonic catalysts therefore prove to be ideal substrate for SERS experiments, since both the high signal enhancement and catalytic activity originate from the hot spot.[30,57] Previous research performed in our group utilized this principle to study the dimerization of 4-NTP to DMAB.[31,32,121] Chemometric methods were applied to obtain a clearer image of the kinetics during the reaction, as is demonstrated in Figure 1.9.[32] Firstly, a one-component principal-component analysis (PCA) removed the spectral blinking from the data, which already resulted in a better understanding of the reaction data with a lower signal to noise ratio. After removal of the spectral blinking, the reaction spectra were taken through a two-component multivariate curve resolution (MCR) that described the reactant and the product, improving the kinetic data even further (Figure 1.9b vs. c). The spectra that were removed from the kinetic data by PCA were subsequently analyzed with a four-component MCR analysis (Figure 1.9d). Two of the components were similar to the two main components (the reactant and the product) in the kinetic data, apart from some slight variations in peak intensities that were caused by differences in orientation. The third and fourth components were low in intensity over the measured time, apart from two single instances for each component. The third component resembled much of DMAB, but the fourth component is a completely unknown structure and is a potential reaction intermediate.[30]

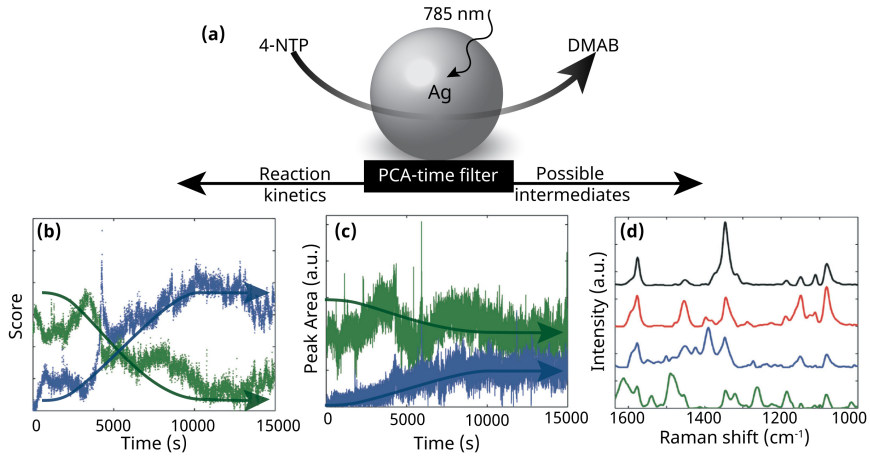

Figure 1.9. The photocatalytic dimerization reaction of 4-NTP to DMAB over Ag nanostructures. (a) 4-NTP dimerization to DMAB is triggered and studied with SERS using a 785 nm laser excitation**. (b)** Spectral fluctuations can be removed from the spectrum with a PCA time filter, after which a two component MCR can further clear up the kinetic data. The kinetic data is now analyzed over full spectra instead of over single peaks, making it less prone to shifts in band positions. **(c)** The conventional method to obtain kinetic data is to plot the peak area over time, which can contain a large amount of noise. **(d)** The discarded data after the PCA time filter can be analyzed with MCR to find possible intermediate structures.[32] Adapted from ref 32.

1.12 Ultrafast Raman Spectroscopy

Most Raman spectrometers are not fit to observe short-lived species, such as intermediates, because they require spectral integration times of at least a second. Recent progress made in the field of ultrafast Raman spectroscopy allows acquisition times in the order of picoseconds with Raman linewidths of tens of cm^{-1}.[33] Fast acquisition times enable the elucidation of a large deal of reaction steps/dynamics, including bond forming and breaking. To extend the potential of time-resolved Raman spectroscopy, it can be combined with other techniques, such as CARS, to improve the signal intensity and SERS to increase the signal intensity even further to detect surface species.[122]

Since the technique generates extremely large electric fields that can potentially damage the sample and the SERS-antenna, the experiments need to be performed in a highly controlled environment. Yampolsky *et al.* managed to reduce the damage to SERS-antennae by encapsulating gold dimers and adsorbed trans-1,2-bis-(4-pyridyl) ethylene (BPE) in thick porous silica shells of about 70-80 nm.[122] The hot spots between the dimer in combination with CARS provided excellent signal enhancement for the observation of BPE near the single-molecule level. By applying a femtosecond laser scanning CARS microscope and by tuning the frequencies of the pump and the Stokes pulses, the authors were able to observe an oscillating signal that was associated with the quantum beating of the closely spaced excited vibrational modes of BPE. It is important to note that a single time

trace was not obtained instantly, but the result was obtained after averaging the signal over an hour.[122]

Ultrafast Raman spectroscopy can lead to promising results where one could actually follow bond formation and breaking. However, the technique suffers from the possibility of sample damage and requires highly controlled environments and thus does not seem fit for the characterization of solid catalysts in their operating conditions yet. Ultimately, time-resolved Raman spectroscopy should be combined with TERS to give a spatial resolution in the nanometer scale and a temporal resolution in the picosecond scale. However, such experiments have to be performed on fixed analytes under ultrahigh vacuum to prevent blinking signal and sample degradation.[123]

1.13 Challenges and Future Prospects

Based on the above considerations it should be clear that SERS and TERS can make the difference in three specific fields. The first field concerns the monitoring of chemical reactions at the molecular level, including the potential to identify reaction intermediates and even transition states. Secondly, the use of SERS in combination with its plasmonic platform opens up ample opportunities to conduct a wealth of chemical reactions at the surface of gold and silver, which are known to be catalytically active. The third one is associated with the heat developed by the plasmonic materials upon illumination providing new opportunities to locally create the proper experimental conditions to trigger a catalytic reaction.

It is important to realize that SERS and TERS have made tremendous progress over the recent years and are becoming mature spectroscopic techniques. Improvements in substrate preparation have made SERS more robust and sensitive, opening the path for the detection of surface species with low Raman scattering cross-sections in a wide range of reaction conditions. Depending on the desired application, the type of SERS substrate can be chosen for optimal results (Table 1). We believe that, following the highlighted examples in this chapter, SERS can become an attractive and versatile characterization method for a wide variety of catalytic materials. However, this will not be a simple task and requires interdisciplinary research for developing stable and inert SERS substrates, combined with intense Raman signal enhancements. Simple spherical plasmonic NPs often do not suffice for heterogeneous catalysis research since their enhancement signal is negligible when they are not in an aggregated state.[124] Dimers or other structures, such as nanorods, are expected to give better results with respect to signal enhancement, but are currently less stable. It is believed that SERS substrates prepared by photolithography can yield more robust and homogeneous Raman signal intensities. Similarly, TERS tips, especially with Ag-coatings, are known to degrade at a fast rate and need development of robust methods of thin, pinhole free protective dielectric coatings for prolonged

measurements in ambient and especially at operating conditions of catalysts at elevated temperatures and pressures.

We believe that SHINERS and its TERS counterpart can play significant roles in the study of heterogeneous catalysis. SHINs have improved thermal and chemical stability in comparison with bare plasmonic nanostructures and can even act as a support material, guaranteeing close contact between catalyst and sensor for heterogeneous catalysis (Table 1). Additionally, alumina-protected TERS tips have proven to be a useful, stable and non-invasive technique for mapping catalytic activity of silver photo-catalysts. Combining the current developments in SERS and TERS with other developments in Raman, such as CARS and ultrafast spectroscopy, will most likely lead to useful mechanistic information regarding catalytic solids.

1.14 Scope of the Thesis

The goals of this PhD thesis are as follows: first, to advance SHINERS towards a more stable and universal characterization technique. Second, to apply SHINERS for the observation and characterization of catalytically relevant surface species during *in situ* and ultimately *operando* spectroscopy. The first three chapters – Chapters 2, 3 and 4 – will focus on the preparation of SHINs and a better understanding of SHINERS signals observed under catalytic studies. The knowledge obtained in these three chapters are then combined in Chapter 5 to develop extrudate sensors for *operando* measurements of surface species during heterogeneous catalysis.

In Chapter 2, TiO_2 and SiO_2 SHINs were prepared for application as SHINERS substrates and were tested for their thermal stability. Both SiO_2 and TiO_2 SHINs were found to be adequate Raman signal enhancers, and maintained their Raman enhancing properties up to temperatures of 400 °C in air. We implemented these nanostructures in Chapter 3 for *in situ* measurements of CO hydrogenation. The two types of SHINs can be used for probing various metal catalysts supported on two support materials, namely TiO_2 and SiO_2. During these initial *in situ* experiments, we ran into difficulties with assigning the Raman signals. This problem was overcome in Chapter 4, by setting up experimental guidelines for the implementation of SHINERS in heterogeneous catalysis. These guidelines involve careful control of experimental conditions to obtain clean substrates for obtaining SHINER spectra without spurious peaks. Finally, in Chapter 5, the knowledge on obtaining optimal SHINERS substrates was applied to prepare extrudate sensors. Using these sensors, we were able to probe the interfaces between metals and support material over three different catalysts: Rh/SiO_2, Rh/TiO_2 and $RhFe/SiO_2$. This resulted in the observations of chemical species that were previously not observed by conventional spectroscopy methods, such as IR. Furthermore, the extrudates contained, next to SHINs, luminescent NPs for probing the local

temperature of a working catalyst. This PhD thesis ends with some concluding remarks and an outlook based on other work found in literature and promising experiments that were performed during various projects that did not make it to the main chapters of this PhD thesis.

Table 1.1. Overview of Different SERS Substrates Including Their Advantages and Disadvantages

SERS substrate	Advantages	Disadvantages
Gold/silver/copper catalyst 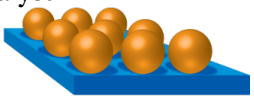	Combined SERS antenna and catalyst Correlate structure to performance Simple synthesis	Plasmon-driven (side-) reactions Hot spots enhance highly locally and not over entire catalyst Low stability
Catalyst particles distributed over existing SERS substrate 	Borrow SERS activity Correlate structure to performance	Gold-reactant interactions Plasmon-driven (side-) reactions Inhomogeneous distribution of particles Low stability
Core-shell particles 	Borrow SERS activity Isolated gold particles	Plasmon-driven (side) reactions Inhomogeneous distribution of particles Low stability Possibly altered catalyst properties
SHINs 	Isolated gold particles Improved stability Can act as support material	Often decreased EFs
TERS 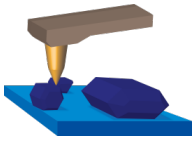	Able to map catalytic activity on the nanoscale Simultaneous topography and chemical information possible Structure-performance correlation	Time consuming Requires metallic substrates for higher EFs Low probe stability, can be improved with dielectric coating

1.15 Author Contributions

This chapter is based on the manuscript: Surface- and Tip-Enhanced Raman Spectroscopy in Catalysis, T. Hartman, C. S. Wondergem, N. Kumar, A. van den Berg, B. M. Weckhuysen, *J. Phys. Chem. Lett.* **2016**, 7, 1570–1584.

The original plan for the manuscript was conceived by Bert Weckhuysen and was further constructed and written by Thomas Hartman and Katinka Wondergem under supervision of Bert Weckhuysen. Naresh Kumar (National Physical Laboratory) contributed with paragraphs on TERS. Albert van den Berg (University of Twente) contributed with paragraphs on micro and nano-structured SERS substrates.

1.16 References

[1] G. Ertl, H. Knözinger, F. Schüth, J. Weitkamp, *Handbook of Heterogeneous Catalysis*, Wiley-VCH, Weinheim, **2008**.
[2] G. A. Somorjai, A. S. Mujumdar, *Dry. Technol.* **1995**, *13*, 507–508.
[3] J. Hagen, *Industrial Catalysis: A Practical Approach*, Wiley-VCH, Weinheim, **2015**.
[4] B. M. Weckhuysen, *Phys. Chem. Chem. Phys.* **2003**, *5*, 4351–43560.
[5] F. Zaera, *Chem. Soc. Rev.* **2014**, *43*, 7624–7663.
[6] A. Savara, E. Weitz, *Annu. Rev. Phys. Chem.* **2014**, *65*, 249–273.
[7] E. Stavitski, B. M. Weckhuysen, *Chem. Soc. Rev.* **2010**, *39*, 4615–4625.
[8] F. Fan, Z. Feng, G. Li, S. Keju, Y. Pinliang, C. Li, *Chem. Eur. J.* **2008**, *14*, 5125–5129.
[9] P. Dufresne, E. Payen, J. Grimblot, J. P. Bonelle, *J. Phys. Chem.* **1981**, *85*, 2344–2351.
[10] C. Li, P. C. Stair, *Catal. Today* **1997**, *33*, 353–360.
[11] H. Knözinger, *Catal. Today* **1996**, *32*, 71–80.
[12] J. W. Niemantsverdriet, *Spectroscopy in Catalysis: An Introduction*, Wiley-VCH, Weinheim, **2007**.
[13] E. Smith, G. Dent, *Modern Raman Spectroscopy—A Practical Approach*, Wiley, Chichester, **2005**.
[14] H. Kim, K. M. Kosuda, R. P. Van Duyne, P. C. Stair, *Chem. Soc. Rev.* **2010**, *39*, 4820–4844.
[15] I. E. Wachs, *Catal. Today* **1996**, *27*, 437–455.
[16] I. E. Wachs, C. A. Roberts, *Chem. Soc. Rev.* **2010**, *39*, 5002–5017.
[17] M. A. Bañares, *Adv. Catal.* **2009**, *52*, 43–128.
[18] J.-X. Cheng, X. S. Xie, *J. Phys. Chem. B* **2004**, *108*, 827–840.
[19] S. Schlücker, *Angew. Chem. Int. Ed.* **2014**, *53*, 4756–4795.
[20] Z.-Q. Tian, B. Ren, D.-Y. Wu, *J. Phys. Chem. B* **2002**, *106*, 9463–9483.

[21] W. Xie, S. Schlücker, *Reports Prog. Phys.* **2014**, *77*, 116502.
[22] Y. Zhang, Y.-R. Zhen, O. Neumann, J. K. Day, P. Nordlander, N. J. Halas, *Nat. Commun.* **2014**, *5*, 4424.
[23] F. M. Hoffmann, *Surf. Sci. Rep.* **1983**, *3*, 107–192.
[24] G. Rupprechter, *Adv. Catal.* **2007**, *51*, 133–263.
[25] Y. R. Shen, *Nature* **1989**, *337*, 519–525.
[26] H. L. Han, G. Melaet, S. Alayoglu, G. A. Somorjai, *ChemCatChem* **2015**, *7*, 3625–3638.
[27] G. A. Somorjai, H. Frei, J. Y. Park, *J. Am. Chem. Soc.* **2009**, *131*, 16589–16605.
[28] K. M. Bratlie, M. O. Montano, L. D. Flores, M. Paajanen, G. A. Somorjai, *J. Am. Chem. Soc.* **2009**, *128*, 12810–12816.
[29] R. Zhang, Y. Zhang, Z. C. Dong, S. Jiang, C. Zhang, L. G. Chen, L. Zhang, Y. Liao, J. Aizpurua, Y. Luo, J. L. Yang, J. G. Hou, *Nature* **2013**, *498*, 82–86.
[30] R. Long, Y. Li, L. Song, Y. Xiong, *Small* **2015**, *11*, 3873–3889.
[31] E. M. van Schrojenstein Lantman, T. Deckert-Gaudig, A. J. G. Mank, V. Deckert, B. M. Weckhuysen, *Nat. Nanotechnol.* **2012**, *7*, 583–586.
[32] E. M. van Schrojenstein Lantman, P. de Peinder, A. J. G. Mank, B. M. Weckhuysen, *ChemPhysChem* **2015**, *16*, 547–554.
[33] E. L. Keller, N. C. Brandt, A. A. Cassabaum, R. R. Frontiera, *Analyst* **2015**, *140*, 4922–4931.
[34] K. Hu, D. Li, J. Cui, Y. Cao, Y. Long, *RSC Adv.* **2015**, *5*, 97734–97737.
[35] V. Joseph, C. Engelbrekt, J. Zhang, U. Gernert, J. Ulstrup, J. Kneipp, *Angew. Chem. Int. Ed.* **2012**, *51*, 7592–7596.
[36] D. Cialla, S. Pollok, C. Steinbrücker, K. Weber, J. Popp, *Nanophotonics* **2014**, *3*, 383–411.
[37] F. Peng, Y. Su, Y. Zhong, C. Fan, S. T. Lee, Y. He, *Acc. Chem. Res.* **2014**, *47*, 612–623.
[38] S.-Y. Ding, J. Yi, J.-F. Li, B. Ren, D.-Y. Wu, R. Panneerselvam, Z.-Q. Tian, *Nat. Rev. Mater.* **2016**, *1*, 16021.
[39] B. Pettinger, *Mol. Phys.* **2010**, *108*, 2039–2059.
[40] J. A. Dieringer, A. D. Mcfarland, N. C. Shah, D. A. Stuart, A. V Whitney, C. R. Yonzon, M. A. Young, X. Zhang, R. P. Van Duyne, *Faraday Discuss.* **2006**, *132*, 9–26.
[41] M. Moskovits, *Phys. Chem. Chem. Phys.* **2013**, *15*, 5301–5311.
[42] P. G. Etchegoin, E. C. Le Ru, in *Surf. Enhanc. Raman Spectrosc. Anal. Biophys. Life Sci. Appl.* (Ed.: S. Schlücker), Wiley-VCH, Weinheim, **2010**, pp. 1–37.
[43] P. G. Etchegoin, E. C. Le Ru, *Phys. Chem. Chem. Phys.* **2008**, *10*, 6079–6089.
[44] M. Shanthil, R. Thomas, R. S. Swathi, K. G. Thomas, *J. Phys. Chem. Lett.* **2012**, *3*, 1459–1464.

[45] N. Félidj, J. Aubard, G. Lévi, J. R. Krenn, M. Salerno, G. Schider, B. Lamprecht, A. Leitner, F. R. Aussenegg, *Phys. Rev. B* **2002**, *65*, 075419.
[46] M. E. Stewart, C. R. Anderton, L. B. Thompson, J. Maria, S. K. Gray, J. A. Rogers, R. G. Nuzzo, *Chem. Rev.* **2008**, *108*, 494–521.
[47] M. Fan, G. F. S. Andrade, A. G. Brolo, *Anal. Chim. Acta* **2011**, *693*, 7–25.
[48] L. L. T. Ngoc, M. Jin, J. Wiedemair, A. van den Berg, E. T. Carlen, *ACS Nano* **2013**, *7*, 5223–5234.
[49] M. Jin, V. Pully, C. Otto, A. van den Berg, E. T. Carlen, *J. Phys. Chem. C* **2010**, *114*, 21953–21959.
[50] D.-Y. Wu, J.-F. Li, B. Ren, Z.-Q. Tian, *Chem. Soc. Rev.* **2008**, *37*, 1025–1041.
[51] T. Yuan, L. L. T. Ngoc, J. van Nieuwkasteele, M. Odijk, A. van den Berg, H. Permentier, R. Bischo, E. T. Carlen, *Anal. Chem.* **2015**, *87*, 2588–2592.
[52] P. H. McBreen, M. Moskovits, *J. Catal.* **1987**, *103*, 188–199.
[53] S. Boghosian, S. Bebelis, C. G. Vayenas, G. N. Papatheodorou, *J. Catal.* **1989**, *117*, 561–565.
[54] Y. Mikami, A. Dhakshinamoorthy, M. Alvaro, H. García, *Catal. Sci. Technol.* **2012**, *3*, 58–69.
[55] P. Christopher, H. Xin, S. Linic, *Nat. Chem.* **2011**, *3*, 467–472.
[56] P. B. Dorain, K. U. Von Raben, R. K. Chang, B. . Laube, *Chem. Phys. Lett.* **1981**, *84*, 405–409.
[57] Z. Zhang, T. Deckert-Gaudig, V. Deckert, *Analyst* **2015**, *140*, 4325–4335.
[58] K. A. Bethke, H. H. Kung, *J. Catal.* **1997**, *102*, 93–102.
[59] A. Marimuthu, J. Zhang, S. Linic, *Science* **2013**, *339*, 1590–1593.
[60] A. Karelovic, P. Ruiz, *Catal. Sci. Technol.* **2015**, *5*, 869–881.
[61] J. L. Wang, R. A. Ando, P. H. C. Camargo, *ACS Appl. Mater. Interfaces* **2014**, *4*, 3815–3819.
[62] R. He, Y. C. Wang, X. Wang, Z. Wang, G. Liu, W. Zhou, L. Wen, Q. Li, X. Wang, X. Chen, J. Zeng, J. G. Hou, *Nat. Commun.* **2014**, *5*, 4327.
[63] J. C. Santos Costa, P. Corio, L. Marcia Rossi, *Nanoscale* **2015**, *7*, 8536–8543.
[64] T. Kiyonaga, Q. Jin, H. Kobayashi, H. Tada, *ChemPhysChem* **2009**, *10*, 2935–2938.
[65] I. Laoufi, M. C. Saint-Lager, R. Lazzari, J. Jupille, O. Robach, S. Garaudée, G. Cabailh, P. Dolle, H. Cruguel, A. Bailly, *J. Phys. Chem. C* **2011**, *115*, 4673–4679.
[66] S. E. J. Bell, M. R. McCourt, *Phys. Chem. Chem. Phys.* **2009**, *11*, 7455–7462.
[67] Q. Zhang, D. A. Blom, H. Wang, *Chem. Mater.* **2014**, *26*, 5131–5142.
[68] Q. Zhang, H. Wang, *ACS Catal.* **2014**, *4*, 4027–4033.
[69] Q. Cui, A. Yashchenok, L. Zhang, L. Li, A. Masic, G. Wienskol, H. Möhwald, M. Bargheer, *ACS Appl. Mater. Interfaces* **2014**, *6*, 1999–2002.
[70] W. Xie, B. Walkenfort, S. Schlücker, *J. Am. Chem. Soc.* **2012**, *135*, 1657–1660.

[71] E. M. van Schrojenstein Lantman, Raman Nanospectroscopy of a Photo-Catalytic Reaction, Utrecht University, PhD thesis, **2014**.
[72] M. Sun, H. Xu, *Small* **2012**, *8*, 2777–2786.
[73] C. E. Harvey, B. M. Weckhuysen, *Catal. Lett.* **2014**, *145*, 40–57.
[74] X.-J. Chen, G. Cabello, D.-Y. Wu, Z.-Q. Tian, *J. Photochem. Photobiol. C Photochem. Rev.* **2014**, *21*, 54–80.
[75] F. Pashaee, R. Hou, P. Gobbo, M. S. Workentin, F. Lagugné-Labarthet, *J. Phys. Chem. C* **2013**, *117*, 15639–15646.
[76] M. Tabatabaei, A. Sangar, N. Kazemi-zanjani, P. Torchio, A. Merlen, F. Lagugné-Labarthet, *J. Phys. Chem. C* **2013**, 14778–14786.
[77] W.-L. Liu, F.-C. Lin, Y.-C. Yang, C.-H. Huang, S. Gwo, M. H. Huang, J.-S. Huang, *Nanoscale* **2013**, *5*, 7953–7962.
[78] Z. Zhang, T. Deckert-Gaudig, P. Singh, V. Deckert, *Chem. Commun.* **2015**, *51*, 3069–3072.
[79] P. Wang, B. Huang, Y. Dai, M.-H. Whangbo, *Phys. Chem. Chem. Phys.* **2012**, *14*, 9813–9825.
[80] M. Rycenga, Z. Wang, E. Gordon, C. M. Cobley, A. G. Schwartz, C. S. Lo, Y. Xia, *Angew. Chem. Int. Ed.* **2009**, *48*, 9924–9927.
[81] T. Kang, S. Hong, Y. Choi, L. P. Lee, *Small* **2010**, *6*, 2649–2652.
[82] L.-B. Zhao, Y.-F. Huang, X.-M. Liu, J. R. Anema, D.-Y. Wu, B. Ren, Z.-Q. Tian, *Phys. Chem. Chem. Phys.* **2012**, *14*, 12919–12929.
[83] M. Pelaez, N. T. Nolan, S. C. Pillai, M. K. Seery, P. Falaras, A. G. Kontos, P. S. M. Dunlop, J. W. J. Hamilton, J. A. Byrne, K. O. Shea, M. H. Entezari, D. D. Dionysiou, *Appl. Catal. B, Environ.* **2012**, *125*, 331–349.
[84] Y.-F. Huang, D.-Y. Wu, H.-P. Zhu, L.-B. Zhao, G.-K. Liu, B. Ren, Z.-Q. Tian, *Phys. Chem. Chem. Phys.* **2012**, *14*, 8485–8497.
[85] W. Xie, C. Herrmann, K. Kömpe, M. Haase, S. Schlücker, *J. Am. Chem. Soc.* **2011**, *133*, 19302–19305.
[86] W. Huang, Q. Jing, Y. Du, B. Zhang, X. Meng, M. Sun, K. S. Schanze, H. Gao, P. Xu, *J. Mater. Chem. C* **2015**, *3*, 5285–5291.
[87] M. W. Knight, N. S. King, L. Liu, H. O. Everitt, P. Nordlander, N. J. Halas, *ACS Nano* **2014**, *8*, 834–840.
[88] J. M. McMahon, S. K. Gray, G. C. Schatz, *Phys. Chem. Chem. Phys.* **2009**, *15*, 5415–5423.
[89] P.-G. Yin, L. Jiang, T.-T. You, W. Zhou, L. Li, L. Guo, S. Yang, *Phys. Chem. Chem. Phys.* **2010**, *12*, 10781–10785.
[90] Z.-Q. Tian, B. Ren, J.-F. Li, Z.-L. Yang, *Chem. Commun.* **2007**, *34*, 3514–3534.
[91] K. N. Heck, B. G. Janesko, G. E. Scuseria, N. J. Halas, M. S. Wong, *J. Am. Chem. Soc.* **2008**, *130*, 16592–16600.
[92] M. A. Mahmoud, B. Garlyyev, M. A. El-sayed, *J. Phys. Chem. Lett.* **2014**, *5*, 4088–4094.
[93] A. M. El-Aziz, L. A. Kibler, D. M. Kolb, *Electrochem. Commun.* **2002**, *4*,

535–539.
[94] G. A. Attard, J. A. Bennett, I. Mikheenko, P. Jenkins, S. Guan, L. E. Macaskie, J. Wood, A. J. Wain, *Faraday Discuss.* **2013**, *162*, 57–75.
[95] J. F. Li, Y. F. Huang, Y. Ding, Z. L. Yang, S. B. Li, X. S. Zhou, F. R. Fan, W. Zhang, Z. Y. Zhou, D. Y. Wu, B. Ren, Z. L. Wang, Z. Q. Tian, *Nature* **2010**, *464*, 392–395.
[96] X. Li, M. Liu, J. Lee, D. Ding, L. A. Bottomley, S. Park, M. Liu, *Phys. Chem. Chem. Phys.* **2015**, *17*, 21112–21119.
[97] X. Li, J.-P. Lee, K. S. Blinn, D. Chen, S. Yoo, B. Kang, L. A. Bottomley, M. A. El-Sayed, S. Park, M. Liu, *Energy Environ. Sci.* **2014**, *7*, 306–310.
[98] A. V. Whitney, J. W. Elam, P. C. Stair, R. P. Van Duyne, *J. Phys. Chem. C* **2007**, *111*, 16827–16832.
[99] N. M. Kha, C.-H. Chen, W.-N. Su, J. Rick, B.-J. Hwang, *Phys. Chem. Chem. Phys.* **2015**, *17*, 21226–21235.
[100] Z. Rong, R. Xiao, C. Wang, D. Wang, S. Wang, *Langmuir* **2015**, *31*, 8129–8137.
[101] W. Xie, S. Schlu, *Nat. Comm* **2015**, *6*, 7570.
[102] S. Guan, O. Donovan-sheppard, C. Reece, D. J. Willock, A. J. Wain, G. A. Attard, *ACS Catal.* **2016**, *6*, 1822–1832.
[103] Z. W. Seh, S. Liu, S. Y. Zhang, M. S. Bharathi, H. Ramanarayan, M. Low, K. W. Shah, Y. W. Zhang, M. Y. Han, *Angew. Chem. Int. Ed.* **2011**, *50*, 10140–10143.
[104] X. D. Lin, V. Uzayisenga, J. F. Li, P. P. Fang, D. Y. Wu, B. Ren, Z. Q. Tian, *J. Raman Spectrosc.* **2012**, *43*, 40–45.
[105] X. Sun, Y. Li, *Langmuir* **2005**, *21*, 6019–6024.
[106] E. V. Formo, Z. Wu, S. M. Mahurin, S. Dai, *J. Phys. Chem. B* **2011**, *115*, 9068–9073.
[107] I. L. C. Buurmans, B. M. Weckhuysen, *Nat. Chem.* **2012**, *4*, 873–886.
[108] C. E. Harvey, E. M. van Schrojenstein Lantman, A. J. G. Mank, B. M. Weckhuysen, *Chem. Commun.* **2012**, *48*, 1742–1744.
[109] N. Kumar, S. Mignuzzi, W. Su, D. Roy, *EPJ Tech. Instrum.* **2015**, *2*, 1–23.
[110] K. F. Domke, B. Pettinger, *ChemPhysChem* **2009**, *10*, 1794–1798.
[111] P. Singh, T. Deckert-Gaudig, H. Schneidewind, K. Kirsch, E. M. van Schrojenstein Lantman, B. M. Weckhuysen, V. Deckert, *Phys. Chem. Chem. Phys.* **2015**, *17*, 2991–2995.
[112] M. Sun, Z. Zhang, H. Zheng, H. Xu, *Sci. Rep.* **2012**, *2*, 1–4.
[113] N. Kumar, B. Stephanidis, R. Zenobi, A. J. Wain, D. Roy, *Nanoscale* **2015**, *7*, 7133–7137.
[114] Z. Zhang, L. Chen, M. Sun, P. Ruan, H. Zheng, H. Xu, *Nanoscale* **2013**, *5*, 3249–3252.
[115] M. Chaigneau, G. Picardi, R. Ossikovski, *Surf. Sci.* **2010**, *604*, 701–705.
[116] T. Ichimura, S. Fujii, P. Verma, T. Yano, Y. Inouye, S. Kawata, *Phys. Rev. Lett.* **2009**, *102*, 186101.

[117] V. Poborchii, T. Tada, T. Kanayama, P. Geshev, *J. Raman Spectrosc.* **2009**, *40*, 1377–1385.
[118] Z. Yang, J. Aizpurua, H. Xu, *J. Raman Spectrosc.* **2009**, *40*, 1343–1348.
[119] P. G. Etchegoin, E. C. Le Ru, M. Meyer, *J. Am. Chem. Soc.* **2009**, *131*, 2713–2716.
[120] H. Shen, X. Zhou, N. Zou, P. Chen, *J. Phys. Chem. C* **2014**, *118*, 26902–26911.
[121] E. M. van Schrojenstein Lantman, O. L. J. Gijzeman, A. J. G. Mank, B. M. Weckhuysen, *ChemCatChem* **2014**, *6*, 3342–3346.
[122] S. Yampolsky, D. A. Fishman, S. Dey, E. Hulkko, M. Banik, E. O. Potma, V. A. Apkarian, *Nat. Photonics* **2014**, *8*, 650–656.
[123] E. A. Pozzi, M. D. Sonntag, N. Jiang, N. Chiang, T. Seideman, M. C. Hersam, R. P. Van Duyne, *J. Phys. Chem. Lett.* **2014**, *5*, 2657–2661.
[124] Y. Zhang, B. Walkenfort, J. H. Yoon, S. Schlücker, W. Xie, *Phys. Chem. Chem. Phys.* **2014**, *17*, 21120–21126.

2

Synthesis of Shell-Isolated Nanoparticles

The preparation of two types of shell-isolated nanoparticles (SHINs) is described in this chapter and they were tested for their Raman signal enhancing effectiveness. TiO_2- and SiO_2-coatings were grown over plasmonic Au cores by colloidal synthesis methods. The Raman signal enhancing effectiveness was tested using the dye molecule rhodamine 6G and their isolating properties using pyridine probe molecules. All coatings up to 3 nm thick were found to give sufficient signal enhancement (enhancement factors of larger than 10^4) for shell-isolated nanoparticle-enhanced Raman spectroscopy (SHINERS). However, coatings of less than 2 nm lost their Raman signal enhancing properties at elevated temperatures and were therefore deemed not applicable for implementation in heterogeneous catalysis.

2.1 Introduction

Shell-isolated nanoparticles (SHINs) with noble metal cores and metal oxide shells were recently invented for application as a non-invasive characterization technique as extension for surface-enhanced Raman spectroscopy (SERS).[1,2] The noble metal cores, typically Au and Ag nanoparticles (NPs), contain free surface electrons in the conduction band which can resonate with the frequency of electromagnetic radiation in the visible regime.[3] This process, which is referred to as localized surface plasmon resonance (LSPR), induces a very intense and localized electromagnetic field within a few nanometers of the surface of the metal core and can be applied for the enhancement of Raman scattering by a factor of 10^6.[4] To minimize interactions of the metal core with the analyte, SiO_2 coatings were synthesized over the Au or Ag nanostructures and this was then doped "shell-isolated nanoparticle-enhanced Raman spectroscopy", or SHINERS.[5]

These shell-isolated materials are promising for heterogeneous catalysis, as they are expected to be more thermally stable and inert during the study of reactions in comparison to uncoated, or bare, noble metal nanostructures.[6] The metal-oxide core protects the Au and Ag NPs from sintering at elevated temperatures and will reduce interferences from the plasmonic cores. Furthermore, the SHINs can mimic a metal oxide support material as found in conventional heterogeneous catalysis.[7]

In this chapter, we demonstrate the preparation of TiO_2- and SiO_2-SHINs using wet colloidal synthesis techniques. The optimal size of Au cores for the enhancement of Raman scattering with a 785 nm excitation wavelength was first investigated using Au NPs with controlled diameters between 30-100 nm. They were subsequently coated with 1-4 nm thick TiO_2 and SiO_2 shells to obtain SHINERS substrates with a Raman enhancement factor inversely proportional to the coating thickness. An optimal balance between thermal stability and signal enhancement was found for a coating thickness between 2-2.5 nm over Au cores of around 80 nm in size. These typical nanostructures are stable under oxidative treatments, such as heating in air up to 400 °C, and can therefore be used for exploitation in heterogeneous catalysis.

2.2 Results and Discussion

In order to study catalytic reactions with SHINERS, a substrate with optimal signal enhancement and stability is required. The first step is to find an optimal core size for enhancing Raman scattering under 785 nm wavelength laser illumination. A 785 nm laser as excitation source, in combination with Au NPs, is used to limit potential plasmonic side reactions.[8–10] Au NPs of various sizes were prepared between approximately 40 and 100 nm using a seed-mediated growth to realize a satisfying control over the Au particle size and were analyzed with transmission electron microscopy (TEM).[11–13] Small Au seeds of 16 nm were first prepared according to the Turkevich method, by reducing $HAuCl_4$ with sodium citrate in water at 100 °C

(Figure 2.1a$_1$).[11,14] These small Au NPs served then as seeds for the reduction of Au^{3+} over the Au surfaces using $NH_2OH{\cdot}HCl$ as reducing agent at room temperature. The final Au NPs were controlled in sizes up to 104 nm, depending on the amount of seeds. An example of 104 nm Au NPs can be found in Figure 2.1a$_2$. The Au cores were then coated with ultrathin TiO_2 and SiO_2 shells in a controlled manner. A new method, that was based on two existing literature examples,[15,16] was developed for the growth of controlled TiO_2 shell materials (Figure 2.1b). At room temperature, titanium(IV) (triethanolaminato) isopropoxide was hydrolyzed in a 2-propanol/water mixture to obtain TiO_2 coatings between 1-4 nm. A controlled growth of the TiO_2 was obtained as a result of the chelating TiO_2 precursor. SiO_2 coatings were produced according to a recent example and relied on the slow hydrolysis of sodium silica in water at around pH 10 (Figure 2.1c).[1,17] The complete synthesis protocol can be found in the experimental section.

All samples were analyzed with UV-Vis spectroscopy (Figure 2.2) to examine the quality of the colloidal solution. Well-dispersed colloidal Au NPs exhibit a localized surface plasmon resonance (LSPR) between 530-600 nm, that decreases in energy with increasing size (Figure 2.2a). After the growth of a coating, the LSPR can red-shift with increasing coating thickness, and is related to the increase in the dielectric constant from TiO_2 in comparison to water (Figure 2.2b).[18–20] When aggregation occurs, the LSPR of two or more Au NPs can couple, which results in the observation of additional bands.

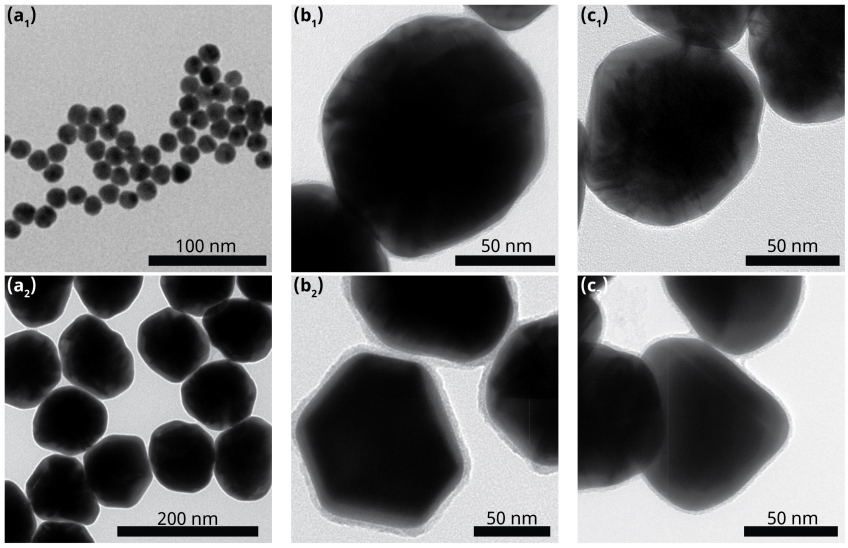

Figure 2.1. Transmission electron microscopy (TEM) images of Au NPs and SHINs. (a$_1$) 17 nm Au seeds; **(a$_2$)** 104 nm Au NPs; **(b$_1$)** 104 nm Au core with 1.5 nm TiO_2 coating ; **(b$_2$)** 104 nm Au core with 4.1 nm TiO_2 shell; **(c$_1$)** 76 nm Au core with 1.2 nm SiO_2 shell; **(c$_2$)** 76 nm Au core with 3.3 nm SiO_2 shell.

Due to the low stability of Au NPs in water-isopropanol mixtures, a shoulder or peak between 700-800 nm was sometimes observed for samples with very thin TiO_2 coatings. This effect becomes even more pronounced when the particles are dried on a Si wafer before SHINERS experiments. Aggregated Au NPs after drying show a broad band extinction up to the infrared regime (Figure 2.2d). The aggregated state of the Au NPs after the drying step is necessary for SERS and SHINERS to enhance the Raman signal when using a 785 nm laser. Without aggregation - to be more precise: without close contact of the plasmonic cores - there is no enhancement of the Raman signal observed.[21]

The effectiveness of Au and Au@TiO_2 NPs for SERS and SHINERS was evaluated by measuring the Raman signal intensity of the xanthene ring stretch of Rh6G aqueous solutions at 1362 cm^{-1}.[22] The dye molecule Rh6G is a prototype molecule for testing SERS substrates. Due to its inherent large Raman scattering cross-section it is often used to compare effectiveness of SERS substrates. The dye molecule has been used for single molecule experiments due to its resonance at 528 nm, however, in this work, Rh6G is not in resonance with the applied 785 nm laser.[22]

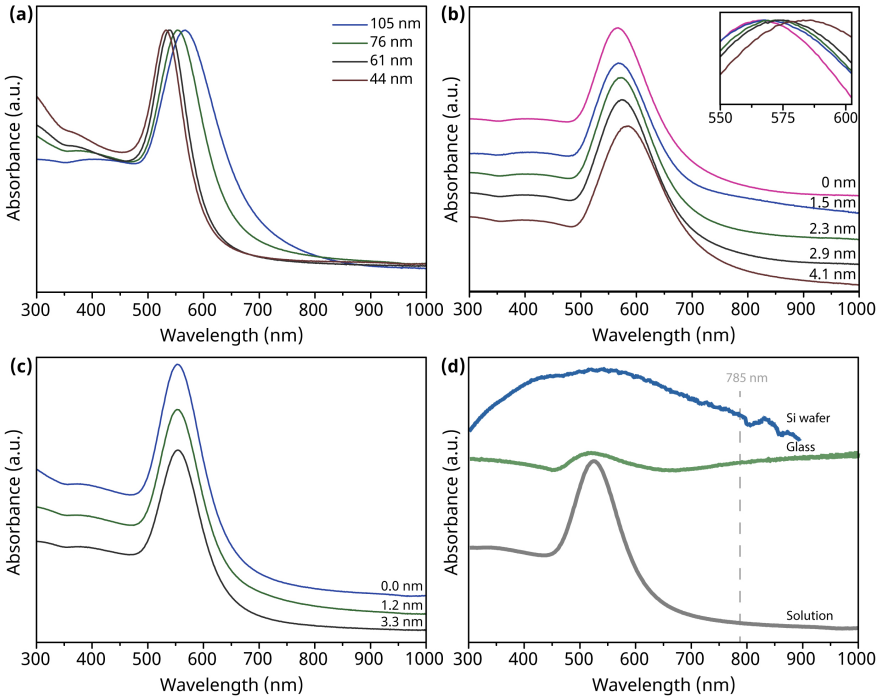

Figure 2.2. UV-Vis spectra of Au, Au@SiO_2- and Au@TiO_2-NPs. (a) UV-Vis spectra of Au NPs of various sizes, from left to right: 44, 61, 76, 105 nm. **(b)** UV-Vis spectra of Au@TiO_2 NPs with a 76 nm Au core and a controlled coating thickness. The inset shows a zoom-in of the peak locations **(c)** UV-Vis spectra of Au@SiO_2 NPs with a 76 nm Au core and a controlled coating thickness. **(d)** UV-Vis spectra of Au NPs in solution and after drying on glass and silicon wafers.

By measuring aqueous solutions, the analyte is dispersed homogeneously over the S(HIN)ERS substrates without drying effects that might lead to local concentration variations. As a result of the heterogeneous nature of the drop-casted S(HIN)ERS substrates, the Raman signal intensity might fluctuate between different spots in the sample. Therefore, 40 random point scans were measured for each sample of which the 20 most intense signals were averaged, as can be seen in Figure 2.3a for bare Au NPs. Without S(HIN)ERS substrates, it was impossible to measure a Raman spectrum of aqueous Rh6G (0.1mM) as shown in Figure 2.3a. The analytical enhancement factor (AEF) was therefore estimated by comparing the S(HIN)ERS signal to the Raman spectrum of solid Rh6G (Figure 2.3a). When comparing the signal intensity at 1362 cm^{-1} between SERS samples we found an optimal plasmon core size between 70-90 nm with estimated AEFs between 10^4-10^5 for TiO_2-coated NPs (Figure 2.3a,b); calculations can be found in the experimental section.[23] All Au NPs were coated with various TiO_2 coating thicknesses. As expected, the intensity of the 1362 cm^{-1} band decreases drastically with increasing TiO_2-coating thickness; examples of SHINER spectra of Rh6G over 76 nm Au core with various TiO_2 coatings are depicted in Figure 2.3c.

When comparing the relative intensity of all the Au cores with various TiO_2 coating thicknesses (Figure 2.3d) it was observed that the shell thickness can be increased for larger plasmonic cores, while preserving sufficient electromagnetic enhancement. Larger Au cores still enhance the Raman signal with coatings up to 4 nm, whereas smaller cores already lose complete Raman signal under the current measurement conditions with thinner coatings below 3 nm. This so-called probing distance found here is similar to what has been observed by Kumari *et al.*[24] on Ag@SiO_2 substrates; the probing distance improves with increasing particle size (Figure 2.3d is based on averaged spectra of all the different substrates). Also in our own work on Au@SiO_2, we find the same dependency of SHINERS signal intensity on the coating thickness (Figure 2.3e).

The uniformity of the metal oxide shells is important during catalysis as it isolates the Au core from sintering and any undesired side reactions. The shell can be tested for any pin holes by measuring the Raman signal of aqueous pyridine (10 mM) over SHINERS substrates.[1] Pyridine adsorbed to nanostructured Au will result in a very intense signal at 1008 and 1036 cm^{-1} originating from two ring breathing modes[25] due to the local enhancement at the surface and the strong affinity of pyridine to Au (Figure 2.3f). When a shell insufficiently covers the Au core, pyridine molecules can adsorb to the metal surface. As a result, the pyridine can now be observed using SERS, whereas for completely isolated Au cores, the signal is too weak to be observed because of the weak adsorption of pyridine to the metal oxides.

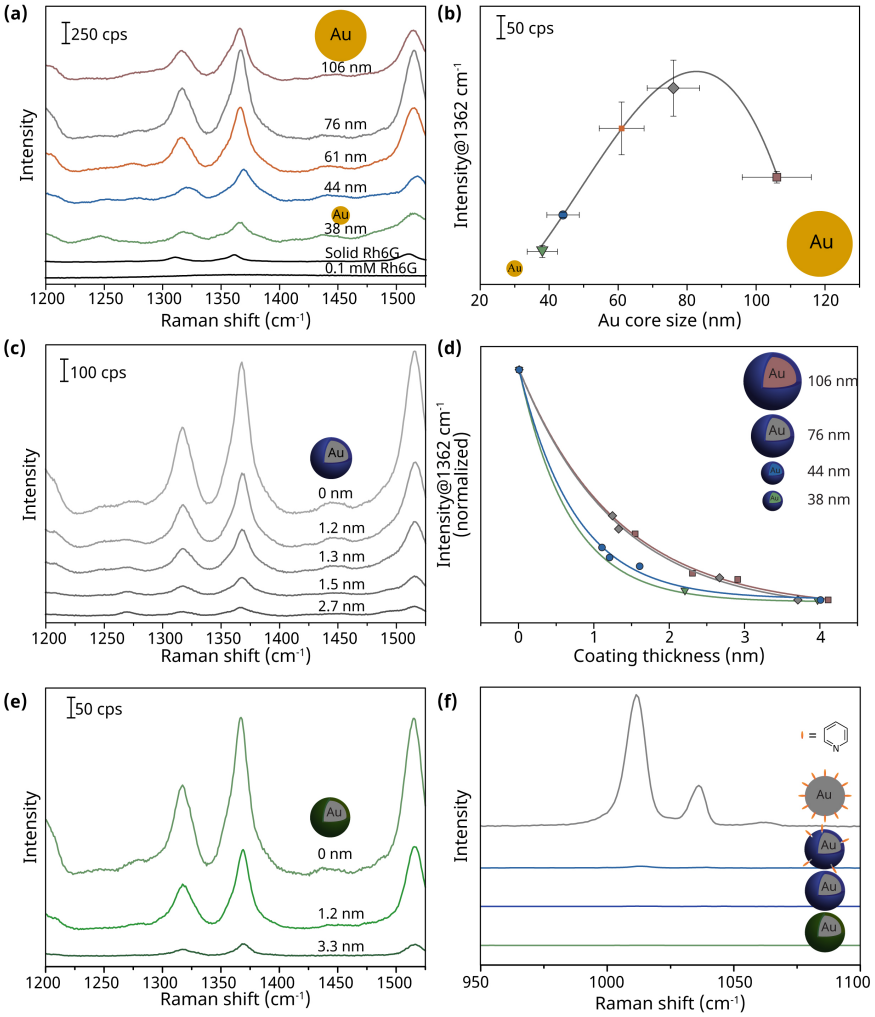

Figure 2.3. SERS and SHINERS signal enhancement tests. (a) SER spectra of 0.1 mM aqueous Rh6G over Au NPs SERS substrates sized between 38 and 106 compared with aqueous Rh6G and solid Rh6G without SERS enhancement; **(b)** The averaged intensity of the Rh6G band at 1362 cm^{-1} for various Au NP sizes between 38 and 106 nm; **(c)** The average SHINER spectra of Rh6G over 76 nm Au NPs with controlled TiO_2 coating; **(d)** The average intensity of the 1362 cm^{-1} band for various Au NP sizes with controlled TiO_2 thickness normalized to its value for uncoated Au NPs. **(e)** The average SHINER spectra of Rh6G over 76 nm Au NPs with controlled SiO_2 coating. **(f)** SHINER spectra of the pyridine adsorption test for pin holes in the oxide coatings (λ= 785 nm; P= $2.0 \cdot 10^5$ $W \cdot cm^{-2}$)

For SHINERS to be viable in heterogeneous catalysis, the substrates need to be stable at elevated temperatures. Unstable substrates will result in signal loss due to sintering, or worse: additional Raman scattering signals due to accessible gold surfaces. In order to verify the stability, Au, Au@TiO_2 and Au@SiO_2 NPs were put to the test by exposing them to 300, 400 and 500 °C in air for 3h. Under the

optical microscope, the benefits of SHINs for improved thermal stability are clearly visible. Without metal oxide coatings, Au NPs sintered on the Si wafer, forming large bulk structures (Figure 2.4a). The SHINs on the other hand, remained stable and kept their appearance (Figure 2.4b and c). In the SHINER spectra, chemical changes were observed for the three different substrates. Au NPs lost all features, except for the broad features at 1350 and 1600 cm^{-1}, which are typical for carbon species. For Au@TiO_2, a broad band at 700 cm^{-1} intensifies strongly when subjected to heat treatments above 300 °C and another peak is observed at 800 cm^{-1} above 400 °C (Figure 2.4e).[26] It has been suggested that the phase transition temperature of amorphous TiO_2 to anatase is around 400 °C, but that this shifts to around 500 °C when heating amorphous NPs.[27] Beyond 300 °C the TiO_2-coating starts to densify and crystallize[27] and around 500 °C it definitely cracks open which allows the Au cores to sinter. The amorphous SiO_2 coating also changes structure with temperatures above 300 °C, as can be observed by the growth of D_1, D_2 and Si-OH stretching vibrations at respectively 480, 800 and 990 cm^{-1} in the Raman spectra of Au@SiO_2 after heat treatments (Figure 2.4f).[28,29]

The stability for Raman signal enhancement was tested by comparing the signal intensity of aqueous Rh6G at 1362 cm^{-1} before and after the heat treatments. Using this method, samples can be tested and compared rapidly. Furthermore, by performing the stability tests *ex situ* with aqueous Rh6G, we can rule out any effects of thermal wandering or decomposition of the analyte during *in situ* measurements. It was observed that for many samples under study, the Rh6G signal drops to lower intensities after thermal treatment. The results are summarized in Figure 2.5.

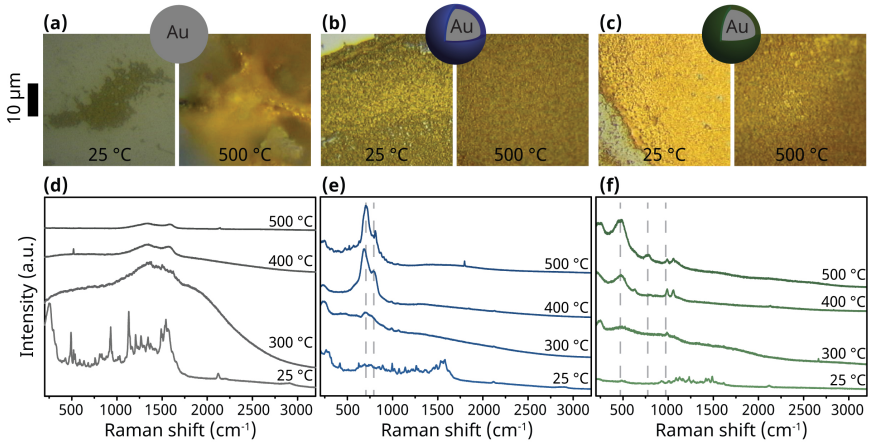

Figure 2.4. Substrate inspection after thermal treatments using optical microscopy and SHINERS. **(a)** Bare Au NPs before and after thermal treatment at 500 °C in air. **(b)** Au@TiO_2 NPs before and after thermal treatment at 500 °C in air. **(c)** Au@SiO_2 NPs before and after thermal treatment at 500 °C in air. **(d)** SHINER spectra of Au NPs before and after thermal treatment at 300, 400 and 500 °C. SHINER spectra of Au NPs before and after thermal treatment at 300, 400 and 500 °. **(e)** SHINER spectra of Au@TiO_2 NPs before and after thermal treatment at 300, 400 and 500 °C. The dotted lines are placed at 700 cm^{-1} and 800 cm^{-1}. **(f)** SHINER spectra of Au@SiO_2 NPs before and after thermal treatment at 300, 400 and 500 °C. The dotted lines are placed at 480, 800 and 990 cm^{-1}.

For both type of dielectric coating materials, the Raman signal intensity does not remain stable above 300 °C when a coating is thinner than 2 nm and starting from 500 °C, all substrates are completely changed in morphology as is observed in the extremely low Rh6G signal (Figure 2.5a and c) and the strongly improved pyridine/Rh6G ratio (Figure 2.5b and d). Due to the densification of the coatings, it is recommended to stay below 400 °C when using SiO_2- and TiO_2-SHINS.

Over Au@TiO_2 substrates with coatings thinner than 3 nm, a very weak Raman signal of pyridine could sometimes be detected (Figure 2.5b). The pyridine signal was, however, at least a factor 10^2 weaker in comparison to uncoated Au NP. For this reason, the pyridine/Rh6G ratio was used to compare between samples, so that the signal enhancement of the substrate was compensated for.

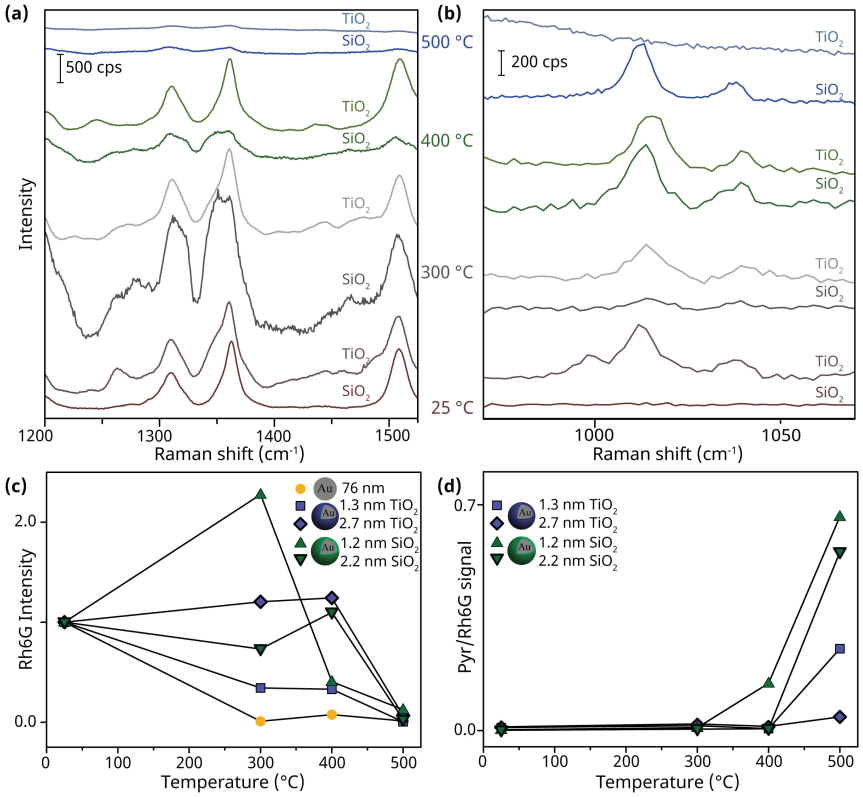

Figure 2.5. Thermal stability tests of SHINs and Au NPs. (a) SHINER spectra of Rh6G over Au@SiO_2 and Au@TiO_2 before and after thermal treatment for 3h at the specified temperatures. **(b)** SHINER spectra of pyridine over the same Au@SiO_2 and Au@TiO_2 substrates after the thermal treatments. **(c)** The Rh6G 1362 cm^{-1} peaks were compared with their initial value after the heat treatments. **(d)** The intensity of pyridine at 1008 cm^{-1} was related to the Rh6G intensity at 1364 cm^{-1} to test the uniformity of the coating. (λ= 785 nm; P= $2.0 \cdot 10^5$ W·cm^{-2})

The thermal stability of Au@TiO_2 and Au@SiO_2 NPs can be related to the thickness of the dielectric coating. A completely pin hole free coating was not obtained for coatings under 3 nm. However, the pyridine signal intensity was very low and coatings were found to be stable with a minimum of 2 nm coating (Figure 2.5c and d).

SiO_2 coatings could be grown extremely thin, with a minimum of 1.2 nm without pin holes (Figure 2.3f). However, these thin coatings proved to be unstable above 300 °C, whereas 2.2 nm coatings did remain stable up to 400 °C (Figure 2.5c and d). TiO_2-coating starts to densify and crystallize[27] above 300 °C, and around 500 °C it definitely cracks open which allows the Au cores to sinter. At 500 °C, all substrates are completely changed in structure as is observed in the extremely low Rh6G signal and the strongly improved pyridine/Rh6G ratio (Figure 2.5d). Due to the densification of the coatings, it is recommended to stay below 400 °C when using SiO_2- and TiO_2-SHINS.

So far, we have not been able to produce SHINERS substrates that are stable in air at 500 °C. Only a small fraction of the substrates remains plasmonically active for SERS, as can be seen by the relative ratio of pyridine to Rh6G Raman signal intensity. However, we expect that new shell materials have to be implemented to gain better thermal stabilities.

2.3 Conclusions

In this chapter we have demonstrated the synthesis of thermally stable Au@SiO_2 and Au@TiO_2 shell-isolated nanoparticles and their application for shell-isolated nanoparticle-enhanced Raman spectroscopy (SHINERS). By carefully controlling the Au core size with a seeded growth method, the optimum size Raman signal enhancement was found to be around 80 nm with an enhancement factor of over 10^5. Furthermore, an optimal coating thickness between 2 and 2.5 nm was prepared by controlling the reaction conditions during the hydrolysis of SiO_2 and TiO_2 precursors. Au@TiO_2 and Au@SiO_2 NPs with coatings of at least 2 nm were able to enhance Raman signals by a factor of at least 10^4, even after a heat treatment up to 400 °C. The simple synthesis procedure requires basic laboratory equipment and can therefore be applied in a wide variety of laboratories. They will be implemented for the study of solid metal catalysts in the coming chapters.

2.4 Experimental Section

Chemicals. The following chemicals were purchased and used as received: (3-aminopropyl)trimethoxysilane (APTMS, 97%), sodium silicate solution (27% SiO_2 in 14% NaOH), titanium(IV) (triethanoloaminato) isopropoxide solution (TTEAIP, 80 wt.% in isopropanol), Rhodamine 6G, hydroxylamine hydrochloride (>98%) from Sigma Aldrich; ammonia solution (28-30%) from VWR

International; $HAuCl_4 \cdot 3H_2O$ (99.99% metals basis) from Alfa Aesar; trisodium citrate dihydrate (99%) from Acros Organics; 2-propanol (CHROMASOLV™ LC-MS >99%) from Honeywell; Hydrochloric acid (Emsure, 37%) from Merck. Demineralized water was purified with a Milli-Q (mQ) system (18.2 MΩ) before use.

Preparation of Au seeds. 30 mL of ultra-pure mQ water and 300 μL of 1% (W/V) aqueous $HAuCl_4$ was added to a 250 mL round bottom flask with a clean stirring bar. The solution was rapidly brought to a boil in a preheated oil bath, while stirring at 1000 rpm. As soon as the solution started boiling, 0.9 mL of 1% (W/V) aqueous trisodium citrate solution was added. The flask was removed from heat after 10 min, once nanoparticle maturation was complete as indicated by the color transition from light yellow to ruby red.[13]

Preparation of 80-90 nm Au NPs. 1.0 mL of the colloidal seeds solution was added to 112 mL mQ water and 2.0 mL 1% (W/V) trisodium citrate was added. Au NPs were grown carefully by adding dropwise 2.8 mL aqueous $NH_2OH \cdot HCl$ (10 mM) and 1 % (W/V) $HAuCl_4$ over 30 min. The volume of the droplets was estimated to be around 10 μL. After fully growing the particles, the solution was left stirring for an additional 10 min.[1] The size of the final Au NPs was controlled by varying the volume of seed solution added.

1-3 nm SiO_2 coating. 0.4 mL of a 1.0 mM solution of aqueous (3-aminopropyl)trimethoxysilane (APTMS) was added dropwise to a 15 mL colloidal solution of Au NPs and stirred for 20 min. Subsequently, 1.0-1.6 mL of an aqueous sodium silicate solution (diluted to 0.54 wt.% with mQ water and adjusted to pH 10.6-10.8 with HCl) was added dropwise under vigorous stirring at 2000 rpm. The flask was placed in an aluminium starfish at 90 °C and stirred for 30-90 min depending on the required coating thickness. After synthesis, the particles were centrifuged and washed 3 times in mQ water and finally stored in 5 mL mQ water in the fridge at 4 °C.[17]

1-4 nm TiO_2-coating. 10 mL colloidal Au particles were concentrated to 1 mL after centrifugation and subsequently mixed with 3 mL isopropanol. While stirring at 2000 rpm, 80 μL aqueous APTMS (1.1 mM) was added. After 10 min, 50-200 μL TTEAIP (2.5 mM in isopropanol) was added dropwise, depending on the desired coating thickness. 1 h later, 50 μL of a solution containing ammonia (28-30%) was added and stirred overnight to prepare a shell of 1-4 nm. After synthesis, the NPs were centrifuged and washed 2 times in isopropanol and 2 times in mQ water.[15,16]

SERS and SHINERS sample preparation. 10 μL of a colloidal solution was drop-casted on a Si wafer and dried under vacuum in a desiccator for 30 min. Raman intensity tests were performed by drop-casting aqueous rhodamine 6G (0.1 mM) solutions over the drop-casted substrates and were covered with a glass cover-sheet to prevent evaporation of the solvent. Pin hole tests were performed by drop-castings aqueous pyridine (10 mM) solutions over the drop-casted substrates and were covered with a glass cover-sheet to prevent evaporation of the solvent. The

thermal stability of the substrates was tested by measuring before and after thermal treatment at 300 and 400 °C (5 °C/min) under air for 3 h.

Characterization. UV-Vis spectra were obtained using a Varian Cary 50 UV-Vis Spectrophotometer in the range of 250-1000 nm and a Craic UV-Vis microscope. Transmission electron microscopy (TEM) images were recorded using a FEI tecnai 12 Icor TEM operating at 120 kV. Samples were prepared by drop-casting a colloidal solution on a carbon-coated TEM grid, which were left to dry in air. Scanning transmission electron microscopy-energy dispersive X-ray analysis (STEM-EDX) images were obtained on a FEI Talos F200X electron microscope operating at 200 kV. Raman spectroscopy measurements were performed on a Renishaw InVia Raman microscope, using 785 nm diode laser excitation through a 50x objective (0.9 NA). *Ex situ* experiments were all performed under 0.24 mW (i.e., $1.12 \cdot 10^5$ W·cm^{-2}), with an integration time of 10 s. All spectra are shown as obtained: no smoothing, background correction, or baseline subtraction.

Enhancement factor. To express the effectiveness of SERS and SHINERS substrates, the enhancement factor (EF) is often used. Here we used the analytical enhancement factor (AEF) as described by Le Ru *et al.*[23], which gives a good indication of the signal to expect. To calculate the AEF, we have compared the Raman signal intensity of dry Rhodamine 6G (Rh6G) with that of the Raman signal intensity obtained from 0.1 mM of an aqueous solution of Rh6G over a SERS/SHINERS substrate under identical experimental conditions. Following the description in the work by Le Ru *et al.* we assumed that the probed volume was identical and ignored the fact that SERS is a surface-sensitive technique. The equation is as follows:

$$AEF = \frac{I_{SERS}/C_{SERS}}{I_{RS}/C_{RS}} \tag{2.1}$$

With: $C_{SERS} = 10^{-7} mol/cm^3$

And $C_{RS} = 1.26 \frac{g}{cm^3} / 479.02\ g/mol$

For example, when we calculate the AEF of a Au@TiO$_2$ sample with a core size of 76 nm and a coating thickness of 2.6 nm, which has a signal intensity of 17,380 counts at 1360 cm^{-1}, compared to dry Rh6G with a signal intensity of 6,795 counts we obtain:

$$AEF = 7 \cdot 10^4 = \frac{17{,}830/10^{-7}}{6{,}795/1.26\ /479.02} \tag{2.2}$$

Over Au NPs with a core size of 76 nm with a signal intensity of 72,911 we obtain AEF = $2.8 \cdot 10^5$.

2.5 Author Contributions and Acknowledgements

This chapter is based on the manuscript: Thermally Stable TiO_2- and SiO_2-Shell-Isolated Au Nanoparticles for In Situ Plasmon-Enhanced Raman Spectroscopy of Hydrogenation Catalysts, T. Hartman, B. M. Weckhuysen, *Chem. Eur. J.* **2018**, *24*, 3733–3741.

Bert Weckhuysen and Thomas Hartman conceived the research plans. Thomas Hartman executed the experimental work under supervision of Bert Weckhuysen. The manuscript was written by Thomas Hartman with feedback and corrections by Bert Weckhuysen.

The following people are furthermore gratefully acknowledged for their contributions: Hans Meeldijk and Wouter Lamme, both from Utrecht University (UU) for their contributions with the TEM-EDX measurements. Katinka Wondergem (UU) is thanked for her valuable input on the experimental and written work.

2.6 References

[1] J. F. Li, Y. F. Huang, Y. Ding, Z. L. Yang, S. B. Li, X. S. Zhou, F. R. Fan, W. Zhang, Z. Y. Zhou, D. Y. Wu, B. Ren, Z. L. Wang, Z. Q. Tian, *Nature* **2010**, *464*, 392–395.

[2] S.-Y. Ding, J. Yi, J.-F. Li, B. Ren, D.-Y. Wu, R. Panneerselvam, Z.-Q. Tian, *Nat. Rev. Mater.* **2016**, *1*, 16021.

[3] E. Petryayeva, U. J. Krull, *Anal. Chim. Acta* **2011**, *706*, 8–24.

[4] S. Schlücker, *Angew. Chem. Int. Ed.* **2014**, *53*, 4756–4795.

[5] J.-F. Li, Y.-J. Zhang, S.-Y. Ding, R. Panneerselvam, Z.-Q. Tian, *Chem. Rev.* **2017**, *117*, 5002–5069.

[6] A. V. Whitney, J. W. Elam, P. C. Stair, R. P. Van Duyne, *J. Phys. Chem. C* **2007**, *111*, 16827–16832.

[7] T. Hartman, C. S. Wondergem, N. Kumar, A. Van Den Berg, B. M. Weckhuysen, *J. Phys. Chem. Lett.* **2016**, *7*, 1570–1584.

[8] E. M. van Schrojenstein Lantman, T. Deckert-Gaudig, A. J. G. Mank, V. Deckert, B. M. Weckhuysen, *Nat. Nanotechnol.* **2012**, *7*, 583–586.

[9] S. K. Cushing, N. Wu, *J. Phys. Chem. Lett.* **2016**, *7*, 666–675.

[10] C. E. Harvey, B. M. Weckhuysen, *Catal. Lett.* **2014**, *145*, 40–57.

[11] B. V. Enüstün, J. Turkevich, *J. Am. Chem. Soc.* **1963**, *85*, 3317–3328.

[12] G. Frens, *Nat. Phys. Sci.* **1973**, *241*, 20–22.

[13] W. Haiss, N. T. K. Thanh, J. Aveyard, D. G. Fernig, *Anal. Chem.* **2007**, *79*, 4215–4221.

[14] J. Kimling, M. Maier, B. Okenve, V. Kotaidis, H. Ballot, A. Plech, *J. Phys. Chem. B* **2006**, *110*, 15700–15707.

[15] Z. W. Seh, S. Liu, S. Y. Zhang, M. S. Bharathi, H. Ramanarayan, M. Low, K. W. Shah, Y. W. Zhang, M. Y. Han, *Angew. Chem. Int. Ed.* **2011**, *50*, 10140–10143.

[16] N. Zhou, L. Polavarapu, N. Gao, Y. Pan, P. Yuan, Q. Xu, *Nanoscale* **2013**, *5*, 4236–4241.

[17] J. F. Li, X. D. Tian, S. B. Li, J. R. Anema, Z. L. Yang, Y. Ding, Y. F. Wu, Y. M. Zeng, Q. Z. Chen, B. Ren, Z. L. Wang, Z. Q. Tian, *Nat. Protoc.* **2013**, *8*, 52–65.
[18] K. L. Kelly, E. Coronado, L. L. Zhao, G. C. Schatz, *J. Phys. Chem. B* **2003**, *107*, 668–677.
[19] W.-L. Liu, F.-C. Lin, Y.-C. Yang, C.-H. Huang, S. Gwo, M. H. Huang, J.-S. Huang, *Nanoscale* **2013**, *5*, 7953–7962.
[20] S. Mubeen, S. Zhang, N. Kim, S. Lee, S. Kramer, H. Xu, *Nano Lett.* **2012**, *12*, 2088–2094.
[21] Y. Zhang, B. Walkenfort, J. H. Yoon, S. Schlücker, W. Xie, *Phys. Chem. Chem. Phys.* **2014**, *17*, 21120–21126.
[22] L. Jensen, G. C. Schatz, *J. Phys. Chem. A* **2006**, *110*, 5973–5977.
[23] E. C. Le Ru, E. Blackie, M. Meyer, P. G. Etchegoin, *J. Phys. Chem. C* **2007**, *111*, 13794–13803.
[24] G. Kumari, J. Kandula, C. Narayana, *J. Phys. Chem. C* **2015**, *119*, 20057–20064.
[25] C. Zuo, P. W. Jagodzinski, *J. Phys. Chem. B* **2005**, *109*, 1788–1793.
[26] S. Degioanni, A. M. Jurdyc, F. Bessueille, J. Coulm, B. Champagnon, D. Vouagner, *J. Appl. Phys.* **2013**, *114*, 234307.
[27] O. Khatim, M. Amamra, K. Chhor, A. M. T. Bell, D. Novikov, D. Vrel, A. Kanaev, *Chem. Phys. Lett.* **2013**, *558*, 53–56.
[28] S. Degioanni, A. M. Jurdyc, A. Cheap, B. Champagnon, F. Bessueille, J. Coulm, L. Bois, D. Vouagner, *J. Appl. Phys.* **2015**, *118*, 153103.
[29] A. Perriot, D. Vandembroucq, E. Barthel, V. Martinez, L. Grosvalet, C. H. Martinet, B. Champagnon, *J. Am. Ceram. Soc.* **2006**, *89*, 596–601.

3

In Situ SHINERS for Catalysis

Raman spectroscopy is known as a powerful technique for solid catalyst characterization as it provides vibrational fingerprints of (metal) oxides, reactants and products. It can become even a strong surface-sensitive technique by implementing shell-isolated nanoparticle-enhanced Raman spectroscopy (SHINERS). Au@TiO_2 and Au@SiO_2 shell-isolated nanoparticles, prepared in Chapter 2, were therefore used as support materials for a variety of hydrogenation catalysts (Pt, Pd, Rh, Ru), so that they can be used as a tool for SHINERS to study surface reactions over heterogeneous catalysts, including the influence of support material. Both SiO_2- and TiO_2-SHINs were found to effectively enhance the Raman signal intensity under the applied reactions conditions for CO hydrogenation. The signal enhancing properties remained stable under reaction conditions (i.e. temperatures higher than 200 °C under CO/H_2 atmosphere for 8h) and the differences between Ru/Au@TiO_2 and Ru/Au@SiO_2 could be explored. With SHINERS, we observed that Ru supported on Au@TiO_2 was more reactive than Ru supported on Au@SiO_2 in the CO hydrogenation reaction. The work shown in this chapter, demonstrates that SHINERS can be effectively applied to study heterogeneous catalysts *in situ*.

3.1 Introduction

In situ characterization techniques are important for understanding the working principles and deactivation mechanisms of solid catalysts.[1–3] *Ex situ* knowledge is often insufficient, because the surface structure and chemical composition of heterogeneous catalysts are influenced by the reaction environment, as induced by temperature, pressure and gas composition.[4,5]

Spectroscopic techniques, such as Raman spectroscopy, are valuable tools to understand (bulk) catalyst structures and catalyst-reactant interactions by diagnostic analysis of vibrational fingerprints.[6,7] The technique can be easily applied to characterize solid catalysts under working conditions, including the liquid-phase.[8,9] However, Raman spectroscopy intrinsically suffers from low signal intensities due to the low Raman cross-sections and is therefore not always optimally equipped for detecting surface reactions.[10]

A technique that can significantly boost the Raman signal intensity is surface-enhanced Raman spectroscopy (SERS).[11,12] The foundation for SERS relies on noble metal nanostructures with plasmonic properties.[13–15] Plasmonic nanostructures prepared from Ag, Au and Cu generate strong localized electromagnetic fields at the surface under illumination with visible light.[16,17] Such local enhancement can drastically increase the detection limit of Raman spectroscopy, reaching even single-molecule sensitivity under optimal conditions.[18] Additionally, due to the highly localized surface sensitivity, it can be used to observe possible intermediate structures during reactions.[19,20]

To improve the applicability as a universal surface characterization technique, shell-isolated nanoparticle-enhanced Raman spectroscopy (SHINERS) was recently developed.[21] By coating gold or silver cores with SiO_2, the plasmonic core is passivated so that virtually any substrate can be characterized with this technique.[22–24] For example, shell-isolated nanoparticles (SHINs) can be assembled over catalytically active single-crystal surfaces to investigate structure-sensitive reactions.[25] Additionally, oxide coatings provide improved thermal stability and inertness. These features, combined with the possibility to anchor solid catalysts to the surface, make SHINERS an interesting characterization technique for heterogeneous catalysis research.[26] An important step forward in the development of SHINERS in catalysis was recently realized by Tian *et al.* by demonstrating SHINs as a universal support material and nano-antenna for various solid catalyst nanoparticles.[27] In a follow-up study, they proved that with SHINERS, the type of coating material has an evident effect on the behavior of solid catalysts.[28]

In this chapter, we present a relatively facile colloidal method to prepare metal/Au@TiO_2 and metal/Au@SiO_2 shell-isolated nanoparticles (SHINs) and illustrate their potential in the field of heterogeneous catalysis. Both SiO_2 and TiO_2 metal oxide shells prepared in Chapter 2 provided stable SHINERS substrates that

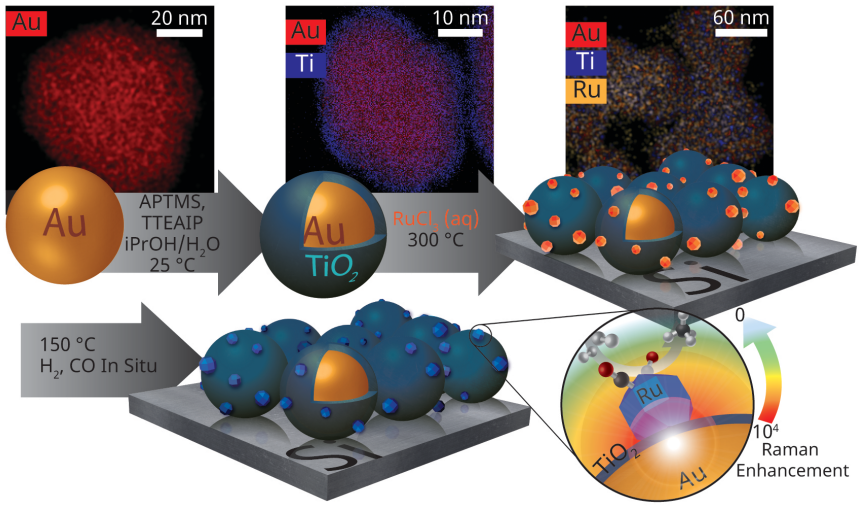

Figure 3.1. Schematic illustration of the synthesis steps involved in the preparation of TiO_2-SHINs. **(Top)** Element maps of the intermediate steps of Au NPs, Au@TiO_2 and oxidized Ru/Au@TiO_2 as obtained with STEM-EDX (Scanning transmission electron microscopy-energy dispersive X-ray analysis). **(Middle)** Schematic of the various steps involved in the synthesis of Ru/Au@TiO_2, and **(Bottom)** Schematic of the SHINERS principle of Ru/Au@TiO_2 during CO hydrogenation at elevated temperatures. The following chemical compounds are used for the synthesis: iPrOH = 2-propanol, APTMS = (3-aminopropyl)trimethoxysilane and TTEAIP = titanium(IV) (triethanolaminato)isopropoxide.

can withstand temperatures up to 400 °C in air without losing Raman signal intensity enhancement. The Au@TiO_2 and Au@SiO_2 SHINs were therefore used as support material for the preparation of Ru and Rh hydrogenation catalysts in this chapter. The obtained Ru/SHINs and Rh/SHINs were implemented to study the effect of catalyst material and shell material on CO hydrogenation. In other words, we have designed local sensor materials enabling the qualitative probing of catalytic CO hydrogenation by making use of the SHINERS principle and transition metals as active hydrogenation catalysts. A visual interpretation of the aim of the work described in this chapter is illustrated in Figure 3.1.

3.2 Results and Discussion

In the previous chapter, it was revealed by SHINERS studies that Au cores were stabilized by the isolating TiO_2 and SiO_2 coatings, even after being subject to 400 °C in air. The Raman signal enhancing effectiveness remained intact with enhancement factors (EF) of at least 10^4. SERS and SHINERS are surface-sensitive characterization techniques,[15] meaning that the highest signal will be obtained at the surface of the isolating shell. This makes SHINERS an interesting method for the study of various metal-support interactions. We therefore introduced hydrogenation catalysts to the best TiO_2- and SiO_2-based SHINs in terms of both overall stability and Raman signal intensity: 76 nm Au NPs with 2.6 nm TiO_2 and

2.2 nm SiO_2 coating. Using these two different substrate materials, we were interested to implement SHINERS for studying the effect of catalyst and support material on the catalytic hydrogenation of CO over active metals.

First, two different catalysts were prepared through wet-impregnation: Ru/Au@SiO_2 and Ru/Au@TiO_2. They were prepared by mixing an aqueous solutions $RuCl_3$ with the colloidal solution and subsequently dried on a Si wafer. After UV-Ozone treatment and a gentle calcination step, the $RuCl_3$ was oxidized, resulting in RuO_2/Au@SiO_2 and RuO_2/Au@TiO_2 SHINs. Before catalysis, the metal precursors were activated in H_2 at temperatures between 150-250 °C. In Figure 3.2, TEM and STEM-EDX images are shown of Ru NPs deposited on the Au@TiO_2 and Au@SiO_2 SHINS after reduction in H_2 at 150 °C.

Using SHINERS, we were able to follow the preparation of Ru catalysts *in situ*, while supported on Au@TiO_2, Au@SiO_2, and Stöber SiO_2 (respectively

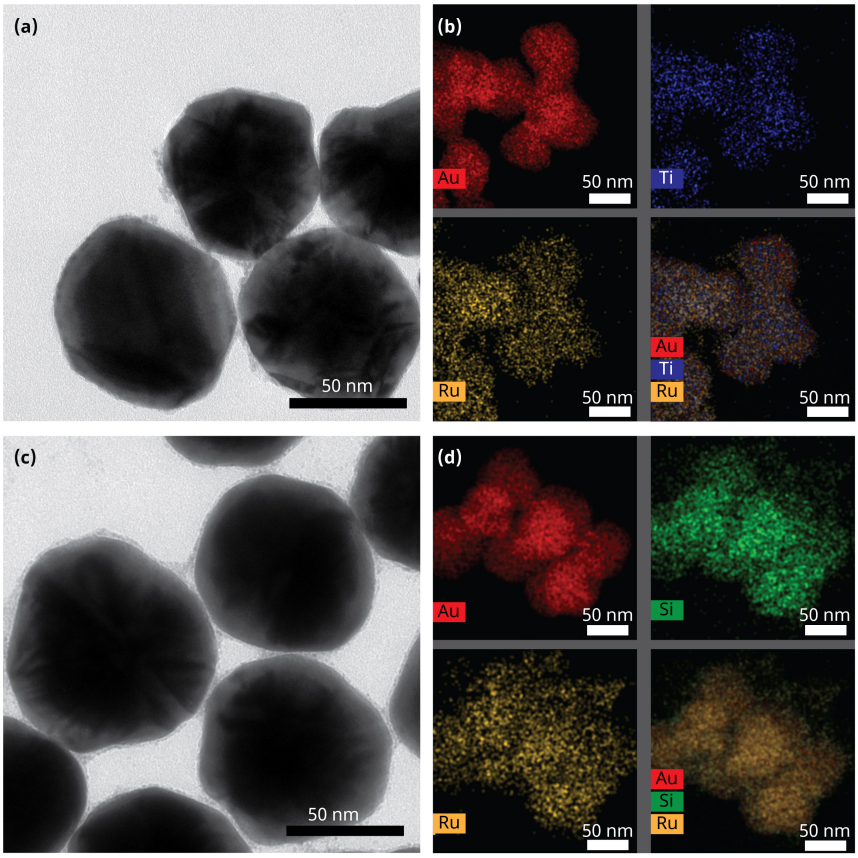

Figure 3.2. Electron microscopy imaging of Ru/Au@TiO_2 and Ru/Au@SiO_2. **(a)** TEM image and **(b)** STEM-EDX elemental map of RuO_x@TiO_2@Au; **(c)** TEM image; and **(d)** STEM-EDX elemental map of RuO_x@SiO_2@Au.

Figure 3.3a, b and c). various bands between 100-500 cm^{-1}, which are typical for Ru-Cl stretching and bending vibrations of $RuCl_3$. Furthermore hydrate species are observed at around 800 cm^{-1}. The SHINERS signal intensity is about 20 times stronger than the Raman signal observed with conventional Raman spectroscopy over 200 nm Stöber SiO_2 NPs. An EF of 20 appears to be much weaker than the factor 10^4-10^5 we observed in Chapter 2. This can be explained by the fact that there is only a small fraction of $RuCl_3$ present in the hot spots, while $RuCl_3$ can already be observed by conventional Raman spectroscopy. Another observation can be made of the relative intensities of the Ru-Cl and Ru-OH_2 bands. Especially the hydrate species are improved in intensity, which might be related to the Ru-SiO_2 interface.

After a heat treatment in air at 300 °C, $RuCl_3$ is fully oxidized to RuO_2, as is apparent from the intense broad bands between 100-700 cm^{-1}. The Raman signals of nano-sized RuO_2 are known to broaden and red-shift with respect to bulk RuO_2 Raman bands at 528, 644 and 716 cm^{-1} due to finite-size effects and stress induced by lattice.[29] However, the broadening of the RuO_2 bands in the SHINER spectra is much stronger in comparison to what is seen before in literature of Raman spectra of RuO_2. Furthermore, in the control experiment with RuO_2 on 200 nm Stöber SiO_2, we see better defined (and weaker) Raman peaks (Figure 3.3c, the intense peak at 520 cm^{-1} originates from the Si wafer). This can be explained by the fact that very small NPs were formed and probed at the Ru-SHINs interfaces, thus more strain is observed in comparison to conventional Raman.[30,31] RuO_2 was then reduced to Ru^0 in a 10 mL/min H_2 in 40 mL/min Ar flow at 150 °C. *In situ* SHINERS verified the reduction of the catalysts by the absence of the Ru-O and Ru-Cl stretches in the spectrum between 100-700 cm^{-1} in Figure 3.3. The remaining Raman bands are associated with amorphous TiO_2 (700 cm^{-1})[32] and Si-OH (990 cm^{-1}) and Si (520 cm^{-1}) from the Si wafer.[33] After reduction, CO was introduced to the catalysts at room temperature. As demonstrated in Figure 3.3a and b, both catalysts show stretching vibrations of chemisorbed carbonyl species directly after exposure to CO gas. We could not observe CO adsorption on similar Ru/SiO_2 samples without SHINERS in Figure 3.3c.

The observation of adsorbed carbonyls reinforces the conclusion that metallic catalysts are indeed formed after H_2 reduction, and that the SHINs are still active for Raman signal enhancement. CO was only observed in a linear position on metallic Ru, with 2 characteristic Raman bands at around 485 and 2020 cm^{-1}, which are the stretching vibrations of respectively Ru-CO and RuC-O.[34–36] Minor differences were observed between Ru/Au@SiO_2 and Ru/Au@TiO_2, but were not convincingly clear bearing in mind a spectral resolution of ~3 cm^{-1}.

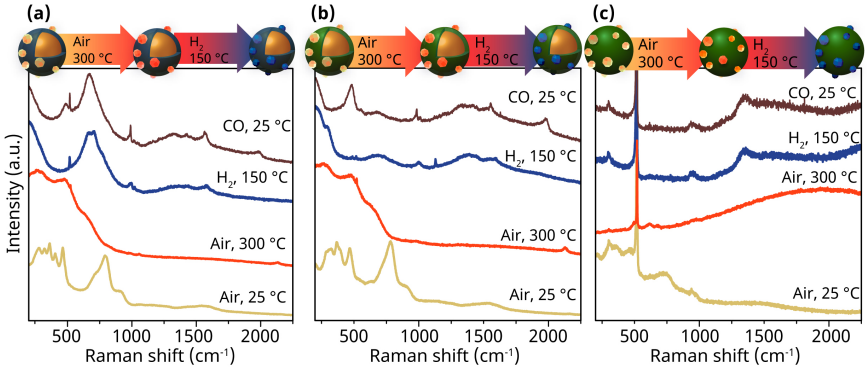

Figure 3.3. SHINER study of supported Ru catalysts. Raman spectra of $RuCl_3$ (yellow), RuO_2 after oxidation at 300 °C in air (orange) and Ru after reduction at 150 °C in 10-40 mL/min H_2-Ar (blue), followed by CO adsorption at room temperature, supported on **(a)** Au@TiO_2 SHINs, **(b)** Au@SiO_2 and **(c)** Stöber SiO_2. (λ= 785 nm; P= 2.6 ▪ 10^5 W ▪ cm^{-2})

Finally, the CO hydrogenation properties of the Ru/SHINs catalysts were tested by hydrogenating the adsorbed CO in a H_2 atmosphere. The effect of shell material on the catalytic properties was investigated using Ru/Au@TiO_2 (Figure 3.4a) and Ru/Au@SiO_2 (Figure 3.4b). The gas feed was switched to 10 mL/min H_2 in 40 mL/min Ar and the temperature was increased stepwise to 250 °C. All bands associated with M-CO stretching vibrations decreased in intensity above 150 °C. Only the removal of linearly adsorbed carbonyls was observed. We do not see the appearance of new adsorbed species, such as different Ru-C or Ru-O interactions, between 100-100 cm^{-1} under the applied methanation conditions.

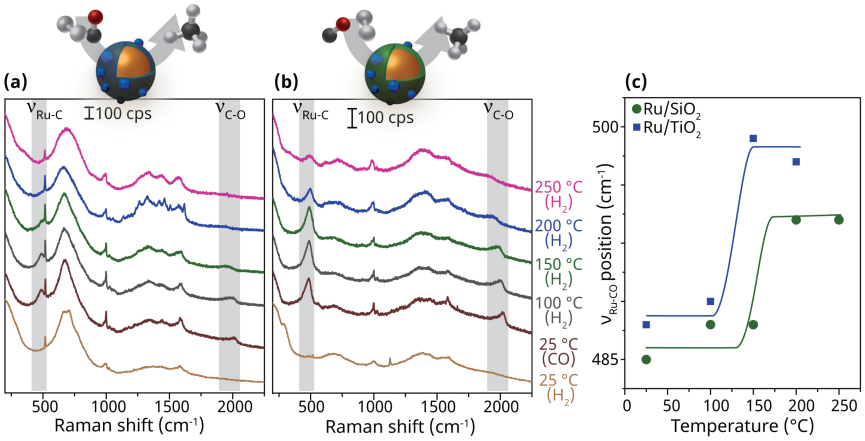

Figure 3.4. CO hydrogenation over supported Ru catalysts on TiO_2- and SiO_2-SHINs as observed with SHINERS. (a) SHINER spectra of Ru/Au@TiO_2 after reduction, CO adsorption and hydrogenation. **(b)** SHINER spectra of Ru/Au@SiO_2 after reduction, CO adsorption and hydrogenation. The $\nu_{M\text{-}C}$ and $\nu_{C\text{-}O}$ vibrational regions are indicated by the highlighted areas around respectively 480 and 2000 cm^{-1}. **(c)** Peak position of the stretching vibration of Ru-CO measured on Ru supported on Au@TiO_2 (blue squares) and Au@SiO_2 (green dots) after reduction, CO adsorption and hydrogenation. (λ= 785 nm; P= 2.6 10^5 W cm^{-2}).

This is unfortunate for the implementation of SHINERS as a tool to study reaction pathways during CO hydrogenation. However, it became clear that TiO_2 and SiO_2 support materials do have a different effect on the reduction properties of the supported Ru NPs when studied by SHINERS. At temperatures above 150 °C, the Ru-CO stretching vibrations are shifted to higher energies, coupled with a stronger decrease in intensity for the Ru/Au@TiO_2 system (Figure 3.4c). This demonstrates the difference induced by a TiO_2 layer for the CO hydrogenation over Ru in comparison to the Ru/SiO_2 system and is in line with what is known in literature.[37–39] After complete CO hydrogenation at 250 °C, the temperature was set to 150 °C and the H_2 atmosphere was changed back to CO. This resulted in the observation of the CO bands again with a signal intensity equal to the initial values.

Thus, SHINERS substrates were successfully prepared and implemented for studying the preparation and operation of heterogeneous catalysts. We have focused on CO adsorption and hydrogenation over supported Ru catalysts using SHINERS. The TiO_2- and SiO_2-SHINS were stable under the reaction conditions, with the intensity of $\nu_{Ru\text{-}C}$ preserving their signal strength - 80-100% - after reaction at 250 °C under hydrogen atmosphere. To investigate the universality of this method, we applied it to a wide range of catalyst materials with ease of preparation.

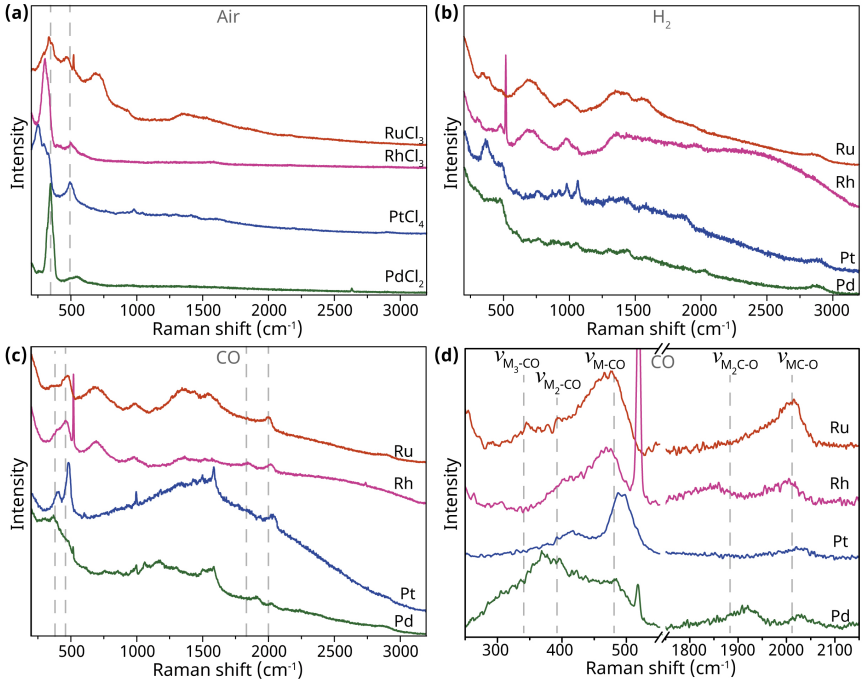

Figure 3.5. SHINERS study of the preparation of heterogeneous catalysts. (a) SHINER spectra directly after UV-O_3 treatment of metal chloride impregnated SiO_2-SHINs in air. The dotted line indicates the position of the M-Cl stretching vibrations. **(b)** SHINER spectra of the same substrates after reduction in 10 mL/min H_2 and 40 mL/min Ar at 150 °C (5 °C/min ramp). **(c)** SHINER spectra of CO adsorption at 150 °C after reduction. **(d)** Zoom-in of the spectra obtained in (c), the stretching vibrations of adsorbed carbonyls are indicated with the dotted line. (λ= 785 nm; P= $2.0 \cdot 10^5$ W·cm^{-2})

For example, similar structures with Rh, Pt and Pd catalysts were prepared using the aqueous MCl_x impregnation method (Figure 3.5). The synthesis steps of all catalysts can be followed (Figure 3.5a) and after reduction (Figure 3.5b), the various preferred adsorption geometries of carbonyl are observed (Figure 3.5c and d). M-Cl vibrations were clearly observed for all metal chlorides in Figure 3.5a, and other synthesis steps of active catalysts can all be followed *in situ* with accurate SHINERS signals.

Because SHINERS signals of metal chlorides and oxides can differ from bulk Raman signals, we see a potential in this technique not only for catalysis, but also for nanostructures characterization. Another example of SHINERS as a characterization tool for nanomaterials analysis and catalysis can be found in Figure 3.6, where the study of alloying Rh with Fe was studied. In this example, Rh-Fe alloys were prepared in the molar ratios 1:0, 4:1 and 1:1 by mixing aqueous $RhCl_3$ and $FeCl_3$ with $Au@SiO_2$ SHINs at a constant total concentration of aqueous MCl_3 (0.2 mM). The MCl_3 spectra in Figure 3.6a only differ in the stretching vibration energy of M-Cl bond. Increasing the Fe content shifts the peak position from 295 to 308 cm^{-1}. After oxidizing the materials at 300 °C, the typical Rh_2O_3 appears at

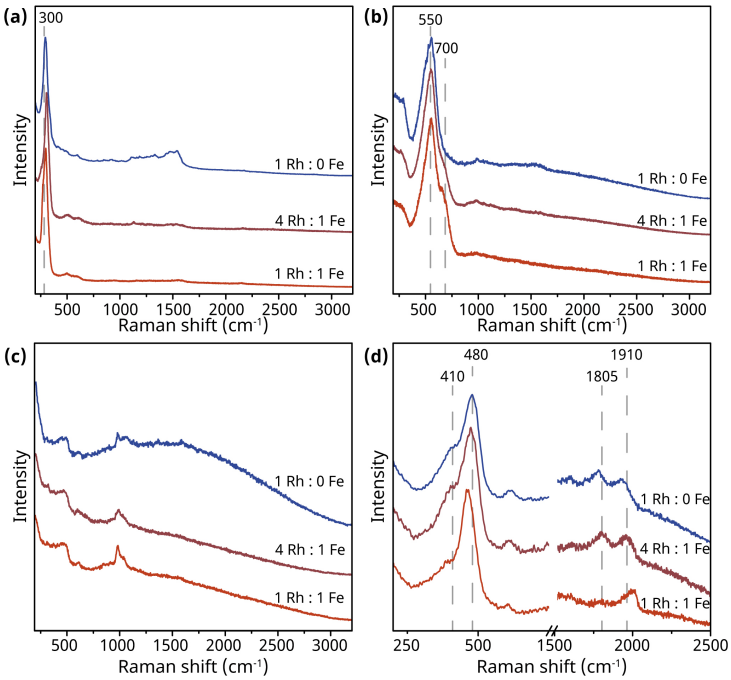

Figure 3.6. SHINERS study of Rh-Fe alloys assembled over $Au@SiO_2$ SHINs. (a) SHINER spectra of $RhCl_3$ mixed with $FeCl_3$ in air at room temperature. **(b)** SHINER spectra of Rh_2O_3 and mixed states with Fe_3O_4 after a heat treatment in 20% O_2 at 300 °C. **(c)** SHINER spectra of metallic Rh and Fe after reduction in 20% H_2 at 250 °C. **(d)** SHINER spectra of CO adsorption after reduction at 250 °C in H_2 over the different Rh catalysts. (λ= 785 nm; P= $8.1 \cdot 10^4$ $W \cdot cm^{-2}$)

550 cm^{-1}, and the Fe containing materials contain an additional shoulder at around 670 cm^{-1} due to the Fe_3O_4 magnetite structures present (Figure 3.6b).[40,41] After reduction in H_2 at 250 °C in Figure 3.6c, only the SiO_2 Raman background was observed and the particles were exposed to a syngas mixture (1 CO:2 H_2) in Figure 3.6d. Now the effect of alloying Rh with Fe was clearly observed by the change in the preferred adsorption sites for carbonyls. As expected for Rh/Au@SiO_2, CO adsorbed in two configurations: 305 (Rh_2-CO) and 1860 cm^{-1} (Rh_2C-O) are associated with CO adsorption in a bridged position, and 470 (Rh-CO) and 2000 cm^{-1} (RhC-O) peaks are associated with linear carbonyls. When the atomic ratio of Rh:Fe increases to 1:1, CO hardly adsorbs in configurations with double bonds. (This indicates less C-O dissociation during hydrogenation reactions. In Chapter 5 we look more into the consequences of this observation for catalysis.

3.3 Conclusions

In this chapter, thermally stable Au@TiO_2 and Au@SiO_2 were successfully applied for *in situ* characterization of working solid catalysts using SHINERS. The simple synthesis procedure requires basic laboratory equipment and can therefore be applied in a wide variety of laboratories. Nano-sized materials can be assembled over the SHINs by wet impregnation to study catalyst preparation to active catalysts. Subsequently, the obtained catalyst/SHINs can be exposed to reactants in the gas phase for *in situ* characterization of the catalyst structure and interfaces with improved intensity. These materials demonstrated their potential for the study of catalytic solids with SHINERS as was observed by the different activity in CO hydrogenation over Ru/Au@TiO_2 and Ru/Au@SiO_2 SHINs.

However, there are more challenges left to tackle. First of all, the stability of the SHINs is limited above 300 °C under reaction conditions. Future work could be performed on more stable or flexible coating materials, such as graphene. Second: during sample preparation, but also during reaction, contamination of the sample can occur, obstructing the interpretation of the data. And third, it is difficult to couple SHINERS results to catalytic activity due to the small quantities of the substrates. In the next chapters, we will demonstrate methods to solve these obstacles.

3.4 Experimental Section

Chemicals. The following chemicals were purchased and used as received: (3-aminopropyl)trimethoxysilane (APTMS, 97%), sodium silicate solution (27% SiO_2 in 14% NaOH), titanium(IV) (triethanoloaminato) isopropoxide solution (TTEAIP, 80 wt.% in isopropanol), Rhodamine 6G, $RuCl_3.xH_2O$ (40-49% Ru content), $RhCl_3$ (98%), H_2PtCl_6 (8 wt% in H_2O), $PdCl_2$ (≥99.9%), hydroxylamine

hydrochloride (>98%) from Sigma Aldrich; ammonia solution (28-30%) from VWR International; $HAuCl_4 \cdot 3H_2O$ (99.99% metals basis) from Alfa Aesar; trisodium citrate dihydrate (99%) from Acros Organics; 2-propanol (CHROMASOLV™ LC-MS >99%) from Honeywell; Hydrochloric acid (Emsure, 37%) from Merck. Demineralized water was purified with a Milli-Q system (18.2 MΩ) before use.

Catalytic studies with SHINERS. 0.1 mL SHINs were mixed with 10-15 μL of an aqueous metal chloride (MCl_x, 2 mM) solution and mixed intensely by shaking and ultrasonic treatment. 10 μL of these mixtures were then dried under vacuum on a Si wafer. The obtained substrates for catalytic studies with SHINERS where subsequently cleaned wit UV-Ozone treatment for 1 h. To obtain metal-containing catalyst materials, the substrates were reduced *in situ* by exposure to 10 mL/min H_2 in 40 mL/min Ar at minimally 150 °C in a Linkam THMS600 heating microscope stage. Raman spectroscopy measurements were performed on a Renishaw InVia Raman microscope, using 785 nm diode laser excitation through a 20x objective (0.4 NA). *In situ* experiments were all performed under 2 mW (i.e., $2.6 \cdot 10^5$ W·cm^{-2}), with an integration time of 10 s. *Ex situ* experiments were performed with a 50x objective (0.5 NA) under 0.24 mW (i.e., $1.12 \cdot 10^5$ W·cm^{-2}), with an integration time of 10 s. All spectra are shown as obtained: no smoothing, background correction, baseline subtraction.

Characterization. Transmission electron microscopy (TEM) images were recorded using a FEI tecnai 12 Icor TEM operating at 120 kV. Samples were prepared by drop-casting a colloidal solution on a carbon-coated TEM grid, which were left to dry in air. Scanning transmission electron microscopy-energy dispersive X-ray analysis (STEM-EDX) images were obtained on a FEI Talos F200X electron microscope operating at 200 kV.

3.5 Author Contributions and Acknowledgements

This Chapter is based on the manuscript: Thermally Stable TiO_2- and SiO_2-Shell-Isolated Au Nanoparticles for In Situ Plasmon-Enhanced Raman Spectroscopy of Hydrogenation Catalysts, T. Hartman, B. M. Weckhuysen, *Chem. Eur. J.* **2018**, *24*, 3733–3741.

The research was conceived by Bert Weckhuysen and Thomas Hartman. Thomas Hartman performed the experimental work under supervision of Bert Weckhuysen. The work was written by Thomas Hartman with feedback and corrections by Bert Weckhuysen.

The following people are furthermore gratefully acknowledged for their contributions: Hans Meeldijk and Wouter Lamme, both from Utrecht University (UU)for their contributions with the TEM-EDX measurements. Katinka Wondergem (UU) is thanked for her valuable input on the experimental and written work.

3.6 References

[1] M. A. Bañares, *Adv. Mater.* **2011**, *23*, 5293–5301.
[2] S. J. Tinnemans, J. G. Mesu, K. Kervinen, T. Visser, T. A. Nijhuis, A. M. Beale, D. E. Keller, A. M. J. Van Der Eerden, B. M. Weckhuysen, *Catal. Today* **2006**, *113*, 3–15.
[3] E. Stavitski, B. M. Weckhuysen, *Chem. Soc. Rev.* **2010**, *39*, 4615–4625.
[4] B. M. Weckhuysen, *Chem. Commun.* **2002**, 97–110.
[5] I. L. C. Buurmans, B. M. Weckhuysen, *Nat. Chem.* **2012**, *4*, 873–886.
[6] I. E. Wachs, *Catal. Today* **1996**, *27*, 437–455.
[7] M. A. Bañares, *Adv. Catal.* **2009**, *52*, 43–128.
[8] G. Mestl, *J. Mol. Catal. A Chem.* **2000**, *158*, 45–65.
[9] I. E. Wachs, C. A. Roberts, *Chem Soc Rev* **2010**, *39*, 5002–5017.
[10] H. Knözinger, *Catal. Today* **1996**, *32*, 71–80.
[11] D. L. Jeanmaire, R. P. van Duyne, *J. Electroanal. Chem. Interfacial Electrochem.* **1977**, *84*, 1–20.
[12] H. Kim, K. M. Kosuda, R. P. Van Duyne, P. C. Stair, *Chem. Soc. Rev.* **2010**, *39*, 4820–4844.
[13] M. Moskovits, *J. Chem. Phys.* **1978**, *69*, 4159–4161.
[14] M. G. Albrecht, J. A. Creighton, *J. Am. Chem. Soc.* **1977**, *99*, 5215–5217.
[15] S.-Y. Ding, E.-M. You, Z.-Q. Tian, M. Moskovits, *Chem. Soc. Rev.* **2017**, *46*, 4042–4076.
[16] S. Schlücker, *Angew. Chem. Int. Ed.* **2014**, *53*, 4756–4795.
[17] S.-Y. Ding, J. Yi, J.-F. Li, B. Ren, D.-Y. Wu, R. Panneerselvam, Z.-Q. Tian, *Nat. Rev. Mater.* **2016**, *1*, 16021.
[18] K. Kneipp, Y. Wang, H. Kneipp, L. T. Perelman, I. Itzkan, R. R. Dasari, M. S. Feld, *Phys. Rev. Lett.* **1997**, *78*, 1667–1670.
[19] E. M. van Schrojenstein Lantman, P. de Peinder, A. J. G. Mank, B. M. Weckhuysen, *ChemPhysChem* **2015**, *16*, 547–554.
[20] H. K. Choi, W. H. Park, C. G. Park, H. H. Shin, K. S. Lee, Z. H. Kim, *J. Am. Chem. Soc.* **2016**, *138*, 4673–4684.
[21] J. F. Li, Y. F. Huang, Y. Ding, Z. L. Yang, S. B. Li, X. S. Zhou, F. R. Fan, W. Zhang, Z. Y. Zhou, D. Y. Wu, B. Ren, Z. L. Wang, Z. Q. Tian, *Nature* **2010**, *464*, 392–395.
[22] Z.-Q. Tian, B. Ren, J.-F. Li, Z.-L. Yang, *Chem. Commun.* **2007**, *34*, 3514–3534.
[23] C. E. Harvey, E. M. van Schrojenstein Lantman, A. J. G. Mank, B. M. Weckhuysen, *Chem. Commun.* **2012**, *48*, 1742–1744.
[24] J.-F. Li, Y.-J. Zhang, S.-Y. Ding, R. Panneerselvam, Z.-Q. Tian, *Chem. Rev.* **2017**, *117*, 5002–5069.
[25] S. Guan, O. Donovan-sheppard, C. Reece, D. J. Willock, A. J. Wain, G. A. Attard, *ACS Catal.* **2016**, *6*, 1822–1832.

[26] T. Hartman, C. S. Wondergem, N. Kumar, A. Van Den Berg, B. M. Weckhuysen, *J. Phys. Chem. Lett.* **2016**, *7*, 1570–1584.
[27] H. Zhang, C. Wang, H. Sun, G. Fu, S. Chen, Y. Zhang, B. Chen, J. R. Anema, Z. Yang, J. Li, Z. Tian, *Nat. Commun.* **2017**, *8*, 15447.
[28] H. Zhang, X.-G. Zhang, J. Wei, C. Wang, S. Chen, H.-L. Sun, Y.-H. Wang, B.-H. Chen, Z.-L. Yang, D.-Y. Wu, J.-F. Li, Z.-Q. Tian, *J. Am. Chem. Soc.* **2017**, *139*, 10339–10346.
[29] S. Y. Mar, C. S. Chen, Y. S. Huang, K. K. Tiong, *Appl. Surf. Sci.* **1995**, *90*, 497–504.
[30] G. Gouadec, P. Colomban, *Prog. Cryst. Growth Charact. Mater.* **2007**, *53*, 1–56.
[31] E. V. Formo, Z. Wu, S. M. Mahurin, S. Dai, *J. Phys. Chem. B* **2011**, *115*, 9068–9073.
[32] S. Degioanni, A. M. Jurdyc, F. Bessueille, J. Coulm, B. Champagnon, D. Vouagner, *J. Appl. Phys.* **2013**, *114*, 234307.
[33] P. F. McMillan, R. L. Remmele, *Am. Mineral.* **1986**, *71*, 772–778.
[34] L. H. Leung, M. J. Weaver, *Langmuir* **1988**, *4*, 1076–1083.
[35] M. A. Barteau, J. Q. Broughton, D. Menzel, *Surf. Sci.* **1983**, *133*, 443–452.
[36] G. H. Yokomizo, C. Louis, A. T. Bell, *J. Catal.* **1989**, *120*, 1–14.
[37] S. Tada, R. Kikuchi, K. Urasaki, S. Satokawa, *Appl. Catal. A Gen.* **2011**, *404*, 149–154.
[38] A. M. Abdel-Mageed, D. Widmann, S. E. Olesen, I. Chorkendorff, J. Biskupek, R. J. Behm, *ACS Catal.* **2015**, *5*, 6753–6763.
[39] T. Komaya, A. T. Bell, Z. Weng-Sieh, R. Gronsky, F. Engelke, T. S. King, M. Pruski, *J. Catal.* **1994**, *150*, 400–406.
[40] C. T. Williams, C. A. Black, M. J. Weaver, C. G. Takoudis, *J. Phys. Chem. B* **1997**, *101*, 2874–2883.
[41] D. Bersani, P. P. Lottici, A. Montenero, *J. Raman Spectrosc.* **1999**, *30*, 355–360.

4

Guidelines for SHINERS in Catalysis

Shell-isolated nanoparticle-enhanced Raman spectroscopy (SHINERS) can be used as a characterization tool for surface species in heterogeneous catalysis research by exploiting the localized electromagnetic fields. However, because of the extremely strong local electric fields, minor amounts of contaminants already have a large impact on the quality and interpretation of the obtained spectroscopic data. Often, a large part of the organic fingerprint region (1100-1700 cm^{-1}) is omitted from SHINER spectra as this is not the main region of interest. In this chapter, we show that bands in this region are an important indication of the cleanliness of the substrate and can be removed so that the entire spectroscopic range of Raman can be used. Furthermore, we propose robust synthesis and measurement protocols to obtain clean SHINERS substrates amenable for catalysis research.

4.1 Introduction

Surface-enhanced Raman spectroscopy (SERS) has the ultimate potential to elucidate molecular structures in single-molecule events.[1] Raman spectroscopy is already a strong complementary technique to IR spectroscopy as it can probe vibrations of molecules and materials over a wider energy range,[2] but in the case for SERS, this spectroscopic technique even becomes a strong surface characterization tool for *in situ* studies of heterogeneous catalysts.[3–5] SERS has been implemented for the study of surface-reactions since its invention,[6–9] which led to the discovery of various reaction pathways for chemical reactions, including possible intermediates.[10–14] In SERS, noble metal nanostructures with plasmonic properties are applied for the enhancement of the Raman signal. The conduction electrons at the surface of these nanostructures can resonate with the excitation laser wavelength and across the Stokes frequency, resulting in a strong enhancement of the incident light and the scattered light within nanometers of the metal surface.[15] To extend the applicability of SERS, metal overlayers were first prepared over existing Au or Ag surfaces.[16,17] Later, shell-isolated nanoparticle-enhanced Raman spectroscopy (SHINERS) was developed to create a more universal technique.[18] When the plasmonic nanoparticles (NPs) are coated with a dielectric layer, such as SiO_2, the technique can be regarded as a non-invasive characterization tool to study virtually any substrate.[19] In this thesis, SiO_2- and TiO_2-shell-isolated nanoparticles (SHINs) were applied in the previous chapter to study hydrogenation catalysis over a number of metals.[20]

Since SERS and SHINERS are extremely sensitive techniques, contamination of the sample can have a large impact on spectral interpretation. Amorphous carbon is one of the most common contaminants, and was identified as the "bottle-neck" for SERS to be widely applied.[21] Organic residues will be present as a result of the preparation conditions and can be decomposed to form amorphous carbon under the conditions generated by the excitation of the plasmonic nanostructures. Depending on the nature of the plasmonic nanostructures, such conditions are perceived as heating,[22] hot-electron injection[4] or degradation by strong electromagnetic effects.[23] Because coke species have a large Raman scattering cross-section, even a small amount can result in intense signals between 1200-1700 cm^{-1}, with the typical 1350 cm^{-1} disordered (D) carbon band and 1600 cm^{-1} graphitic (G) carbon band as the strongest interferences. More problematic is that SERS and SHINERS can detect local changes in amorphous carbon as blinking spectra with fluctuating spectral intensities and band locations. The random location of these peaks make them difficult to subtract or ignore.[21] Such problems were already observed in the application of SERS for the study of CO hydrogenation over Rh in the 1990s. At elevated temperatures in the absence of oxygen, Weaver *et al.* observed the conversion of organics to coke species over the SERS substrates, resulting in features that obscured the spectra in the 1200-1600 cm^{-1} range.[12,24] This range was therefore left out of the interpretation. Additionally,

the presence of carbon affects the performance of a catalyst as it can block access to the reactive surface and its formation should therefore be prevented.[25]

Because the field of SHINERS in heterogeneous catalysis is relatively new, the information on sample preparation is scarce in the literature and remains often limited to some brief discussions in the experimental section of these articles. We have therefore worked on the development of a valuable set of practical guidelines to inform the scientific community about the possible routes to tackle substrate and spectral contamination. Using these guidelines, the reproducibility of *in situ* experiments is guaranteed, which is a necessity for SHINERS to become a more routine technique in the field of catalysis. Three pretreatments to remove organic residues were investigated in this chapter; a heat treatment in air up to 300 °C, oxidation by UV/O_3 at room temperature and a reduction treatment up to 250 °C in H_2. Furthermore, the purity of the gas feed was found to be critical and can be improved easily with a filter. It was found that minor contaminations in the gas feed caused by impurities have a major effect on the SHINERS spectral interpretation as well as on the catalyst properties. Finally, the guidelines are applied to Ru/Au@TiO_2 and Ru/Ag@SiO_2 SHINs to demonstrate the universality of the methods proposed.

4.2 Results and Discussion

Catalytically active SHINERS substrates were prepared that enhance the Raman signal with a factor of over 10^4.[20] First, small Au seeds of 16 nm were prepared and further grown to 80 nm with $HAuCl_4$, using hydroxylamine hydrochloride as reducing agent.[26] A silica coating of 2 nm was grown over the Au cores using (3-aminopropyl)trimethoxysilane (APTMS) and sodium silicate in water at 90 °C for 40 min.[27] When dried and aggregated over Si wafers, these nanostructures were found to be optimal for enhancing the Raman scattering with a 785 nm laser connected to our Raman microscope.[20] Finally, catalyst precursors were assembled over the SHINs by mixing aqueous $RuCl_3$ and Au@SiO_2 SHINs, followed by drying on a Si wafer. A visual inspection of the steps involved in the synthesis was performed with transmission electron microscopy (TEM), as shown in Figure 4.1a - e. The complete details of the preparation can be found at the end of this chapter. The coating thickness of the SHINs is essential to control; in Chapter 2, it was demonstrated that a coating of minimally 2 nm is required for stable SHINERS signals under elevated temperatures.[20] However, when the isolating shell reaches 3 nm, the signal is strongly diminished and becomes unsuitable for *in situ* measurements.

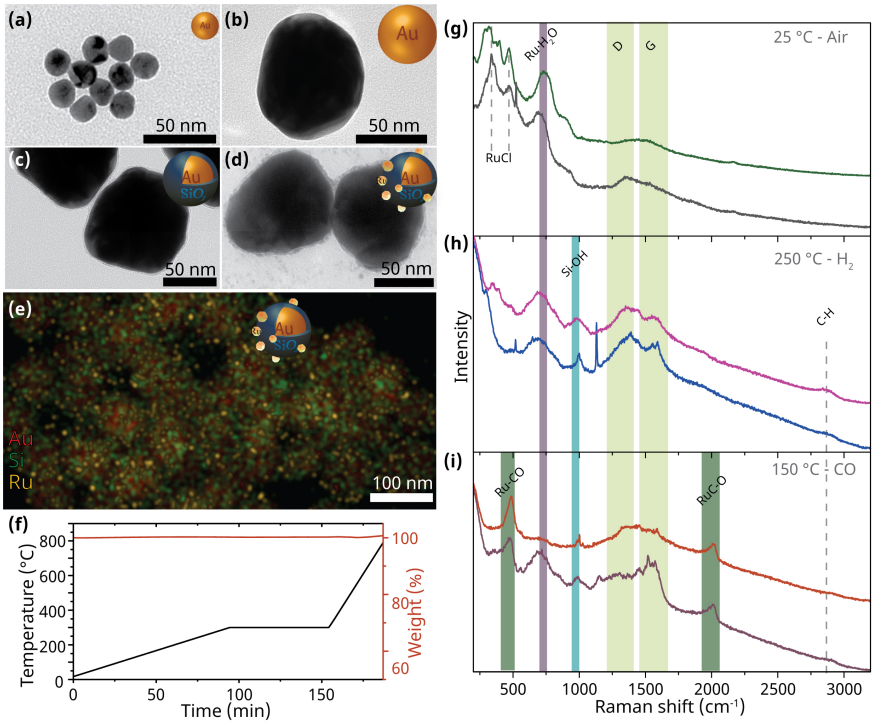

Figure 4.1. The preparation of catalytically active SHINs. TEM and STEM-EDX microscopy images of the synthesis steps involved to prepare Ru/SiO_2@Au based SHINs: **(a)** Au seeds of 16 nm, **(b)** Au nanoparticles (NP) of 80 nm, **(c)** SiO_2-SHIN of 80 nm with 2 nm SiO_2 shell, **(d)** Ru catalysts assembled over SiO_2-SHINS after reduction at 150 °C in H_2. **(e)** STEM-EDX image of Ru catalysts assembled over SiO_2-SHINS after reduction at 150 °C in H_2 with Au indicated with red, Si with green and Ru with yellow. **(f)** Thermal gravimetric analysis (TGA) of 8 mg Au@SiO_2 SHINs. **(g)** *in situ* SHINER spectra of two separate substrates of untreated $RuCl_3$/Au@SiO_2 as obtained after synthesis, **(h)** followed by reduction to Ru/Au@SiO_2 under H_2 at 250 °C, and **(i)** after CO adsorption at 150 °C [785 nm, 0.81 mW, 10 s].

Organic residues are inherent to colloidal synthesis, because the controlled growth of nanoparticles requires several types of directing agents.[28] Therefore, the colloidal products were cleaned by three consecutive centrifugation and washing steps with purified water (demineralized milli-Q, 18.2 MΩ·cm resistivity).

The high sensitivity of SHINERS is demonstrated by the fact that even though with thermogravimetric analysis (TGA) no mass loss was observed over 20-800 °C (Figure 4.1f) organics are still observed in the SHINER spectra of two untreated samples, as illustrated in (Figure 4.1g). Even after several washing steps, a fraction of the molecules remains on the surface and will influence the observed SHINER spectra. The spectra of untreated SHINER substrates vary not only between different samples, but even over different spots within a single sample. The catalyst precursor was then activated by a reduction step in H_2 at 250 °C for 1 h in Figure 4.1h. When the contaminants were not removed, broad features of carbon remain, obscuring the spectra. The substrates can be used for the detection of adsorbed

carbonyls with ν(Ru-CO) at 480 cm^{-1} and ν(RuC-O) at 2000 cm^{-1} in Figure 4.1i. However, the study of adsorbed reactants and products becomes difficult due to the strong features between 1100-1700 cm^{-1} originating from organics. This region is often not measured, as the main focus is metal-adsorbate interactions, with as added benefit a reduced acquisition time. When this spectral region is omitted, important information is excluded from interpretation, as it can be used to evaluate the cleanliness of the sample. For example, when contamination is more substantial, the deposited carbon can isolate the catalyst from reactants, blocking CO from adsorbing on surfaces. This was observed in one example of CO adsorption on heavily contaminated Ru. The substrate was required to be heated to 300 °C in synthesis gas (2 H_2: 1 CO) before CO adsorption was visible (Figure 4.2). This result further demonstrates the need to remove residual organics before catalysis with robust cleaning methods, and that the fingerprint region needs to be included in the analysis to verify the cleanliness.

The contaminants before any treatment are identified as organics in Figure 4.3a, with δ_{as}(CH) at 1440 cm^{-1} and $\nu_s(CO_2^-)$ and $\nu_{as}(CO_2^-)$ of organic carboxylic acid salts at 1340 and 1560 cm^{-1}, respectively, most likely from residual citrates.[29,30] The substrates therefore have to be cleaned prior to *in situ* SHINERS experiments. In contrast to SERS substrates,[24] Au@SiO_2 NPs can withstand strong oxidation treatments to remove organic residues without sacrificing the Raman signal enhancing properties, as demonstrated in Figure 4.3a.[20] Using UV/O_3 for 1 h, all observable organic contaminants can be removed without affecting the $RuCl_3$ spectrum. In addition, heat treatments in air at 200 °C and 300 °C for 1 h will remove all organics and will also oxidize $RuCl_3$ to RuO_2, as is apparent from the intense Raman bands between 100-700 cm^{-1}. The bands observed in this work are much broader than conventional Raman experiments of RuO_2. Although it is known that Raman bands of nano-sized RuO_2 broaden and red-shift with respect to bulk RuO_2 Raman bands at 528, 644 and 716 cm^{-1},[31] hardly any separate bands are detected here with SHINERS. Because of its highly localized sensitivity, SHINERS probes the RuO_2-SiO_2 interface of NPs in the range of 3 nm, and

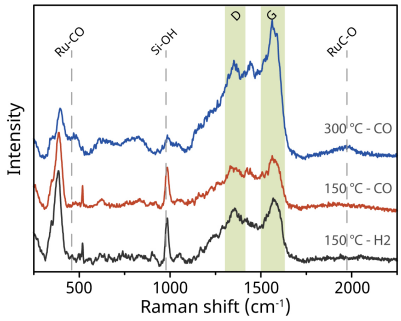

Figure 4.2. SHINERS study of CO adsorption over contaminated Ru catalysts. SHINER spectra of Ru/Au@SiO_2 directly after reduction at 150 °C, followed by CO adsorption at 150 °C and subsequent heating to 300 °C. [785 nm, 0.81 mW, 10 s]

therefore, more strain is observed in comparison to conventional Raman.[32,33]

Two contamination bands remained after the cleaning procedures at 1050 cm^{-1} and 2130-2150 cm^{-1}. They are not related to organic contaminations, but can be ascribed to adsorbed NO_x impurities originating from the atmosphere.[34,35] Nitrates adsorbed in a bridged or bidentate conformation result in features expected at 1050 cm^{-1}. The peak at 2140 cm^{-1} indicates the presence of triple bonded C≡C or C≡N stretching vibrations of adsorbed alkynes or nitriles.

To obtain active hydrogenation catalysts, it is necessary to reduce Ru^{x+} catalyst precursors to metallic Ru^0. The reduction of Ru^{x+} species occurs at temperatures above 150 °C under H_2 atmosphere.[20] After 30 min at 250 °C under 10 mL/min H_2 in 40 mL/min Ar flow all bands associated with RuO_2 or $RuCl_x$ disappeared, indicating the full reduction of the catalyst. The remaining Raman bands are associated with Si-OH (990 cm^{-1}) and Si (520 cm^{-1}) from the Si wafer.[36] However, in contrast to other work,[3] we observed the growth of carbon during the reduction. The major contribution to the SHINER spectra consists of carbonaceous species as is apparent by the carbon D and G bands at respectively 1350 and 1590 cm^{-1} (Figure 4.3b). The bands (re)appeared after reducing samples that were pretreated with UV/O_3 and heat treatment at 200 °C. Furthermore, the presence of other organic materials with $\delta_{as}(CH)$ at 1440 cm^{-1} and $\nu_s(CO_2^-)$ and $\nu_{as}(CO_2^-)$ of organic carboxylate acid salts at 1340 and 1560 cm^{-1} reappeared in the samples treated by UV/O_3.

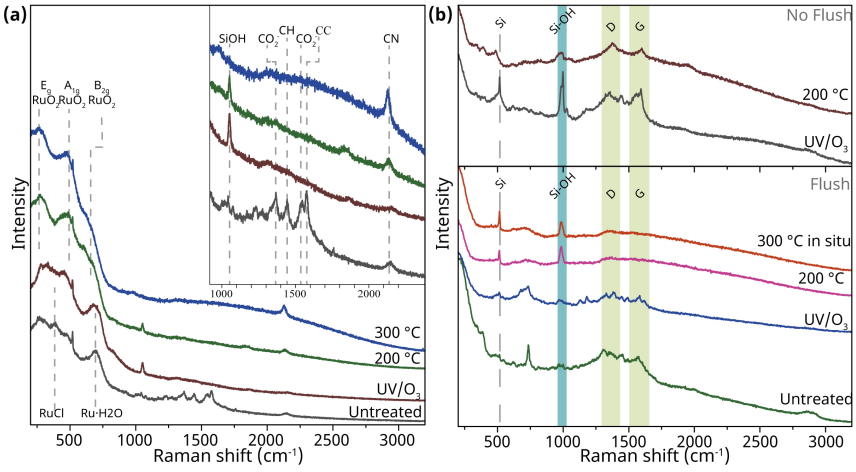

Figure 4.3. SHINERS cleaning method. SHINER spectra of **(a)** $RuCl_3$/SHINs in ambient conditions after heat treatment in air at 300 °C, 200 °C after UV/O_3 treatment and an untreated substrate; **(b)** Ru^0/SHINs after the pretreatments and a subsequent reduction step under H_2 at 250 °C. The top spectra were obtained when the reduction was performed without flushing, the bottom spectra were obtained after an extended flushing step of all gases for 15 min or longer. [785 nm, 0.81 mW, 10 s]

However, the appearance of carbon was still observed. Organic molecules in the gas lines and reaction chamber are the most likely cause. Since the substrates appeared clean prior to reduction, the contamination must come from the reduction treatment. It is therefore important to add an extended flushing period before reduction, to remove any residual organics in the reaction chamber or gas lines. The growth of carbon can be prevented by flushing with the reaction gases for at least 15 min.

Before *in situ* SHINERS experiments we are therefore required to follow two important steps: cleaning the substrate and cleaning the gas feed. These two steps can be optimally combined by cleaning the substrate in the reaction chamber. In this manner, we can assure that the complete reaction chamber is clean, and simultaneously evaluate whether the sample is indeed clean. First, all the gas lines were flushed and then the sample was heated with 3-5 °C/min to 300 °C for 30 min to remove organic molecules. After cooling down to room temperature, the flow was changed to 10 mL/min H_2 in 40 mL/min Ar to reduce the RuO_2 at 250 °C for 30 min. The heating ramp should be limited to 5 °C/min; faster heating rates will result in signal losses, most likely as a result of changes in the nanostructures, such as sintering of the catalyst particles.[37]

Clean substrates can now be applied to study catalytically relevant reactions, such as the Fischer-Tropsch process. When opening the reaction chamber to CO, carbonyls will adsorb to the Ru surface, which is observed in the SHINER spectrum as linearly adsorbed CO with ν(Ru-C) at 480 cm^{-1} and ν(RuC-O) at 2000 cm^{-1}.[38–40] However, over extended measurements of 1 h at 200 °C or higher, strong bands in the D and G region of carbon accumulated, together with the growth of various bands around the M-C and C-O stretching vibrations (Figure 4.4a). The strong bands around 1300 and 1540 cm^{-1} indicate the presence of carbon species. Because their positions in the Raman spectrum are shifted, these species are of a different origin than the previously observed coke bands in Figure 4.3 and relate to more disordered graphite.[41] Furthermore, from 380-430 cm^{-1}, the Raman scattering bands of ν(Fe-CO) and ν(Ni-CO) are observed, between 500-800 cm^{-1} we observe δ(Ni-C-O) and δ(Fe-C-O) and between 1880-2200 cm^{-1} various types of ν(MC-O).[42–44] CO is stored in stainless steel and will therefore carry iron and nickel carbonyls.[45] We therefore assign the Raman bands around 2000 cm^{-1} to the C-O stretching vibrations of Ni and Fe carbonyls that have adsorbed to the SHINs. To prevent contamination by gas phase impurities, a filter was constructed of ZnO, γ-Al_2O_3, and activated carbon in that specific order to capture respectively H_2O, carbonyls, and organics. A microfilter was added to prevent microparticles from entering the reaction chamber. When the filter is applied and under limited laser powers, *in situ* SHINERS studies of CO hydrogenation can be performed up to temperatures of 350 °C without the appearance of carbon species (Figure 4.4b).

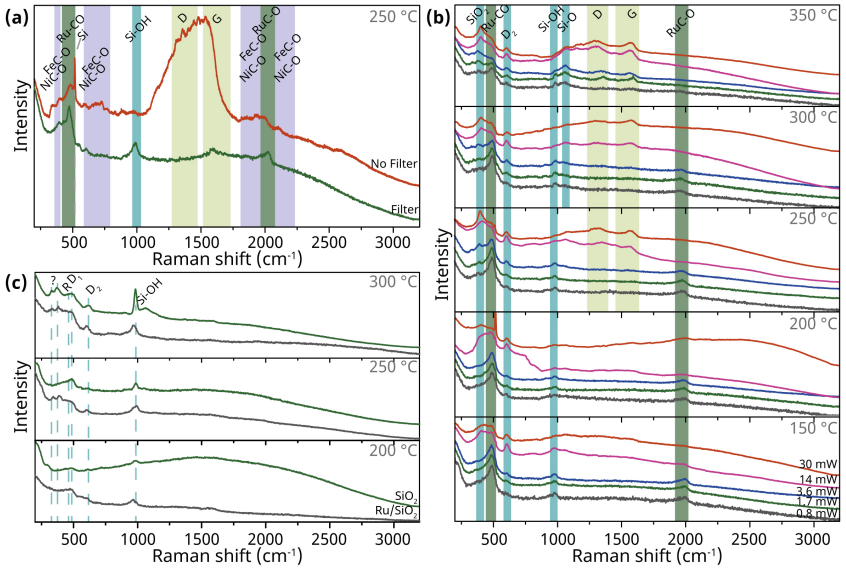

Figure 4.4. The effect of gas filters and laser power. *in situ* SHINER spectra of Ru/SHINs **(a)** Ru/Au@SiO_2 at 250 °C under CO-rich atmosphere with and without the filter consisting of ZnO, γ-Al_2O_3, activated carbon and a microfilter; **(b)** Ru/Au@SiO_2 under FTR conditions (10:20 CO:H_2) at 150-350 °C under changing laser power (0.8, 1.7, 3.6, 14 and 30 mW) **(c)** SHINER spectra of Au@SiO_2 (green) and Ru/Au@SiO_2 (grey) at 200, 250, 300 °C under H_2-rich atmosphere.

We have mainly focused on contamination bands until now, and a number of bands in the previously discussed spectra were left unassigned. These 'spectral contaminants' originate from the Au@SiO_2 substrate. The amorphous SiO_2 restructures as a result of the increased temperature. To understand the changes in the background, clean Au@SiO_2 substrates were subjected to the same reducing conditions as Ru/Au@SiO_2 in Figure 4.4c. The SHINER spectra of Au@SiO_2 and Ru/Au@SiO_2 are very similar, as is expected because metallic Ru does not have Raman bands in the observed region. After reduction, a broad feature at 480 cm^{-1} and a band is observed at 988 cm^{-1}. The 480 cm^{-1} band is associated with the R (symmetric stretching mode of the bridging oxygens between two Si atoms) and D_1 band (4-membered ring breathing mode). The band at 988 cm^{-1} is associated with terminal Si-OH stretching vibration. Heating further to 250 and 300 °C intensifies the bands, and additional bands appear at 630, 800 and 1055 cm^{-1}, that originate from D_2 (3-membered ring breathing mode) and Si-O-Si bond bending, that correspond to bulk SiO_2 studies.[46] These bands were also observed in Chapter 2 after oxidation in air at temperatures up to 500 °C, however, in reducing environments with H_2, the SiO_2 transformation occurs already at 250 °C, and additional bands appear at 335 and 380 cm^{-1} that grow in intensity with the temperature (Figure 4.4c).

In Raman spectroscopy, the effect of the laser power on the sample can be problematic. Stronger laser power results in improved signal to noise ratios, but chances on sample degradation increase. In SERS and SHINERS, the sample and the substrate can both be affected by the strong electromagnetic field. Furthermore, the nanoparticles can create heat and hot electrons to further complicate the effect of the light intensity.[4,22,23] It is therefore important to know the practical limits of laser power before substrate degradation occurs. In Figure 4.4b, the effect of laser power was investigated under CO hydrogenation at different temperatures. The laser power was regulated in a step-wise fashion with discrete filters that allowed control of the total transmission of the light before the sample. Under all the investigated temperatures, increasing the laser power results in a decrease in the intensity of the ν(Ru-CO) and ν(RuC-O) stretching vibrations, the appearance of the D_2 band of SiO_2, and an increase in the unknown SiO_2 bands at 335 and 380 cm^{-1}. Increasing the temperature results in a lower threshold power for the laser to induce the spectral changes. At 150 °C, the SHINER spectrum is affected from 14 mW and higher, whereas at 250 °C the changes are detected already under 3.6 mW, and at 350 °C the changes are detected with 1.7 mW laser power. The effect of the 785 nm laser is therefore limited to heating of the substrate. The related laser power density can be found in Table 4.1 in the experimental section.

To verify the reproducibility of the guidelines and the stability of the SHINERS substrates under the cleaning procedures, two samples were tested for their cleanliness and signal intensity. Substrates that were subjected to 300 °C were found to be free of spurious peaks in the fingerprint region (Figure 4.5a vs. b) measured over 80 random spots, in contrast to the untreated samples that contained several random peaks. Additionally, the SHINERS signal intensity of ν(Ru-CO) (Figure 4.5c vs. d) was found to be uninfluenced by the oxidative pretreatment. The heating step can therefore be applied without consequences to the effectiveness of the substrate for SHINERS.

By following the mentioned guidelines, clean SHINERS substrates are obtained that are ready to use for heterogeneous catalysis. These methods are robust and reliable for study of various solid catalysts over different SHINERS substrates. In fact, clean Au@TiO_2 (Figure 4.6a) and Ag@SiO_2 (Figure 4.6b) can also be obtained using the same methods. By following our guidelines – after flushing the reaction chamber and gas lines, an *in situ* calcination at 300 °C and by applying the filter – clean SHINER spectra were obtained on Ag@SiO_2 under both 532 and 785 nm laser excitation (Figure 4.7).

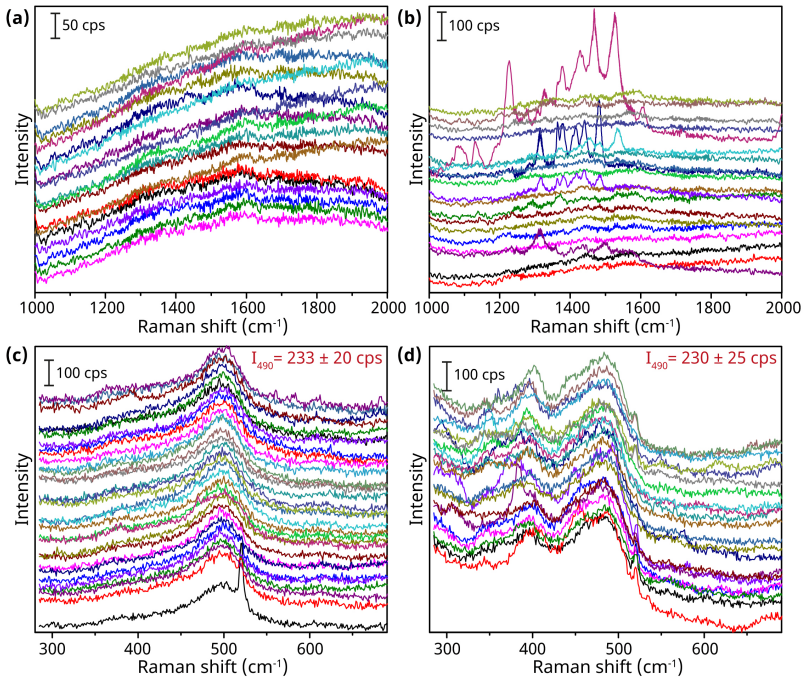

Figure 4.5. Reproducibility tests of SHINERS with and without following the guidelines. SHINER spectra of the *fingerprint* region of **(a)** a heat treated sample in O_2 at 300 °C for 30 min, and **(b)** an untreated sample. SHINER spectra of the *ν*(Ru-CO) stretching vibration region of two treated samples and two untreated samples at 30 °C under a CO-rich atmosphere: **(c)** heat treated under 300 °C for 30 min followed by reduction with H_2 at 250 °C; **(d)** reduced under H_2 at 250 °C. For each sample, 40 spots were measured, the average signal intensity is indicated in the top right corner with counts per second (cps). [785 nm, 0.81 mW, 10 s]

As expected, with a 532 nm excitation wavelength, we observe a stronger Raman signal. This can be related, first of all, to the Raman intensity depending on the excitation wavelength with λ^{-4}.[47] Furthermore, Ag-based SHINs have a stronger plasmon resonance with light in the 400-600 nm range and because of the higher quantum efficiency of the CCD detector for 532 nm lasers, the Raman intensity in the higher wavenumber range is more intense. This results in a relatively stronger *ν*(RuC-O) under CO hydrogenation conditions than observed with a 785 nm laser (Figure 4.7a). The background of fully reduced Ru/Ag@SiO_2 after complete hydrogenation of CO at 300 °C shows the same bands as for Ru/Au@SiO_2 with different relative intensities (Figure 4.7b).

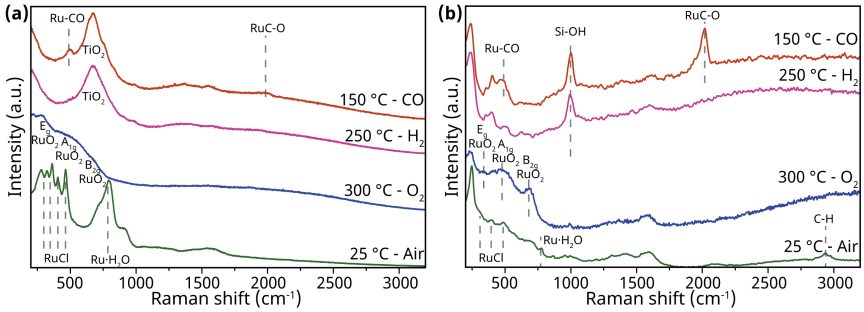

Figure 4.6. Application of guidelines to Au@TiO_2 and Ag@SiO_2 SHINs. (a) SHINER spectra of $RuCl_3$/Au@TiO_2 in air, after 300 °C oxidation, after 250 °C reduction under H_2 and at 150 °C under CO atmosphere. [785 nm, 0.81 mW, 10 s] **(b)** SHINER spectra of $RuCl_3$/Au@Ag@SiO_2 in air, after 300 °C oxidation, after 200 °C reduction under H_2 and at 150 °C under CO atmosphere. [532 nm, 30 μW, 10 s]

An advantage of implementing Ag plasmonic cores is that the stronger Raman signal intensity allows shorter acquisition times so that reactions can be followed with shorter intervals. However, because of the stronger plasmon resonance, the chance increases for degradation of the substrate and adsorbates due to thermal or electromagnetic effects. The threshold for laser induced damage is observed at 160 μW under CO hydrogenation conditions over Ru/Ag@SiO_2 (Figure 4.7c). Under methanation conditions (50 mL/min H_2 and 5 mL/min CO at 210 °C), the *ν*(Ru-CO) and *ν*(RuC-O) of linearly adsorbed carbonyls appear at around respectively 480 and 2000 cm^{-1}. Over time, the signal remains stable with 30 μW incident laser power. As soon as the laser power is increased to 160 μW, a marked growth in the intensity of the D and G graphite Raman bands is observed. The laser power effect can be studied with a 3 s integration time to follow the growth of the D and G band in Figure 4d. When the laser power is switched from 30 to 160 μW, random peaks appear between 1100-1600 cm^{-1} that gradually build up to the known D and G bands. When a new location is measured, we again observe the blinking of various peaks in the spectrum and the rise of the D and G bands. Interestingly, under H_2 at 300 °C after all surface-bound CO has reacted, we can increase the laser power to 360 μW without the observation of any spectral blinking or carbon growth (Figure 4.7b). Since the introduction of CO under stronger laser powers results in the immediate formation of carbons, we can conclude that the cleaning methods are successful, and furthermore, that the cleanliness can be verified simply by increasing the laser power under H_2.

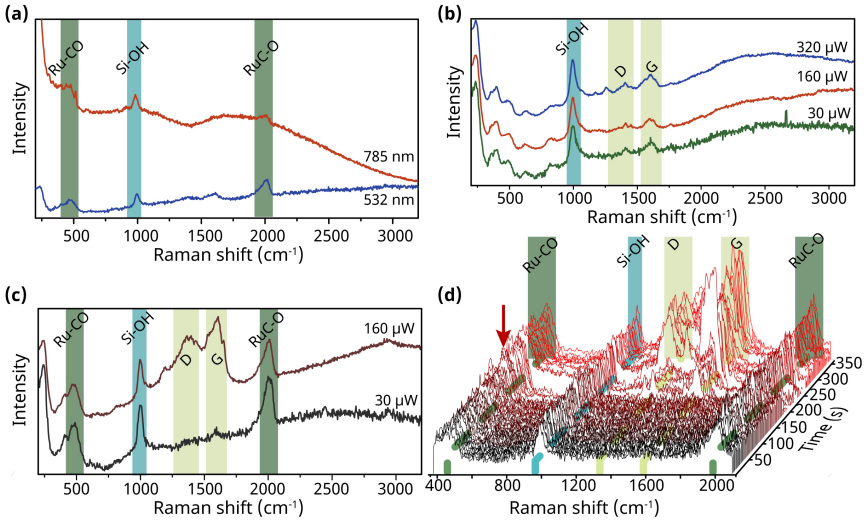

Figure 4.7. The effect of laser power on the SHINERS spectra of Ru/SiO_2@Ag during methanation conditions measured with SHINERS. (a) SHINERS measurements of Ru/SiO_2@Ag in CO-rich atmosphere at 150 °C under 10 s, 30 µW, 532 nm (lower, blue line) and 10 s, 1.7 mW, 785 nm (upper, red line) excitation. **(b)** SHINERS measurements of Ru/SiO_2@Ag in H_2 atmosphere (50 H_2:40Ar mL/min at 300 °C) with 30 µW, 160 µW and 320 µW for 10s integration time. **(c)** SHINERS measurements of Ru/SiO_2@Ag in methanation conditions (50 H_2:5CO:40Ar mL/min at 210 °C) with 30 and 160 µW for 10s integration time. **(d)** Time-dependent SHINERS measurements of Ru/SiO_2@Ag in methanation conditions (50 H_2:5CO:40Ar mL/min at 210 °C) with a 3 s integration time for 360 s. After 180 s, the laser power is changed from 30 to 160 µW, as is indicated by the red arrow. The spectra are normalized to the Ru-CO band at 470 cm^{-1}.

4.3 Conclusions

This chapter aims to provide further insight in the contamination causes of *in situ* SHINERS experiments and put forward a set of practical guidelines to obtain clean substrates. Due to the intense local signal intensity near the plasmonic nanostructures, SHINERS is a technique that will always be prone to contamination. It is therefore of utmost importance to work with clean starting materials and clean reaction materials. However, an optimal SHINERS study should involve the cleaning of the substrate, the gas lines and the reaction products. Therefore, we advise for future experiments to start with a heat treatment of at least 200 °C in an oxygen-rich environment. Since the gas lines have to be cleaned as well, a flushing step of all gases should be considered of at least 15 min. Finally, any contaminants during catalysis that may be found in the CO feed should be removed with a filter. The filter may consist of ZnO, Al_2O_3 and activated coal to remove respectively water, carbonyls, and organics. Furthermore, one should be aware of the Raman laser power effects in combination with the plasmonic nanoparticles. Depending on the electromagnetic enhancement of the SHINs, a

limited laser power or minimized exposure times to prevent carbon growth should be applied. The signal can then be improved by accumulating multiple points with very short exposure times to minimize local sample heating.[21] When these practical steps are followed, a clean(er) SHINER spectrum will be obtained, which can be applied for catalysis research.

4.4 Experimental Section

Chemicals. The following chemicals were purchased and used as received: (3-aminopropyl)trimethoxysilane (APTMS, 97%), sodium silicate solution (27% SiO_2 in 14% NaOH), Rhodamine 6G, $RuCl_3.xH_2O$ (40-49% Ru content), hydroxylamine hydrochloride (>98%) from Sigma Aldrich; ammonia solution (28-30%) from VWR International; $HAuCl_4 \cdot 3H_2O$ (99.99% metals basis) from Alfa Aesar; trisodium citrate dihydrate (99%) from Acros Organics; Hydrochloric acid (Emsure, 37%) from Merck. Demineralized water was purified with a Milli-Q system (18.2 MΩ) before use.

Preparation of Au seeds. 30 mL ultra-pure Milli-Q (mQ) H_2O and 300 µL of 1% (W/V) $HAuCl_4$ was added to a 250 mL round bottom flask with a clean stirring bar. The solution was rapidly brought to a boil in a preheated oil bath, while stirring at 1000 rpm. As soon as the solution started boiling, 0.9 mL of 1% (W/V) trisodium citrate solution was added for 16 nm Au seeds, 0.3 mL citrate was added for 40 nm Au seeds. The flask was removed from heat after 10 min, once nanoparticle maturation was complete as indicated by the color transition from light yellow to red.[26]

Preparation of 80 nm Au nanoparticles. 1.2 mL colloidal solution of 16 nm Au seeds was added to 112 mL mQ water and 2.0 mL 1% (W/V) trisodium citrate was added. Au NPs were grown carefully by adding dropwise 2.4 mL $NH_2OH \cdot HCl$ (10 mM) and 1.7 mL $HAuCl_4$ (1 % W/V) over 30 min. The volume of the droplets was estimated to be around 10 µL. After fully growing the particles, the solution was left stirring for an additional 10 min.[18] The size of the final Au NPs was controlled by varying the volume of seed solution added.

Preparation of 80 nm Ag nanoparticles. 1.7 mL of the colloidal 40 nm Au seeds solution was added to 8.3 mL mQ water. 0.25 mL 1% (W/V) trisodium citrate and 0.368 mL ascorbic acid (50 mM) were added and stirred for 5 minutes. Then, 0.4 mL $AgNO_3$ was added dropwise over the course of 30 minutes. Finally, the mixture was heated at 70 °C for 1 h.

SiO_2 coating of 2 nm. The colloidal solution of Ag NPs was first diluted 2 times in mQ water, and was then mixed with 0.03 mL $NaBH_4$ (100 mM). To both 15 mL Au or Ag NPs, 0.4 mL of a 1.0 mM solution of (3-aminopropyl)trimethoxysilane (APTMS) was added dropwise and stirred for 20 min. Subsequently, 1.4 mL of a sodium silicate solution (diluted to 0.54 wt.% with mQ water and adjusted to pH 10.6-10.8 with HCl) was added dropwise under stirring. The flask was placed in an aluminium starfish at 90 °C and stirred for 40 min. After synthesis, the colloidal

solution was centrifuged and washed 3 times in mQ water and finally stored in 5 mL mQ water in the fridge at 4 °C.[27,48]

SHINERS sample preparation. 0.1 mL SHINs solution was mixed with 10 μL of an aqueous $RuCl_3$ (2 mM) solution and mixed intensely by shaking and ultrasonic treatment. 10 μL of a mixture was then dried under vacuum on a Si wafer. The obtained substrates for catalytic studies with SHINERS were subsequently cleaned using either a heat treatment or UV/O_3. The catalyst substrates were reduced *in situ* by exposure to 10 mL/min H_2 in 40 mL/min Ar at 150 °C in a Linkam THMS600 heating microscope stage.

Characterization. Transmission electron microscopy (TEM) images were recorded using a FEI Tecnai 12 Icor TEM operating at 120 kV. Samples were prepared by drop-casting a colloidal solution on a carbon-coated TEM grid, which were left to dry in air. Raman spectroscopy measurements were performed on a Renishaw InVia Raman microscope, using 785 nm diode laser excitation through a 50x long working distance objective (0.5 NA). All spectra are shown without data processing, unless specified.

Table 4.1. The laser power was controlled with filters that allowed step-wise control of the total transmission of the laser power. The laser power was measured with Ophir Orion power and energy meter. The power density was calculated with the following equation:

$$P(W \cdot cm^{-2}) = \frac{P\ (W)}{\pi \cdot (\frac{\lambda}{2NA})^2} \tag{4.1}$$

	785 nm		**532 nm**	
Transmission (%)	*Power (mW)*	*Power density ($W \cdot cm^{-2}$)*	*Power (mW)*	*Power density ($W \cdot cm^{-2}$)*
100	30.1	$6.22 \cdot 10^6$	37.1	$1.67 \cdot 10^7$
50	14.3	$2.95 \cdot 10^6$	20.5	$9.22 \cdot 10^6$
10	3.59	$7.42 \cdot 10^5$	3.53	$1.59 \cdot 10^6$
5	1.73	$3.57 \cdot 10^5$	1.76	$7.92 \cdot 10^5$
1	0.81	$1.67 \cdot 10^5$	0.32	$1.44 \cdot 10^5$
0.5	0.39	$8.06 \cdot 10^4$	0.16	$7.20 \cdot 10^4$
0.1	0.05	$2.07 \cdot 10^4$	0.03	$1.35 \cdot 10^3$

4.5 Author Contributions and Acknowledgements

This chapter is based on the manuscript: Practical Guidelines for Shell-Isolated Nanoparticle-Enhanced Raman Spectroscopy of Heterogeneous Catalysts, T. Hartman, C.S. Wondergem, B. M. Weckhuysen, *ChemPhysChem* **2018**, 19, 2461-2467

Thomas Hartman and Bert Weckhuysen conceived the research plans. Thomas Hartman executed the experimental work under supervision of Bert Weckhuysen.

The work was written by Thomas Hartman with feedback and corrections by Bert Weckhuysen. Katinka Wondergem contributed to the written text with both textual and scientific input.

The following people are furthermore gratefully acknowledged for their contributions: Hans Meeldijk (UU) is thanked for his contributions to the TEM-EDX measurements, Lennart Weber (UU) is thanked for his contribution to the TGA measurement.

4.6 References

[1] P. G. Etchegoin, E. C. Le Ru, *Phys. Chem. Chem. Phys.* **2008**, *10*, 6079–6089.
[2] H. Knözinger, *Catal. Today* **1996**, *32*, 71–80.
[3] H. Zhang, C. Wang, H. Sun, G. Fu, S. Chen, Y. Zhang, B. Chen, J. R. Anema, Z. Yang, J. Li, Z. Tian, *Nat. Commun.* **2017**, *8*, 15447.
[4] H. Zhang, X.-G. Zhang, J. Wei, C. Wang, S. Chen, H.-L. Sun, Y.-H. Wang, B.-H. Chen, Z.-L. Yang, D.-Y. Wu, J.-F. Li, Z.-Q. Tian, *J. Am. Chem. Soc.* **2017**, *139*, 10339–10346.
[5] T. Hartman, C. S. Wondergem, N. Kumar, A. Van Den Berg, B. M. Weckhuysen, *J. Phys. Chem. Lett.* **2016**, *7*, 1570–1584.
[6] M. Fleischmann, P. J. Hendra, A. J. McQuillan, *Chem. Phys. Lett.* **1974**, *26*, 163–166.
[7] D. L. Jeanmaire, R. P. van Duyne, *J. Electroanal. Chem. Interfacial Electrochem.* **1977**, *84*, 1–20.
[8] M. G. Albrecht, J. A. Creighton, *J. Am. Chem. Soc.* **1977**, *99*, 5215–5217.
[9] M. Moskovits, *J. Chem. Phys.* **1978**, *69*, 4159–4161.
[10] E. M. van Schrojenstein Lantman, T. Deckert-Gaudig, A. J. G. Mank, V. Deckert, B. M. Weckhuysen, *Nat. Nanotechnol.* **2012**, *7*, 583–586.
[11] Z. Zhang, T. Deckert-Gaudig, P. Singh, V. Deckert, *Chem. Commun.* **2015**, *51*, 3069–3072.
[12] C. T. Williams, A. A. Tolia, H. Y. H. Chan, C. G. Takoudis, M. J. Weaver, *J. Catal.* **1996**, *163*, 63–76.
[13] K. N. Heck, B. G. Janesko, G. E. Scuseria, N. J. Halas, M. S. Wong, *J. Am. Chem. Soc.* **2008**, *130*, 16592–16600.
[14] E. M. van Schrojenstein Lantman, P. de Peinder, A. J. G. Mank, B. M. Weckhuysen, *ChemPhysChem* **2015**, *16*, 547–554.
[15] S. Schlücker, *Angew. Chem. Int. Ed.* **2014**, *53*, 4756–4795.
[16] T. Wilke, X. Gao, C. G. Takoudis, M. J. Weaver, *J. Catal.* **1991**, *130*, 62–75.
[17] C. E. Harvey, B. M. Weckhuysen, *Catal. Lett.* **2014**, *145*, 40–57.
[18] J. F. Li, Y. F. Huang, Y. Ding, Z. L. Yang, S. B. Li, X. S. Zhou, F. R. Fan, W. Zhang, Z. Y. Zhou, D. Y. Wu, B. Ren, Z. L. Wang, Z. Q. Tian, *Nature* **2010**, *464*, 392–395.

[19] S.-Y. Ding, J. Yi, J.-F. Li, B. Ren, D.-Y. Wu, R. Panneerselvam, Z.-Q. Tian, *Nat. Rev. Mater.* **2016**, *1*, 16021.
[20] T. Hartman, B. M. Weckhuysen, *Chem. Eur. J.* **2018**, *24*, 3733–3741.
[21] B. S. Yeo, T. Schmid, W. Zhang, R. Zenobi, *Appl. Spectrosc.* **2008**, *62*, 708–713.
[22] T. Kang, S. Hong, Y. Choi, L. P. Lee, *Small* **2010**, *6*, 2649–2652.
[23] S. Linic, U. Aslam, C. Boerigter, M. Morabito, *Nat. Mater.* **2015**, *14*, 567–576.
[24] C. T. Williams, C. A. Black, M. J. Weaver, C. G. Takoudis, *J. Phys. Chem. B* **1997**, *101*, 2874–2883.
[25] C. H. Bartholomew, *Appl. Catal. A Gen.* **2001**, *212*, 17–60.
[26] W. Haiss, N. T. K. Thanh, J. Aveyard, D. G. Fernig, *Anal. Chem.* **2007**, *79*, 4215–4221.
[27] J. F. Li, X. D. Tian, S. B. Li, J. R. Anema, Z. L. Yang, Y. Ding, Y. F. Wu, Y. M. Zeng, Q. Z. Chen, B. Ren, Z. L. Wang, Z. Q. Tian, *Nat. Protoc.* **2013**, *8*, 52–65.
[28] C.-J. Jia, F. Schüth, *Phys. Chem. Chem. Phys.* **2011**, *13*, 2457–2487.
[29] R. L. Craig, A. L. Bondy, A. P. Ault, *Anal. Chem.* **2015**, *87*, 7510–7514.
[30] J. Ofner, T. Deckert-Gaudig, K. A. Kamilli, A. Held, H. Lohninger, V. Deckert, B. Lendl, *Anal. Chem.* **2016**, *88*, 9766–9772.
[31] S. Y. Mar, C. S. Chen, Y. S. Huang, K. K. Tiong, *Appl. Surf. Sci.* **1995**, *90*, 497–504.
[32] G. Gouadec, P. Colomban, *Prog. Cryst. Growth Charact. Mater.* **2007**, *53*, 1–56.
[33] E. V. Formo, Z. Wu, S. M. Mahurin, S. Dai, *J. Phys. Chem. B* **2011**, *115*, 9068–9073.
[34] R. J. Peláez, J. P. Espinós, C. N. Afonso, *Nanotechnology* **2017**, *28*, 175709.
[35] F. Thibault-starzyk, E. Seguin, S. Thomas, M. Daturi, H. Arnolds, D. A. King, *Science* **2009**, *324*, 1048–1051.
[36] P. F. McMillan, R. L. Remmele, *Am. Mineral.* **1986**, *71*, 772–778.
[37] P. Munnik, P. E. De Jongh, K. P. De Jong, *Chem. Rev.* **2015**, *115*, 6687–6718.
[38] L. H. Leung, M. J. Weaver, *Langmuir* **1988**, *4*, 1076–1083.
[39] M. A. Barteau, J. Q. Broughton, D. Menzel, *Surf. Sci.* **1983**, *133*, 443–452.
[40] G. H. Yokomizo, C. Louis, A. T. Bell, *J. Catal.* **1989**, *120*, 1–14.
[41] A. C. Ferrari, *Solid State Commun.* **2007**, *143*, 47–57.
[42] A. M. Ricks, Z. E. Reed, M. A. Duncan, *J. Mol. Spectrosc.* **2011**, *266*, 63–74.
[43] H. Stammreich, K. Kawai, Y. Tavares, P. Krumholz, J. Behmoiras, S. Bril, *J. Chem. Phys.* **1960**, *32*, 1482–1487.
[44] H. Stammreich, K. Kawai, O. S. W. Sala, P. Krumholz, *J. Chem. Phys.* **1961**, *35*, 2168–2174.
[45] R. Smit, C. J. Eijkhoudt, A. J. Van Dillen, J. W. Geus, *Prepr. Pap. - Am. Chem. Soc., Div Fuel Chem.* **1999**, *44*, 119–123.

[46] G. E. Walrafen, M. S. Hokmabadi, N. C. Holmes, *J. Chem. Phys.* **1986**, *85*, 771–776.
[47] E. Smith, G. Dent, *Modern Raman Spectroscopy—A Practical Approach*, Wiley, Chichester, **2005**.
[48] C. Y. Li, M. Meng, S. C. Huang, L. Li, S. R. Huang, S. Chen, L. Y. Meng, R. Panneerselvam, S. J. Zhang, B. Ren, Z. L. Yang, J. F. Li, Z. Q. Tian, *J. Am. Chem. Soc.* **2015**, *137*, 13784–13787.

5

Extrudate Sensors for Catalysis

Insights into the relationship between catalytic activity and catalyst structure, including the underlying reaction mechanism, are required for the development of improved catalysts. For industrial catalysis, extrudate catalysts are widely implemented for their high mechanical strength and to minimize pressure drops. In this chapter, we present a unique set of catalyst extrudate sensors that allow for the simultaneous detection of local temperature and surface species. The extrudate sensor operates two-fold: 1. The temperature is probed up to 600 °C as a function of the applied reactions conditions with an accuracy of 0.3 °C (at 300 °C) using Yb^{3+},Er^{3+} co-doped $NaYF_4$@SiO_2 core/shell nanoparticles; and 2. Surface species are detected using the strongly localized Raman signal enhancement of Au@SiO_2 and Au@TiO_2 core-shell nanoparticles. The principle of this sensing approach has been explored for the characterization of the CO hydrogenation reaction over supported Rh and RhFe catalysts. Luminescence thermometry demonstrated a mismatch between the set temperature and the actual temperature. The local temperature variations could go up to 40 °C, depending on the gas feed. Furthermore, a series of experiments in which the extrudate and catalyst NP composition were varied resulted in the identification of a previously unobserved species on the Rh/SiO_2 interface and allowed for the investigation of the reaction pathways in the investigated catalytic systems. The implementation of this extrudate catalyst sensor as characterization tool provides a unique approach towards the further understanding of the relevant parameters in catalysis.

5.1 Introduction

The design of the ideal heterogeneous catalyst requires detailed knowledge of the interaction with its environment.[1–3] Since chemical reactions over solid catalysts are dictated by their surface properties, a variety of characterization techniques are required to probe the catalyst-reactant interface. To correlate catalyst composition and interfacial interactions to catalyst performance (e.g. selectivity) it is crucial to monitor the catalytic system under *in situ* or *operando* conditions.[4–6]

A new generation of spectroscopic techniques therefore focuses on higher sensitivity and improved spatial and temporal resolution. An example of a recent technique is shell-isolated nanoparticle-enhanced Raman spectroscopy (SHINERS).[7,8] The conduction electrons at the surface of the metal nanoparticles (NPs) resonate in a wide spectral region around the laser wavelength, resulting in a strong enhancement of the Raman signal.[9] The isolating SiO_2 shell ensures a stable nanostructure for characterization of the structure of the catalyst, as well as adsorbed species up to 400 °C.[10] The advantage of using Raman-based spectroscopic techniques in addition to, for example, infrared (IR) spectroscopy, is the ability to observe vibrations in the low wavenumber regime and characterize direct metal-adsorbate interactions. However, the yield of shell-isolated nanoparticles (SHINs) in a typical synthesis is usually not sufficient for practical *operando* experiments in heterogeneous catalysis. *In situ* experiments are therefore carried out separately from product analysis on similar bulk catalysts.[11]

Another recent invention involving NP sensors for heterogeneous catalysis, is bandshape luminescence thermometry.[12,13] Bandshape luminescence thermometry, a technique with many applications ranging from catalysis[14] to bio-imaging,[15] relies on temperature-dependent luminescence in which the ratio between two (or more) emission peaks changes with temperature. Temperature, in addition to catalyst structure and composition, plays an important role for the activity and selectivity of catalytic reactions.[16] To fully correlate catalytic processes to the conditions, it is important to monitor reaction temperature on the same length scale as XAS, IR or SHINERS, i.e. measuring the temperature of an individual catalyst particle. Temperature sensing on the catalyst particle level still proves to be difficult. A few temperature measurements have been performed during catalytic reactions,[17] mainly using nuclear magnetic resonance[18] (NMR), black body radiation[19,20] or by the use of multiple thermocouples.[21] Although using multiple thermocouples can give a general idea of temperature gradients in chemical reactors, monitoring temperatures on smaller length scales is still rather difficult. In addition, thermocouples can disturb a reactor bed and non-invasiveness cannot be guaranteed. IR-thermography is difficult to implement if light absorbing species are present, while the interpretation of NMR-thermometry is often cumbersome and depends on the concentration of the probed species.[18] In order to monitor temperature using a non-invasive method with sufficient spatial resolution, bandshape luminescence thermometry can be exploited.[12,13]

In this chapter, we have developed a set of bifunctional extrudate sensors that can be practically implemented in a reactor bed for both luminescence thermometry and SHINERS (Figure 5.1). SHINs are assembled on the exterior of SiO_2 and TiO_2 extrudates to obtain extrudate sensors with Raman signal enhancement. We furthermore demonstrate that these SHINs can be assembled over SiO_2 extrudates containing Yb^{3+},Er^{3+} co-doped $NaYF_4$@SiO_2 core/shell nanoparticles, which are exploited for their temperature-dependent luminescence of the Er^{3+} dopant.[22,23] The $^4S_{3/2}$ and $^2H_{11/2}$ excited states are separated by an energy difference of ca. 700 cm^{-1} (or several kT at room temperature)[24] and the population of the energy levels is governed by Boltzmann statistics,[25] resulting in unique temperature-dependent luminescence, which can be exploited for thermometry.

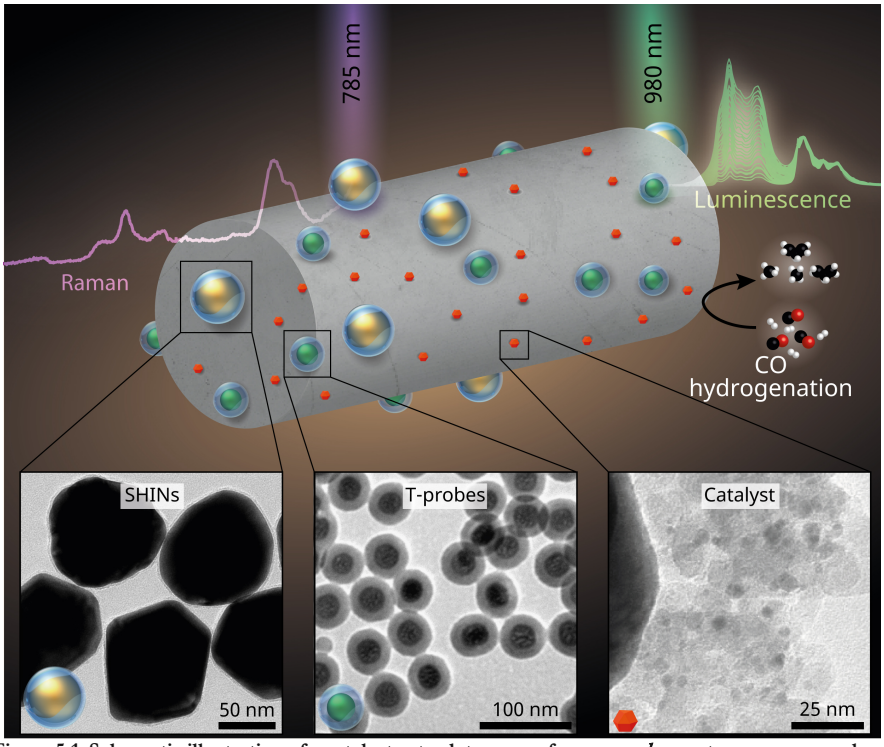

Figure 5.1. Schematic illustration of a catalyst extrudate sensor for *operando* spectroscopy research. The grey SiO_2-extrudate carrying Au@SiO_2 SHINs (gold spheres), Rh catalysts (red particles) and $NaYF_4$@SiO_2 temperature sensors (green spheres) to simultaneously measure temperature and surface species using luminescence thermometry and SHINERS. TEM micrographs of the prepared Au@SiO_2 SHINs (left inset), $NaYF_4$@SiO_2 temperature sensors (middle inset), and Rh catalyst NPs (right inset).

These extrudate sensors are applied for *operando* studies of the CO hydrogenation over Rh and RhFe. In this reaction, syngas (a CO/H_2 mixture) is converted into hydrocarbons, such as alkanes, alkenes and alcohols over catalyst NPs that were obtained with a wet impregnation method. SHINERS allows for the detection of adsorbed carbonyl species, while luminescence thermometry gives local temperature readouts at the same time. The products of CO hydrogenation (i.e. alkanes, alkenes, alcohols, CO_2 and H_2O) were monitored with online MS.

In the first experiments, we demonstrate that the local temperature sensors allow for precise temperature read-outs within a single catalyst particle in a reactor bed with an accuracy of 0.3 °C at 300 °C. The importance of the temperature measurements of the catalytic system itself was demonstrated by monitoring the catalyst temperature during CO hydrogenation, where a mismatch was observed between the set temperature and the local temperature obtained with luminescence thermometry. Moreover, upon changing the CO/H_2 ratio in the gas feed at a constant flow speed, temperature differences of up to 40 °C were observed. The main reason for the temperature mismatch was accredited to heat dissipation in the reactor by H_2. These results show that the local temperature can significantly differ from temperature readouts of 'bulk' methods, emphasizing the need for local temperature measurements during *operando* experiments.

The strong localized sensitivity of SHINERS was exploited for probing the metal-support interfaces during the CO hydrogenation. In the initial *operando* experiments, using the multifunctional extrudate sensors on Rh/SiO_2, the increase of catalytic activity at elevated temperatures was directly correlated with the SHINER spectra under *operando* conditions and was further supported by FT-IR measurements. In addition, the applicability of the extrudate sensors was tested more in-depth by varying the composition of the catalyst NPs, SHINs and extrudate. Using SHINERS, a reaction intermediate was identified which was previously not observed with conventional methods (e.g. IR spectroscopy). The reaction intermediates, in combination with isotope labeling experiments, showed different reaction pathways that were correlated to the product selectivity.

The results presented show the clear potential for luminescence thermometry in combination with other diagnostic tools, such as SHINERS. These tools can be further complemented by the incorporation of e.g. UV-Vis spectroscopy. The potential to simultaneously monitor crucial parameters such as surface species, at the exact local temperature, under reaction conditions at the single catalyst particle level allows for new insights to be obtained for catalytic reaction mechanics, as showcased here for catalytic CO hydrogenation.

5.2 Results and Discussion

To enable SHINERS measurements with simultaneous luminescence thermometry, mm-sized catalyst extrudates containing $NaYF_4@SiO_2$ were prepared with ca. 1:1 weight ratio $NaYF_4@SiO_2$ and SiO_2 binder and subsequently

$Au@SiO_2$ SHINs were deposited on the exterior surface of the extrudate followed by a wet-impregnation with $RhCl_3$ and subsequent oxidation and reduction to form 1 wt.% Rh/SiO_2. The experimental details of the prepared system can be found in the Experimental Section as well as in previous work.[7,10,14,26] Figure 5.1 shows a schematic representation of the prepared sensor system in which SHINERS (purple spectrum) and luminescence thermometry (green spectra) are combined.

The quasi-spherical $Au@SiO_2$ SHINs (yellow spheres, D = 88 ± 7.8 nm; SiO_2 = 2.6 ± 0.4 nm) used for SHINERS are shown in the left inset of Figure 5.1. The $NaYF_4$ cores (green spheres, D = 25.4 ± 1.4 nm) of the $NaYF_4@SiO_2$ NPs (D = 45.9 ± 1.7 nm) are doped with 18% Yb^{3+} and 2% Er^{3+} and are shown in the middle inset of Figure 5.1. The Er^{3+} dopant is responsible for the temperature-dependent luminescence in the visible region (λ_{em} = 500–570 nm), while the Yb^{3+} dopant allows for efficient upconversion excitation[27] in the infrared region (λ_{exc} = 980 nm). The wet-impregnation of the Rh catalyst (red particles, right inset of Figure 5.1) was monitored with SHINERS (in the Experimental Section) and the deposition of the $Au@SiO_2$ SHINs and the presence of $NaYF_4@SiO_2$ were confirmed by scanning electron microscopy (SEM) images of the extrudates (Figure 5.2a). Rh NPs were not observed in the SEM images, most likely due to the small size of the Rh NPs. In order to confirm the presence of all the elements present within the nanostructures, the catalyst extrudates were investigated using STEM-EDX and the results are shown in Figure 5.2b - f. In these images, we can see that all the materials are present and the Rh catalysts are in close contact with the $Au@SiO_2$ SHINs.

In the TEM images, $Au@SiO_2$, $NaYF_4@SiO_2$, Rh and SiO_2 (from the extrudate) can be observed, indicating that all different parts of the system have

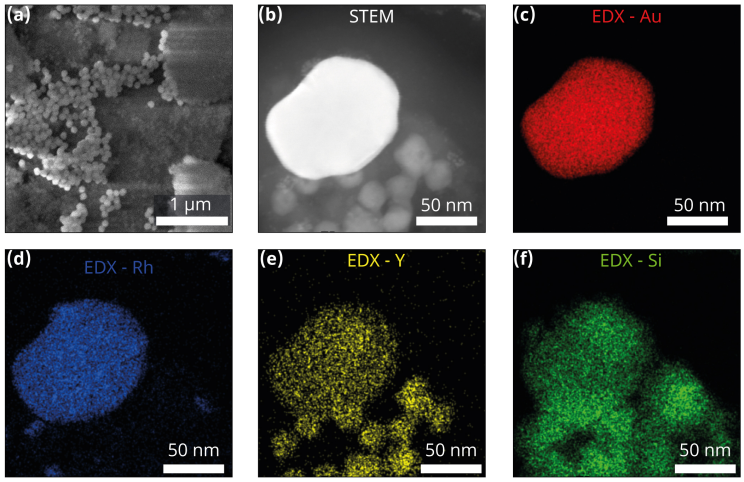

Figure 5.2. Scanning Electron microscopy studies of extrudate sensors. (a) SEM image of an extrudate sensor after CO hydrogenation. **(b)** STEM image of the image of an extrudate sensor after CO hydrogenation. **(c)** STEM-EDX mapping the presence of Au. **(d)** STEM-EDX mapping the presence of Rh. **(e)** STEM-EDX mapping the presence of Y.**(f)** STEM-EDX mapping the presence of Si.

been incorporated successfully. The prepared particles, shown in Figure 5.1, can now be used to monitor catalysis by performing SHINERS, luminescence thermometry as well as on-line mass spectrometry (MS). Using this *operando* spectroscopy approach, surface structures, the local temperature and catalytic activity can be monitored simultaneously and insight into the reaction mechanism can be obtained.

To monitor the temperature using temperature-dependent luminescence, the unique energy levels of the Er^{3+} dopant ions in the $NaYF_4$ were exploited. The three relevant energy levels for this temperature-dependent luminescence are shown in Figure 5.3a. After excitation to a higher lying excited state, the system quickly relaxes to the $^2H_{11/2}$ and $^4S_{3/2}$ levels of Er^{3+}. The energy difference between these excited states is ca. 700 cm^{-1}, or several kT at room temperature. Fast non-radiative relaxation between these thermally coupled states results in a population distribution between the excited states, governed by Boltzmann statistics. Figure 5.3b shows the temperature-dependent luminescence from transitions of the $^2H_{11/2}$ and $^4S_{3/2}$ excited state to the $^4I_{15/2}$ ground state. Higher temperatures result in more thermal energy and a higher population of the higher energy excited state, $^2H_{11/2}$. By increasing the temperature with intervals of 25 K from 298 K/25 °C up to 873 K/600 °C (black to orange) it can be observed in Figure 5.3b that the ratio between the two emitting states changes drastically. The Boltzmann behavior (inset Figure 5.3c), where ΔE is the energy difference between the excited states, C a temperature-independent constant, I_i is the emission intensity from state i, k is the Boltzmann constant and T is temperature, can be exploited to monitor

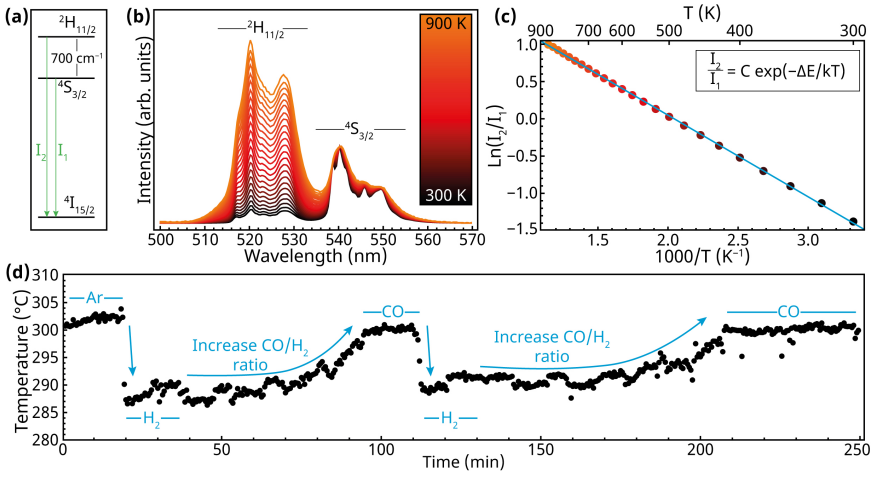

Figure 5.3. Temperature-dependent luminescence of $NaYF_4$:Er^{3+},Yb^{3+}. (a) The energy levels $^2H_{11/2}$ and $^4S_{3/2}$ of Er^{3+} are thermally coupled states, resulting in **(b)** temperature-dependent luminescence which is governed by Boltzmann statistics. **(c)** Due to the Boltzmann statistics as described in the inset, the logarithm of the luminescence intensity ratio plotted versus 1000/T yields a linear fit. The linear fit can be used to monitor local temperatures at the single catalyst level. **(d)** The local temperature varies with gas composition with lower temperatures at higher H_2 gas pressures.

temperatures accurately by plotting the logarithm of the luminescence intensity ratio (I_2/I_1) vs. reciprocal temperature ($1000/T$), as shown in Figure 5.3c.

The datapoints show a clear linear correlation between the logarithm of the luminescence intensity ratio vs. reciprocal temperature and the linear fit (cyan line) shows good agreement ($r^2 = 0.999$). The slope of the fit should correspond to $\Delta E/k$, it was found that ΔE was in good agreement with the value observed in emission spectra (735 vs 690 cm^{-1}). Furthermore, temperature-dependent luminescence characterization of the $NaYF_4$ cores, $NaYF_4$@SiO_2 core/shells and $NaYF_4$@SiO_2 incorporated extrudates all showed similar behavior. These measurements show that the temperature probes can be used to monitor temperature up to at least 900 K by exploiting the calibration curve shown in Figure 5.3c.

The possibility to monitor the reaction temperature with luminescence thermometry in catalytically relevant conditions is shown in Figure 5.3d. Here, gases with different compositions (Ar, H_2 and CO) are introduced with a constant flow speed of 20 mL min^{-1} at a setpoint of 350 °C. However, the local temperature at the catalyst reached only ca. 300 °C. This large offset between catalyst and set temperature is due to the spatial separation of the temperature feedback of the reactor inside the heating elements and the actual catalyst bed. The difference of ca. 50 °C can influence the catalytic reactivity, resulting in a different productivity and selectivity.[28] Furthermore, it was observed that the local temperature is greatly dependent on the gas composition inside the reactor. Gases with low thermal conductivity, such as Ar (22.6 mW m^{-1} K^{-1} at 400 K) and CO (32.3 mW m^{-1} K^{-1} at 400 K), have a smaller influence on the observed temperature. Upon introduction of H_2, the temperature decreases drastically due to the high thermal conductivity of H_2 (230.4 mW m^{-1} K^{-1} at 400 K).[29] These experiments were repeated in Figure 5.4 at a different reaction temperature of ca. 350 °C (setpoint of ca. 400 °C) and reactor loading, here we found that the temperature mismatch could go up to 40 °C depending on the gas composition.

The temperatures obtained under pure Ar or CO atmosphere are very stable, and the temperature during CO flow was therefore evaluated to determine the accuracy of the measurements. The standard deviation was found to be 0.3 °C by

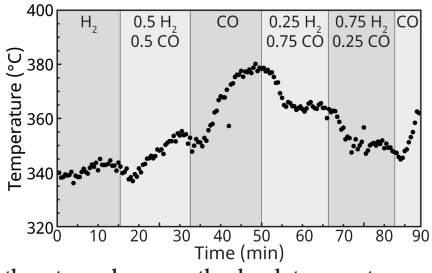

Figure 5.4. Influence of the atmosphere on the local temperature as probed by *operando* luminescence thermometry with on-line mass spectrometry.

evaluating the temperature obtained under pure CO. This demonstrates the very accurate temperature measurements, even at 300 °C.

Furthermore, the temperatures obtained are the local temperatures at the catalyst and take into account temperature fluctuations due to reactor heterogeneities, heat dissipation and possible exo- and endothermic effects. The temperature measurements in a H_2-rich atmosphere show fluctuations. The fluctuations are most likely due to the turbulent flow of the gas since the gas composition is alternated in several steps from pure H_2 to pure CO. A good indication of the temperature accuracy with luminescence thermometry can be obtained by evaluating the temperature output at constant CO atmosphere.

To investigate the effect of temperature on the CO adsorption and the related reaction steps in CO hydrogenation, luminescence thermometry, SHINERS and on-line MS measurements were performed simultaneously. Rh is an interesting metal for the study of CO hydrogenation because it can produce both hydrocarbons, alcohols and other oxygenates, depending on the experimental conditions.[30] Its catalytic properties are often ascribed to the position of Rh in the periodic table. On the left side of Rh and above, elements such as Fe and Co dissociate CO to form hydrocarbons in Fischer-Tropsch synthesis. In contrast, on the right and below, Pd and Pt do not dissociate CO and produce methanol.[30] The selectivity of CO hydrogenation over Rh depends heavily on the preparation method and applied conditions and can therefore be exploited for tuning the product distribution. Rh/TiO_2, for example, is known to produce longer chain hydrocarbons in comparison with Rh/SiO_2,[31] and the selectivity towards alcohols can be greatly improved by the alloying with Fe.[32] We have therefore prepared a set of catalyst extrudates: SiO_2 extrudates containing Rh catalyst NPs, $Au@SiO_2$ SHINs and T-probes (Rh/SiO_2-sensors), TiO_2 extrudates containing Rh catalyst NPs, $Au@TiO_2$ SHINs and T-probes (Rh/TiO_2-sensors) and SiO_2 extrudates containing RhFe catalyst NPs, $Au@SiO_2$ SHINs and T-probes ($RhFe/SiO_2$-sensors). With MS we verified the selectivity of these catalysts under the same reaction conditions at 250 °C with 2.5 mL/min CO and 5 mL/min H_2 (Figure 5.5).

With these observations, it is interesting to find out if SHINERS can contribute to the understanding of the differences between these catalytic systems. We first extensively demonstrate combined luminescence thermometry and SHINERS for the *operando* study of CO hydrogenation over Rh/SiO_2 catalysts (Figure 5.6a). Figure 5.6b shows the production of methane and propane, (CH_4 and C_3H_8), over time (green lines), while heating up the systems to different temperatures (gray boxes). Note that the mentioned temperatures were all measured by luminescence thermometry. The production of CH_4 and C_3H_8, CO_2 and H_2O was determined by integrating the corresponding peaks (m/z = 15, 38–42, 44 and 18, respectively) from the mass spectra. The C_2H_6 production could not be determined reliably, as the MS peaks of CO and C_2H_6 overlapped.

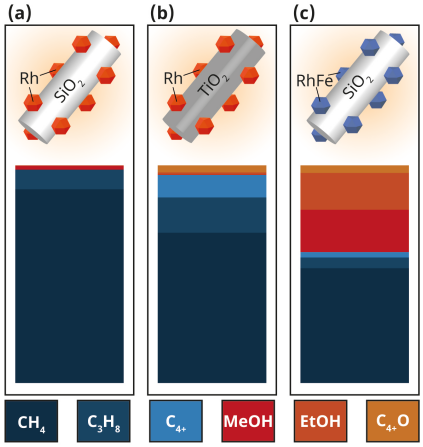

Figure 5.5. Product distribution during the CO hydrogenation at 250 °C. (a) Rh/SiO_2-sensors **(b)** RhTiO_2-sensors and **(c)** RhFe/SiO_2-sensors. The product distribution is based on the MS signal intensity. CH_4 (15 *m/z*), C_3H_8 (41 *m/z*), MeOH (31 *m/z*), EtOH (45 *m/z*), C_{3+} (55, 70, 84 *m/z*), C_{3+} Oxygenates (58, 78 *m/z*).

Figure 5.6b shows that the increase in temperature from RT to 348 °C resulted in a higher catalytic activity as expected for the Rh-catalyzed CO hydrogenation.[28] Furthermore, a low conversion to CO_2 is observed starting at 171 °C and remains constant at 213 °C and above. The H_2O production is, as expected, directly correlated to hydrocarbon production. At the same time, SHINER spectra were obtained at all temperatures, and the increase in catalytic activity can be correlated to structural changes at the catalyst surface. The SHINER spectra in Figure 5.6c show a peak in the lower wavenumber regime at 480 cm^{-1} with a shoulder at 410 cm^{-1}, which are assigned to the stretching vibrations of, respectively, linearly (Rh–CO) and bridged (Rh_2–CO) adsorbed carbonyls.[33,34] The activity of Rh in CO hydrogenation is sometimes associated with the ratio of bridged vs. linear carbonyls,[35] with the activity increasing for an increased amount of bridged carbonyls. Other work demonstrated that single site Rh and Rh^{x+} were the most important for CO insertion and blocking the bridged CO sites led to an improved selectivity towards longer oxygenates.[36,37]

The ratio between the two peaks changes with temperature and is plotted in Figure 5.6d with orange dots; the dashed line is added as a guide for the eye. With increasing temperature, the intensity of the ν(Rh–CO) at 480 cm^{-1} decreases, whereas the intensity of the ν(Rh_2–CO) at 410 cm^{-1} remains similar. At 260 °C, when the first reaction products are observed, the ν(Rh_2–CO)/ν(Rh–CO) intensity ratio reaches the ratio of 0.8, and does not depend on temperature anymore. This observation is in line with previous works[35–37] and was confirmed using IR microspectroscopy; the signal intensity of the linear carbonyls decreases for active Rh catalysts, indicating that these species are reacting on the surface.

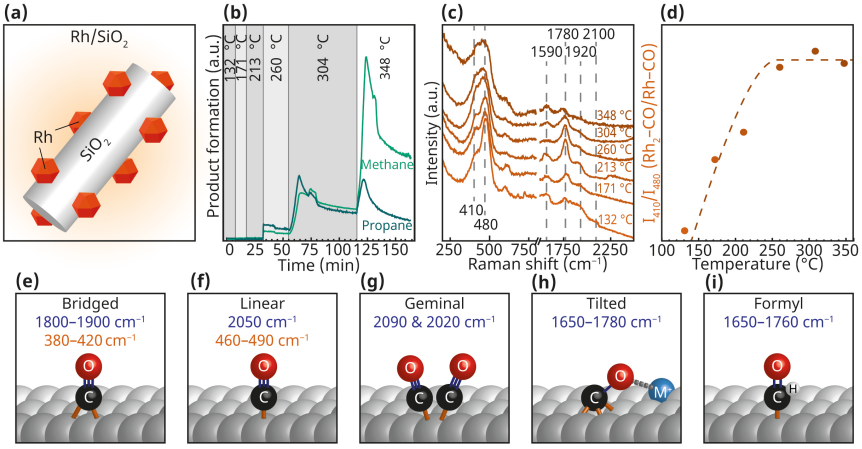

Figure 5.6. Combined *operando* luminescence thermometry with SHINERS and on-line MS. (a) The Rh/SiO_2 catalyst investigated in this experiment **(b)** Methane/Propane production over time (green lines) while continuously monitoring temperature using luminescence thermometry (gray areas) **(c)** SHINER spectra obtained at the temperatures that were determined by luminescence thermometry, specific Raman shifts for adsorbed CO are highlighted with dashed lines. **(d)** The ratio between the intensity of the SHINERS (orange dots + dashed line) for bridged CO and linear CO. **(e–i)** Structures of adsorbed CO on Rh surfaces with typical vibration energies shown in blue and orange.[38]

Furthermore, in the spectral region between 1500–2500 cm^{-1}, a set of bands is observed that are associated with the C–O stretching vibrations of adsorbed carbonyls and intermediates/reaction products (Figure 5.6e - i). Formate species show a peak at 1590 cm^{-1}, broad features of bridged and linear CO are observed between 1800–2000 cm^{-1} and in addition an unknown feature at 1780 cm^{-1} is observed. The intensity of the unknown band increases to a maximum at 213 °C and subsequently decreases at higher temperatures. Two assignments are possible for the band at 1780 cm^{-1}: tilted carbonyls ($Rh_3C–O–M^+$)[39] or adsorbed formyl/aldehyde[38] species (Figure 5.6h-i). In previous work, tilted CO has only been observed with IR spectroscopy on SiO_2-supported Rh catalysts with the presence of a metal oxide promotor.[40] We have confirmed this in our lab by FT-IR microscopy experiments on the same extrudates. The presence of formyls thus seems more likely and indicates that the pathway to alkanes involves hydrogen-assisted CO dissociation, as shown in Figure 5.7a (pathway 2). Furthermore, the maximum conversion to propane during CO hydrogenation was found to coincide with the strongest intensity of the 1780 cm^{-1} band at 260 °C, indicating that the species associated with the 1780 cm^{-1} band potentially plays an important role in the C–C coupling or CO insertion mechanism.

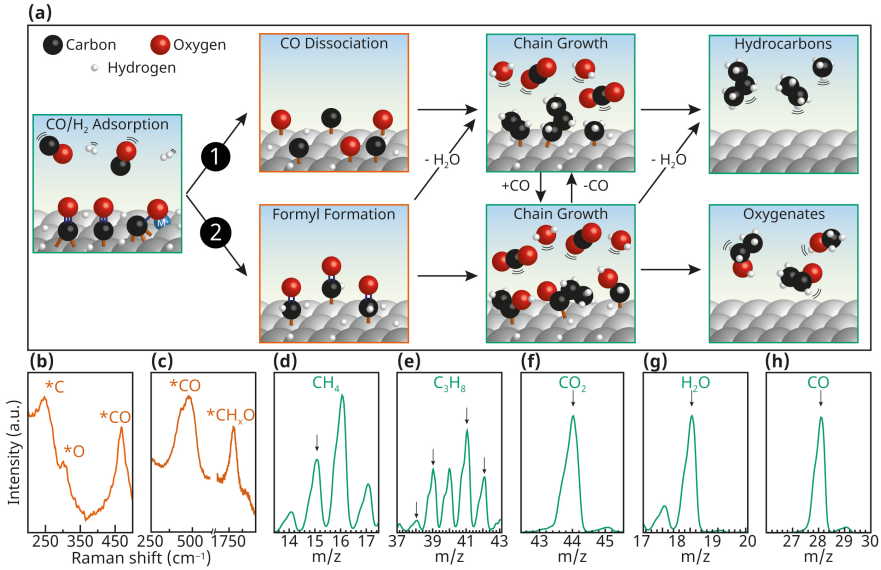

Figure 5.7. Rh-catalyzed CO hydrogenation pathways. (a) The CO hydrogenation pathways with the compounds observed during *operando* measurements; highlighted in green for compounds that are observed with on-line MS, highlighted in orange for compounds that are observed with SHINERS. **(b–c)** The SHINER spectra of the respective adsorbed species. **(d–h)** The MS spectra of the specific regions where the products are detected.

Several adsorbates, intermediates and products that appear in the mechanism can be distinguished using SHINERS (orange, Figure 5.7b - c) and MS (green, Figure 5.7d – h), and together can be used to form a better understanding of the involved pathway. With MS, only trace amounts of alcohols or oxygenates were observed in the products over the Rh/SiO_2 catalysts in this experiment, indicating that the reaction most likely follows pathway 1 in Figure 5.7a, which involves direct CO dissociation. However, because tilted carbonyls are usually observed with SHINERS only when a metal oxide promotor is added, the most likely assignment of the band at 1780 cm^{-1} seems to be formyl or aldehyde species. The reaction pathway should then include pathway 2, with crossover between pathway 1 and 2. This would involve the hydrogen-assisted CO dissociation through formyl species, with the subsequent removal of water so that light alkanes are finally produced.

As was observed in Figure 5.5a and Figure 5.6, Rh/SiO_2 catalysts produce mostly short-chain alkanes, which would make the observation of formyl species rather unlikely, but not impossible. In addition, the selectivity of CO hydrogenation to longer chain hydrocarbons over Rh was greatly improved by changing the support material to TiO_2 (Figure 5.5b). Furthermore, by alloying Rh with Fe, the selectivity was shifted towards the synthesis of oxygenates (Figure 5.5c).

This product distribution should be reflected in the SHINER spectra of the respective catalysts, and could give insights in the nature of the SHINERS signal at below 1800 cm^{-1}. For the purpose of studying the support effects of CO

hydrogenation over Rh, Au@TiO_2 NPs were synthesized (Chapter 2). The support material is expected to have an impact on this typical observation, since reducible support materials tend to have a stronger interaction with the oxygen atom in the tilted conformation of CO. Furthermore, RhFe catalysts were prepared over SHINERS substrates to study the effect of the metal alloying. The synthesis of the three types of catalysts were followed with *in situ* SHINERS, and can be found in the Experimental Section.

The three catalysts were compared under the same CO hydrogenation conditions at 250 °C. The bands of adsorbed carbonyls in the SHINER spectrum of Rh/TiO_2 are very similar to that of Rh/SiO_2, although CO seems to interact slightly stronger as is indicated by the higher energy of the Rh-C stretching vibrations (Figure 5.8a-b). An additional band at 690 cm^{-1} is observed in all the spectra of Rh/TiO_2, and originates from the amorphous TiO_2 shells of Au@TiO_2.[10,41] The RhFe/SiO_2 catalyst, on the other hand, contrasts strongly with the other two catalysts as there is hardly any band observed around 1800 cm^{-1} (Figure 5.8c). This definitely contradicts the conclusion that these sub 1800 cm^{-1} species found on Rh/SiO_2 are related to adsorbed formyls. If they are observed on any catalyst, it should be on RhFe alloys, as a precursor to alcohols and other oxygenates. Although we do not observe formyl species over RhFe/SiO_2 the observation of mostly linear Rh–CO species confirms its importance for the CO insertion reaction.[35]

In order to obtain a definite conclusion about the involved reaction pathway, the origin of the peak at 1780 cm^{-1} was further investigated using isotopic labelling. To distinguish between tilted carbonyl and formyl species, experiments with deuterium (D_2) isotopes were performed to validate the previous findings and assign the 1780 cm^{-1} band. As mentioned above, the peak at 1780 cm^{-1} can be assigned to either tilted carbonyl species ($Rh_3C–O–M^+$) or adsorbed formyls. If adsorbed formyls are present, the C–O stretching vibration is directly influenced by the connected hydrogen. Replacing H_2 with D_2 in the reaction should then result in a redshift of the Raman signal by 10–20 cm^{-1} (Figure 5.8d).[42,43] In contrast, when the unknown band is related to a tilted carbonyl, no shift in the band position is expected. Therefore, H_2, CO and D_2 were introduced in an alternating fashion at 250 °C, when the 1780 cm^{-1} band was at its most intense (Figure 5.8e).

The effect of H_2 on adsorbed carbonyls was directly observed with the increase of the peak intensity at 1795 cm^{-1} and a concurrent red shift to 1767 cm^{-1}. A subsequent introduction of CO returned the band to its initial position. When D_2 was introduced, the unknown band increased in intensity again and shifted to the same position as for H_2 (Figure 5.8f). These results indicate that the band at 1780 cm^{-1} is not a formyl or aldehyde species, but a tilted carbonyl. Although this species has not been observed using IR, a logical assignment of the tilted carbonyl is a CO species at the Rh/SiO_2 interface. Recently, it has been found that $SiO–H^{\delta+}$ species can form at the interface of metal-silica interfaces upon H_2 dissociation and affect

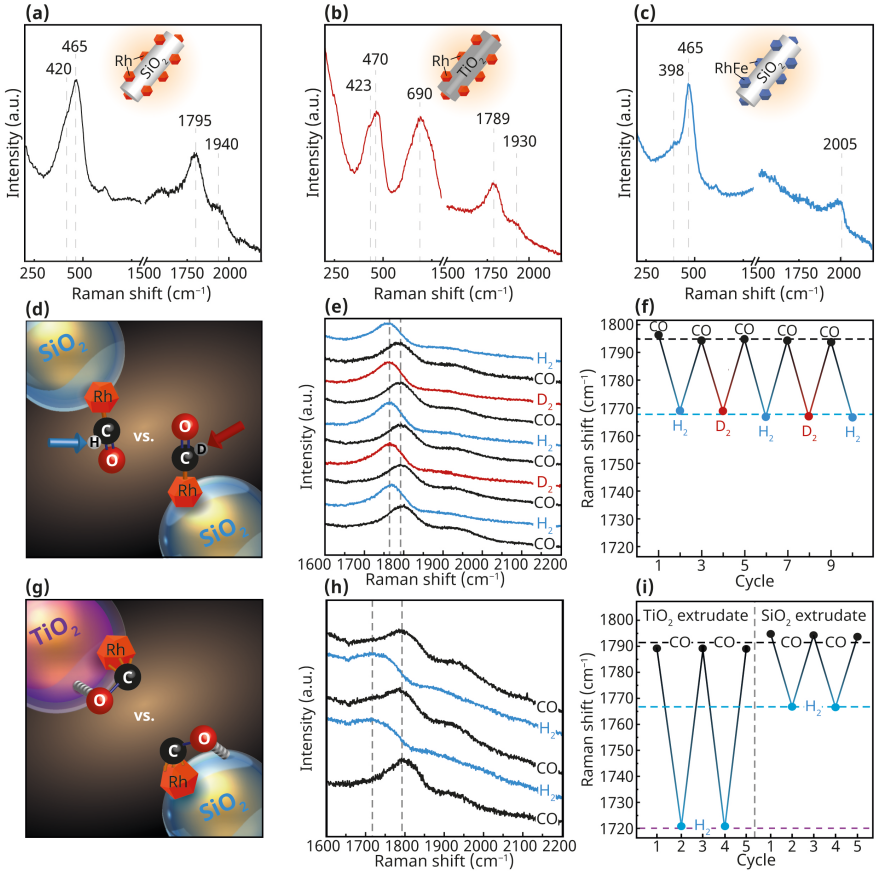

Figure 5.8. Catalyst-support interface probed with SHINERS during CO hydrogenation with 1:2 CO:H_2 at 250 °C. (a) SHINER spectra of Rh/SiO_2 obtained with Au@SiO_2 NPs. **(b)** SHINER spectra of Rh/TiO_2 obtained with Au@TiO_2 NPs. **(c)** SHINER spectra of RhFe/SiO_2 obtained with Au@SiO_2 NPs. **(d)** Molecular structures of formyl species adsorbed on Rh catalysts over Au@SiO_2 SHINERS substrates. **(e)** SHINER spectra of CO hydrogenation at 250 °C over Rh/Au@SiO_2 with alternating introduction of CO, H_2 and D_2. **(f)** The SHINERS peak locations of the unknown band under the specified conditions. **(g)** Molecular structures of tilted carbonyls adsorbed on Rh catalysts over Au@SiO_2 and Au@TiO_2 SHINERS substrates. **(h)** SHINER spectra of CO hydrogenation at 250 °C over Rh/Au@TiO_2 with alternating introduction of CO and H_2. **(i)** The SHINERS peak locations of the unknown band under the specified conditions, as observed over Au@TiO_2 and Au@SiO_2.

the catalytic properties.[44] The strong local sensitivity of SHINERS would explain why it can be observed in the Raman experiments, but is not observed with IR.

A similar experiment consisting of the altered introduction of CO and H_2 was therefore performed on Rh/Au@TiO_2 as well to verify the strength of the interaction of the support (Figure 5.8g). The SHINER spectra of adsorbed carbonyls on SiO_2 and TiO_2 are very similar. However, after switching to a pure H_2 atmosphere, the tilted carbonyl is redshifted much stronger to 1720 cm^{-1} (Figure 5.8h). The band shifts by ca. 70 cm^{-1}, which is a significant different in

comparison to Rh/Au@SiO_2, which shifted by 25 cm^{-1} (Figure 5.8i). These results confirm the stronger interaction of the TiO_2 support material during the catalytic reaction.[45] Furthermore, we can use the knowledge of this interfacial chemistry to explain the higher selectivity towards longer hydrocarbons in the CO hydrogenation for Rh/TiO_2 catalysts.

5.3 Conclusions

Catalyst extrudate sensors were developed for use in applied catalysis that allow for the simultaneous *operando* monitoring of reaction temperature with luminescence thermometry and surface species with SHINERS. They were applied for the study of CO hydrogenation over a Rh/SiO_2 catalyst. The extrudates consisted of SiO_2 and various nanoparticles, namely a Rh catalyst, Au@SiO_2 SHINs and $NaYF_4$@SiO_2 T-probes. With SHINERS, various surface species were observed under CO hydrogenation conditions up to 350 °C that were used for researching the CO hydrogenation reaction. Coupled to the product analysis with on-line MS, a reaction pathway for CO hydrogenation was explored. With the *operando* studies, the active carbonyl species for hydrogenation was found to be linearly adsorbed CO. In addition, a tilted carbonyl was surprisingly observed in the SHINER spectra and was related to Rh/SiO_2 interfacial structures. The interface between Rh NPs and the support was further investigated over Rh/TiO_2 and RhFe/SiO_2 catalysts, where it was found that the support interaction was stronger on Rh/TiO_2, resulting in more CO dissociation (pathway 1) and a higher selectivity towards longer hydrocarbons. Furthermore, the amount of linear carbonyl was increased, while the amount of tilted carbonyls was reduced by alloying Rh with Fe. This resulted in a higher selectivity towards oxygenates as a result of more CO insertion (pathway 2). In addition, luminescence thermometry was applied to effectively determine the local temperature of the catalyst particle up to at least 350 °C with a 0.3 °C accuracy at 300 °C, and demonstrated that the set temperature deviated of the local temperature at the catalyst level. Experiments in which the gas feed was varied, showed that the main reason for a mismatch in the set and observed temperature is caused by heat dissipation; changing the gas composition from H_2 to CO at 300 °C can change the local temperature by 20 °C, and up to 40 °C at 350 °C. The results show that the crucial parameters for chemical reactions (i.e., adsorbed species and temperature) should be monitored under relevant conditions (*operando*) and at relevant length scales (at the catalyst particle). In order to compare results between different *operando* studies, it is paramount that the local temperature can be monitored to account for temperature deviations due to heat dissipation and/or exo- and endothermic reactions at the catalyst surface. Different types of catalyst extrudate sensors, as developed in this chapter, can be prepared for a wide variety of catalysts and support oxides and using on-line activity measurements, the formation of reaction products can be coupled to the observed spectral features of surface reaction intermediates. In other words, the extrudate sensors open up a

new way of assessing catalyst reactivity within a reactor bed, thereby focusing on the local temperature as well as the surface intermediates locally formed within catalyst grains along the reactor bed.

5.4 Experimental Section

Materials. All chemicals were used without further purification. The following chemicals were purchased from Sigma-Aldrich: Cyclohexane (99.5%, CH), oleic acid (90%, OA), ethanol (>99.8%, EtOH), methanol (>99.85%, MeOH), sodium hydroxide (>97%, NaOH), ammonium fluoride (>98%, NH_4F), ammonium hydroxide (28 wt% in H_2O, ammonia), rare-earth acetate hydrates (99.9%, $RE(Ac)_3$), tetraethyl orthosilicate (99.999%, TEOS), IGEPAL CO-520 ($(C_2H_4O)_n$•$C_{15}H_{24}O$ with n ~ 5, average Mn = 441 g mol^{-1}, NP-5) and methylcellulose (4000 CP), (3-aminopropyl)trimethoxysilane (APTMS, 97%), sodium silicate solution (27% SiO_2 in 14% NaOH), Rhodamine 6G, $RhCl_3$ (98, hydroxylamine hydrochloride (>98%). 1-octadecene (90%, ODE) and trisodium citrate dihydrate (99%) were purchased from Acros Organics. Demineralized water was purified with a Milli-Q system (18.2 MΩ) before use.

The purity of the gases used in the experiments was 99.99% and was passed through a filter consisting of ZnO, Al_2O_3 and activated coal. The flow was controlled by Brooks mass flow controllers connected to a Brooks Smart Interface.

Preparation of temperature sensors. $NaYF_4$@SiO_2 nanoparticles (NPs) doped with 18% Yb^{3+} and 2% Er^{3+} of ca. 50 nm were prepared via an initial synthesis of $NaYF_4$ core particles (ca. 25 nm) and subsequent SiO_2 overgrowth as reported earlier[1–4].

Synthesis of catalyst extrudates. Extrudates containing $NaYF_4$@SiO_2 NPs were prepared by mixing 3.2 g of dried $NaYF_4$@SiO_2 NPs with 3.8 g silica (Davicat Si1302), 0.2 g methylcellulose and water in a Caleva Mixer Torque Rheometer. The obtained paste was then transferred to a single mini-screw extruder (Caleva) and extruded into 2 mm diameter cylindrical extrudates. The obtained extrudates were dried overnight at room temperature and afterwards calcined at 873 K.

Synthesis of Au@SiO_2. Au@SiO_2 NPs of ca. 90 nm were prepared via seeded growth of Au core particles (ca. 88 nm) and subsequent SiO_2 overgrowth as reported earlier[5,6].

30 mL H_2O and 300 µL of 1% (W/V) $HAuCl_4$ were added to a 250 mL were rapidly brought to a boil in a preheated oil bath, under vigorous stirring. 0.9 mL of 1% (W/V) trisodium citrate solution was added when the solution was boiling. The flask was removed from heat after 10 min, resulting in a ruby red colloidal solution with Au seeds of ca. 16 nm.[46] 1.4 mL seeds were then added to 112 mL mQ water and 2.0 mL 1% (W/V) trisodium citrate was added. Au NPs were grown by adding dropwise 2.8 mL $NH_2OH{\cdot}HCl$ (10 mM) and 1 % (W/V) $HAuCl_4$ over 30 min. 15 mL of colloidal Au NPs solution was mixed with 0.4 mL aqueous APTMS (1.0 mM) solution and stirred for 20 min. Subsequently, 1.4 mL of a sodium silicate

solution (diluted to 0.54 wt.%, pH 10.8) was added under vigorous stirring. The flask was placed in an aluminum heating mantle at 90 °C and stirred for 45 min. After synthesis, the particles were centrifuged and washed 3 times in mQ water and finally stored in 1 mL mQ water.

Synthesis of Au@TiO_2. 10 mL colloidal particles were concentrated to 1 mL after centrifugation and subsequently mixed with 3 mL isopropanol. While vigorously stirring, 80 µL aqueous APTMS (1.1 mM) was added. After 10 min, 100 µL TTEAIP (2.5 mM in isopropanol) was added dropwise. 1h later, 50 µL of a solution containing ammonia (28–30%) was added and stirred overnight to prepare a shell of ca. 2 nm. After synthesis, the NPs were centrifuged and washed 2 times in isopropanol and 2 times in mQ water.[10]

Deposition of SHINs on extrudates. 0.25 mL of a colloidal solution with shell-isolated nanoparticles (SHINs) (Au@SiO_2 or Au@TiO_2) was concentrated to 25 µL and mixed with 50 µL aqueous $RhCl_3$ (0.01M). The colloidal solution immediately became unstable, resulting in a grey/purple mixture. This mixture was slowly added to a dried extrudate until the pores were filled (1 mL/g for SiO_2 and 0.2 mL/g for TiO_2), leaving the aggregated SHINs on the outside of the extrudate.

***Operando* Catalytic Experiments.** 1 wt% Rh and RhFe catalysts were prepared by a wet-impregnation method: the extrudates, containing shell-isolated nanoparticles (SHINs) and $NaYF_4$@SiO_2 NPs were immersed in 0.1 M aqueous $RhCl_3$ or $RhCl_3$:$FeCl_3$ (1:1 atomic ratio) for 24h. An extrudate (ca. 10 mg) was then loaded into a CCR1000 stage (Linkam) where gas atmosphere and temperature could be controlled. It was first dried at 80 °C for 2h, then at 120 °C for 2h and subsequently at 300 °C (3 °C/min) for 1h, all in 10 mL/min O_2 and 40 mL/min Ar. After calcination, the extrudates were reduced in 10 mL/min H_2 at 250 °C (3°C/min) for 30 min. These synthesis steps were followed with *in situ* SHINERS, and can be found in the Experimental Section. They were then ready for CO hydrogenation experiments. CO hydrogenation was performed under 2.5 mL/min CO and 5 mL/min H_2. *Mass Spectrometry (MS).* The composition of the gas phase was monitored with on-line MS on an Omni Star GSD 320 O2 Analytical system (Pfeiffer Vacuum). The inlet was heated to 150 °C.

Luminescence Thermometry. Upconversion luminescence spectrum were obtained with an MDL-III-980nm-2W continuous wave laser, Ocean Optics VIS-NIR combined light source and detection probe, Ocean optics QEPro CCD detector and Ocean Optics software.

Shell-Isolated Nanoparticle-Enhanced Raman Spectroscopy (SHINERS). Raman spectroscopy measurements were performed on a Renishaw InVia Raman microscope, using 785 nm diode laser excitation through a 50x objective (0.5 NA). *In situ* experiments were all performed under 0.8 mW (i.e., $1.67 \cdot 10^5$ $W \cdot cm^{-2}$), with an integration time of 10s. SHINER spectra of $RhCl_3$ and Rh_2O_3 were obtained with 1s integration time. All spectra are shown without data processing, unless specified.

Fourier-Transform Infrared (FT-IR) Microspectroscopy. FT-IR spectra were obtained on a Spotlight 400 FT-IR microscope (PerkinElmer) equipped with a MCT array (mercury cadmium telluride) detector. Measurements were taken with an aperture size of 100 × 100 μm and integrated over 256 scans, with 4 cm^{-1} resolution.

Transmission electron microscopy (TEM). TEM images were recorded using a FEI Tecnai 12 Icor TEM operating at 120 kV. Samples were prepared by drop-casting a colloidal solution on a carbon-coated copper grid, which were left to dry in air. TEM images of the extrudate were obtained by gently scraping the outer surface of the spent catalyst and dispersing it in 2-propanol after which a drop was dried on a carbon coated copper grid. Scanning transmission electron microscopy-energy dispersive X-ray analysis (STEM-EDX) images were obtained on a FEI Talos F200X electron microscope operating at 200 kV.

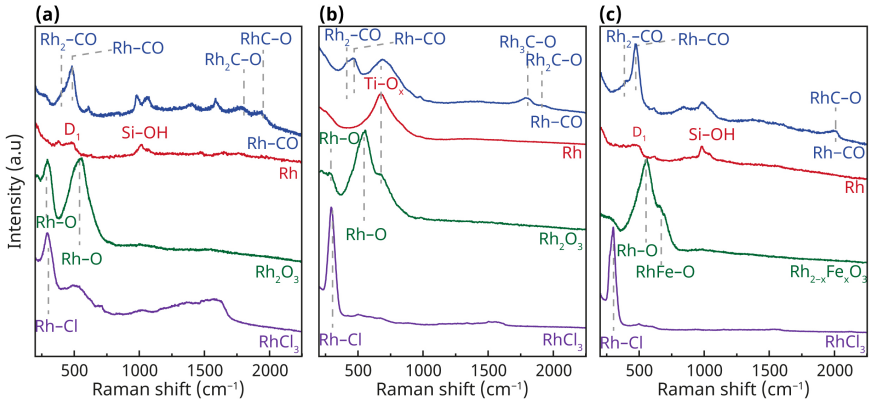

Figure 5.9. SHINERS study of catalyst preparation for CO hydrogenation catalysis. All samples were treated as follows: $RhCl_3$ in air, followed by oxidation in 20% O_2 at 300 °C, then treated in H_2 at 250 °C and finally CO hydrogenation at 250 °C. **(a)** $RhCl_3$/Au@SiO_2; **(b)** $RhCl_3$/Au@TiO_2; **(c)** (RhFe)Cl_3/Au@SiO_2. [785 nm, 10s, $1.67 \cdot 10^5$ $W \cdot cm^{-2}$]

5.5 Author Contributions and Acknowledgements

This chapter is based on the manuscript: Extrudate Sensors for Probing Metal-Support Interfacial Catalytic Reactions Using *Operando* SHINERS and Luminescence Thermometry, T. Hartman, R.G. Geitenbeek, G.T. Whiting, B.M. Weckhuysen, *in revision for publication.*

Bert Weckhuysen conceived the original plans for the manuscript, the research was designed together with Thomas Hartman and Robin Geitenbeek. $NaYF_4$@SiO_2 NPs were prepared by Robin Geitenbeek and were used by Gareth Whiting to prepare extrudates; Thomas Hartman prepared and deposited

$Au@SiO_2$ SHINs with Rh on the extrudates; the *operando* experiments were performed by Thomas Hartman and Robin Geitenbeekk. Thomas Hartman and Robin Geitenbeek contributed equally to the manuscript.

The following people are gratefully acknowledged for their contributions: Andries Meijerink (Utrecht University, UU) for his valuable input and discussions. Nynke Krans (UU) is thanked for her contributions to the TEM-EDX measurements, while Iris ten Have (UU) is thanked for her contributions to the SEM measurements.

5.6 References

[1] G. Ertl, *Reactions at Solid Surfaces*, Wiley, Hoboken, **2009**.
[2] G. Ertl, H. Knözinger, F. Schüth, J. Weitkamp, *Handbook of Heterogeneous Catalysis*, Wiley-VCH, Weinheim, **2008**.
[3] G. A. Somorjai, A. S. Mujumdar, *Dry. Technol.* **1995**, *13*, 507–508.
[4] M. A. Bañares, *Adv. Mater.* **2011**, *23*, 5293–5301.
[5] I. L. C. Buurmans, B. M. Weckhuysen, *Nat. Chem.* **2012**, *4*, 873–886.
[6] B. M. Weckhuysen, *Phys. Chem. Chem. Phys.* **2003**, *5*, 4351–43560.
[7] J. F. Li, Y. F. Huang, Y. Ding, Z. L. Yang, S. B. Li, X. S. Zhou, F. R. Fan, W. Zhang, Z. Y. Zhou, D. Y. Wu, B. Ren, Z. L. Wang, Z. Q. Tian, *Nature* **2010**, *464*, 392–395.
[8] S.-Y. Ding, J. Yi, J.-F. Li, B. Ren, D.-Y. Wu, R. Panneerselvam, Z.-Q. Tian, *Nat. Rev. Mater.* **2016**, *1*, 16021.
[9] S. Schlücker, *Angew. Chem. Int. Ed.* **2014**, *53*, 4756–4795.
[10] T. Hartman, B. M. Weckhuysen, *Chem. Eur. J.* **2018**, *24*, 3733–3741.
[11] H. Zhang, C. Wang, H.-L. Sun, G. Fu, S. Chen, Y.-J. Zhang, B.-H. Chen, J. R. Anema, Z.-L. Yang, J.-F. Li, Z.-Q. Tian, *Nat. Commun.* **2017**, *8*, 15447.
[12] D. Jaque, F. Vetrone, *Nanoscale* **2012**, *4*, 4301–4326.
[13] C. D. S. Brites, P. P. Lima, N. J. O. Silva, A. Millán, V. S. Amaral, F. Palacio, L. D. Carlos, *Nanoscale* **2012**, *4*, 4799–4829.
[14] R. G. Geitenbeek, A. Nieuwelink, T. S. Jacobs, B. B. V Salzmann, J. Goetze, A. Meijerink, B. M. Weckhuysen, *ACS Catal.* **2018**, 2397–2401.
[15] F. Vetrone, R. Naccache, A. Zamarrón, A. Juarranz de la Fuente, F. Sanz-Rodríguez, L. Martinez Maestro, E. Martín Rodriguez, D. Jaque, J. García Solé, J. a Capobianco, *ACS Nano* **2010**, *4*, 3254–3258.
[16] S. Hwang, R. Smith, *Chem. Eng. Commun.* **2009**, *196*, 616–642.
[17] J. D. Grunwaldt, J. B. Wagner, R. E. Dunin-Borkowski, *ChemCatChem* **2013**, *5*, 62–80.
[18] I. V. Koptyug, A. V. Khomichev, A. A. Lysova, R. Z. Sagdeev, *J. Am. Chem. Soc.* **2008**, *130*, 10452–10453.
[19] B. Kimmerle, J. D. Grunwaldt, A. Baiker, P. Glatzel, P. Boye, S. Stephan, C. G. Schroer, *J. Phys. Chem. C* **2009**, *113*, 3037–3040.

[20] M. Simeone, L. Salemme, C. Allouis, G. Volpicelli, *AIChE J.* **2008**, *54*, 2689–2698.
[21] I. Yarulina, F. Kapteijn, J. Gascon, *Catal. Sci. Technol.* **2016**, *6*, 5320–5325.
[22] T. Li, C. Guo, S. Zhou, C. Duan, M. Yin, *J. Am. Ceram. Soc.* **2015**, *98*, 2812–2816.
[23] X. Xu, Z. Wang, P. Lei, Y. Yu, S. Yao, S. Song, X. Liu, Y. Su, L. Dong, J. Feng, H. Zhang, *ACS Appl. Mater. Interfaces* **2015**, *7*, 20813–20819.
[24] W. T. Carnall, H. Crosswhite, H. M. Crosswhite, *Energy Level Structure and Transition Probabilities of the Trivalent Lanthanides in LaF_3*, Argonne National Laboratory, **1977**.
[25] O. Svelto, *Principles of Lasers*, Springer, New York, **2010**.
[26] R. G. Geitenbeek, P. T. Prins, W. Albrecht, A. Van Blaaderen, B. M. Weckhuysen, A. Meijerink, *J. Phys. Chem. C* **2017**, *121*, 3503–3510.
[27] F. Auzel, *Chem. Rev.* **2004**, *104*, 139–73.
[28] T. Inoue, T. Iizuka, K. Tanabe, *Appl. Catal.* **1989**, *46*, 1–9.
[29] J. R. Rumble, *CRC Handbook of Chemistry and Physics, 98th Edition*, CRC Press, Boca Raton, **2017**.
[30] J. J. Spivey, A. Egbebi, *Chem. Soc. Rev.* **2007**, *36*, 1514–1528.
[31] J. R. Katzer, A. W. Sleight, P. Gajardo, J. B. Michel, E. F. Gleason, S. McMillan, *Faraday Discuss. Chem. Soc.* **1981**, *72*, 121–133.
[32] Y. Liu, F. Göeltl, I. Ro, M. R. Ball, C. Sener, I. B. Aragão, D. Zanchet, G. W. Huber, M. Mavrikakis, J. A. Dumesic, *ACS Catal.* **2017**, *7*, 4550–4563.
[33] C. T. Williams, C. A. Black, M. J. Weaver, C. G. Takoudis, *J. Phys. Chem. B* **1997**, *101*, 2874–2883.
[34] C. T. Williams, K.-Y. Chen, C. G. Takoudis, M. J. Weaver, *J. Phys. Chem. B* **1998**, *102*, 4785–4794.
[35] H. Arakawa, T. Fukushima, M. Ichikawa, K. Takeuchi, T. Matsuzaki, Y. Sugi, *Chem. Lett.* **1985**, *14*, 23–26.
[36] S. S. C. Chuang, S.-I. Pien, *J. Catal.* **1992**, *138*, 536–546.
[37] S. S. C. Chuang, S. I. Pien, *J. Catal.* **1992**, *135*, 618–634.
[38] S. S. C. Chuang, R. W. Stevens, R. Khatri, *Top. Catal.* **2005**, *32*, 225–232.
[39] M. Tóth, J. Kiss, A. Oszkó, G. Pótári, B. László, A. Erdohelyi, *Top. Catal.* **2012**, *55*, 747–756.
[40] K. I. Hadjiivanov, G. N. Vayssilov, *Adv. Catal.* **2002**, *47*, 307–511.
[41] S. Degioanni, A. M. Jurdyc, F. Bessueille, J. Coulm, B. Champagnon, D. Vouagner, *J. Appl. Phys.* **2013**, *114*, 234307.
[42] S. X. Weng, A. Anderson, B. H. Torrie, *J. Raman Spectrosc.* **1989**, *20*, 789–794.
[43] W. J. Mitchell, J. Xie, T. A. Jachimowski, W. H. Weinberg, *J. Am. Chem. Soc.* **1995**, *117*, 2606–2617.
[44] C. Xu, G. Chen, Y. Zhao, P. Liu, X. Duan, L. Gu, G. Fu, Y. Yuan, N. Zheng, *Nat. Commun.* **2018**, *9*, 3367.
[45] A. Erdöhelyi, F. Solymosi, *J. Catal.* **1983**, *84*, 446–460.

[46] W. Haiss, N. T. K. Thanh, J. Aveyard, D. G. Fernig, *Anal. Chem.* **2007**, *79*, 4215–4221.

6

Summary, Outlook and Conclusions

This thesis focused on the development of SHINERS towards a functioning characterization tool for heterogeneous catalysis. In this chapter, the most important findings are summarized, and we will look forward towards the future of SHINERS and other relevant developments in the field and end with some conclusions.

6.1 Summary

This thesis started with an introduction and a future perspective on the state of SERS and TERS for catalysis. It was clear from the start that SHINERS plays an important role in moving plasmon-enhanced Raman spectroscopy forward as application in heterogeneous catalysis. The technique provides non-invasive Raman signal enhancement in combination with improved thermal and chemical stability. Two types of coatings were successfully prepared for thermally stable SHINERS experiments. Au@SiO_2 and new Au@TiO_2 NPs were developed for the purpose of studying the Fischer-Tropsch process. However, the initial SHINERS results were not consistent, and we therefore focused more on obtaining reliable SHINERS substrates for application in heterogeneous catalysis. After this research, we can prepare reliable SHINERS substrates that are proven effective characterization tools for performing *operando* spectroscopy to investigate interfacial chemical reactions during catalysis. In other words, the work in this thesis opens up a new way of assessing catalyst-reactant interactions. In the following paragraphs the main findings of each chapter are summarized and are visually displayed in Figure 6.1.

In Chapter 2, the synthesis of thermally stable Au@SiO_2 and Au@TiO_2 was demonstrated. By carefully controlling the Au core size with a seeded growth method, the optimal size for Raman signal enhancement was found to be around 80 nm with an enhancement factor of over 10^5. The SiO_2- and TiO_2-shells were carefully grown over the Au cores by controlling the hydrolysis of silicates and an organic titanates in aqueous solutions. As expected, the Raman signal enhancement was inversely proportional to the coating thickness, which resulted in the loss of all enhancing properties once the coating reached a thickness of 4 nm. An important balance between the Raman signal enhancement and thermal stability was therefore found for a minimum coating thickness of 2 nm and a maximum thickness of 2.5 nm. SHINs with 80 nm Au cores and 2 nm SiO_2 or TiO_2 coatings still provided Raman signal enhancement factors of over 10^4 and were unaffected by thermal treatments up to 400 °C.

These nanostructures were applied in Chapter 3 for the *in situ* study of catalysts. The synthesis of nano-sized metal catalysts could be followed over the SHINs after a wet impregnation of the Au@SiO_2 and Au@TiO_2 colloids with aqueous $RuCl_3$. More importantly, the SHINERS materials were proven effective Raman signal enhancers for catalysis when comparing the Raman spectra of various samples after a CO adsorption step. Adsorbed carbonyls were clearly observed on metallic Ru/Au@TiO_2 and Ru/Au@SiO_2 SHINs in contrast to Ru/SiO_2. Using the SiO_2- and TiO_2-SHINs, the support effects on the CO hydrogenation were studied. It was found that CO was hydrogenated at lower temperature over Ru/Au@TiO_2 in comparison to Ru/Au@SiO_2. Finally, other Pt-group metals were impregnated on Au@SiO_2 NPs to demonstrate the universality of the method. Successful substrates for SHINERS were acquired using Rh, Pd and Pt on Au@SiO_2.

Depending on the metals present, all these substrates showed various adsorption geometries of carbonyls, such as linear and bridged carbonyls. Also the effect of alloying was demonstrated by a wet impregnation of aqueous $RhCl_3$ and $FeCl_3$. When more Fe was present in the alloy, the carbonyls were present in a more linear geometry instead of bridged.

However, during these initial catalytic experiments, many bands were observed in the fingerprint region of the SHINER spectra that were difficult to assign. Since the origin of these bands were unknown, the fingerprint region could not be used for the study of reaction pathways. Additionally, contamination of the catalysts most likely affects the activity and should therefore be removed. Even more so, due to their intense signal and random positions, they obscured further interpretation of the SHINER spectra. In Chapter 4, we therefore investigated different approaches to obtain spectra free of contamination. The best approaches were presented as guidelines for SHINERS in heterogeneous catalysis. The chapter was presented as a guideline to obtain useful SHINERS data as a result of effective cleaning pretreatments. It was found of utmost importance to work with clean starting materials and clean reaction materials. Therefore, we advised for future experiments to start with a heat treatment of 300 °C in an oxygen-rich environment, including a flushing step of at least 15 min of all gases. Finally, any contaminants during catalysis that may be found in the CO feed should be removed with a filter. The filter may consist of ZnO, Al_2O_3 and activated coal to remove respectively water, carbonyls, and organics. Furthermore, one should be aware of the Raman laser power effects in combination with the plasmonic nanoparticles. Depending on the electromagnetic enhancement of the SHINs, a limited laser power or minimized exposure times to prevent carbon growth should be applied. When these practical steps are followed, a clean(er) SHINER spectrum will be obtained, which can be applied for catalysis research.

The knowledge and materials that were obtained in the preceding chapters were applied to prepare a new type of sensor for *operando* SHINERS in combination with luminescence thermometry. In Chapter 5, catalyst extrudate sensors were developed for use in applied catalysis that allowed for the simultaneous operando monitoring of reaction temperature with luminescence thermometry and surface species with SHINERS. They were applied for the study of CO hydrogenation over supported Rh catalysts. With SHINERS, various surface species were observed under CO hydrogenation conditions up to 350 °C that were used for researching the CO hydrogenation reaction. The most important finding was that SHINERS can observe interfacial species of catalyst and support that are not detected with conventional techniques, such as IR spectroscopy. These species are dependent on the nature of the catalyst and support, as was demonstrated with Rh/SiO_2, Rh/TiO_2 and $RhFe/SiO_2$ catalysts. In addition, luminescence thermometry was applied to effectively determine the local temperature of the catalyst particle up to at least 350 °C with a 0.3 °C accuracy at 300 °C, and demonstrated that the set temperature deviated of the local temperature at the catalyst level. Experiments in

which the gas feed was varied showed that the main reason for temperature discrepancies is heat dissipation; variations of up to 40 °C were observed. The results show that the crucial parameters for chemical reactions (i.e., adsorbed species and temperature) should be monitored under relevant conditions (operando) and at relevant length scales (at the catalyst particle).

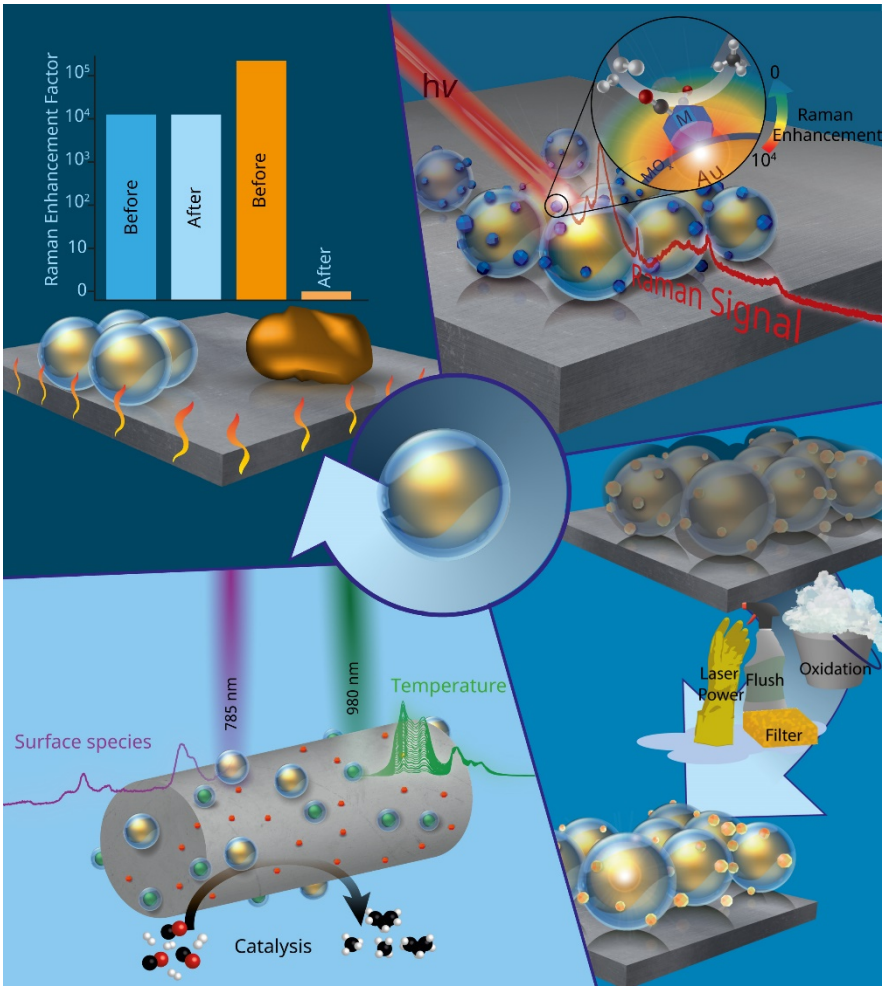

Figure 6.1. Summarizing figure of the main projects of this thesis. Starting at Chapter 2 and moving clockwise through the Chapters. In Chapter 2, the preparation and applicability of SHINs for thermally stable SHINERS experiments was demonstrated. In Chapter 3, the prepared SHINs were successfully implemented as tools for studying heterogeneous catalysis. In Chapter 4, the limitations of contamination were solved so that finally, in Chapter 5, SHINs were used as an *operando* probing tool for interfacial chemistry during a catalytic reaction.

6.2 Outlook

The work on shell-isolated nanoparticles (SHINs) described in this thesis has contributed to a more universal application of SHINERS for heterogeneous catalysis. With Chapter 5 as the culmination of the research: SHINERS was applied for observing interfacial catalytic reactions in *operando* experiments. Many improvements can still be made, for example in substrate engineering and theoretical understanding. Research is still ongoing to find substrates with stronger Raman signal enhancement factors, coupled with improved thermal and chemical stability. New materials will open up extra possibilities to acquire Raman spectra faster at even more demanding conditions. These two fields are deemed highly important for the further development of plasmon enhanced Raman in heterogeneous catalysis:

1. Substrate engineering will lead to improved stability, allowing measurements at higher temperatures over a longer reaction time. If we can couple this to an improved sensitivity, we can obtain better signals at faster acquisition times.
2. Improved theoretical understanding of plasmons and visualizing their shape and size will help us understand the area we are probing.

Substrate engineering

Although the thermal stability of plasmon enhanced Raman spectroscopy is improved with SHINERS up to temperatures of 400 °C in air, it remains limited under reaction conditions. Future work could be performed on more stable or flexible coating materials, such as graphene.[1] We therefore investigated the preparation of Cu@C nanostructures. Cu@C NPs were obtained from the pyrolysis of the metal organic framework (MOF) HKUST-1 in N_2.[2] The pyrolysis of MOFs is gaining popularity for the synthesis of catalysts, but was used here to generate plasmonic Cu cores. This highly simple but practical synthesis procedure can generate large amounts (on the scale of several grams) of SHINERS substrates. The Cu NPs were rather small (20 nm, Figure 6.2), but in the correct size range for effective SHINERS. However, in combination with the thick carbon coating, they did not exhibit any Raman signal enhancement. By controlling the pyrolysis temperature and gas atmosphere in future experiments, the appropriate synthesis parameters can be found to obtain quickly and cheaply a large amount of Cu NPs for SHINERS.

The Raman signal enhancement can be improved by tuning the size, the shape and the material of the plasmonic core. In this thesis, we focused on spherical SHINs, because spheres are energetically the most favorable shape and will suffer the least from restructuring at high temperature. Au plasmonic cores were predominantly applied, because of their inertness and ease of storage. However, Ag is known to have a better activity for PERS. Spherical Ag@SiO_2 and Ag@TiO_2

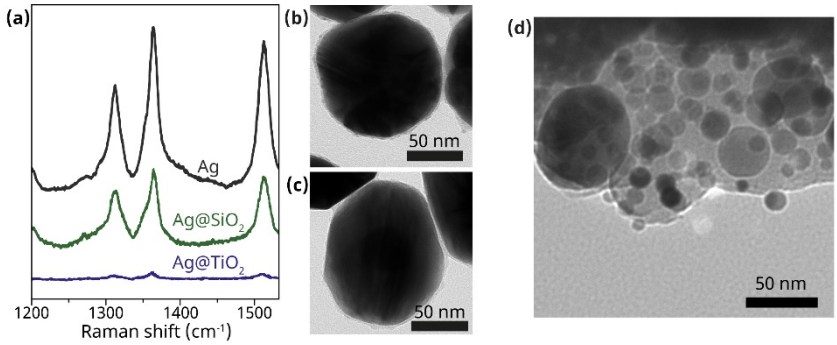

Figure 6.2. First experiments with Ag@TiO_2 SHINs. (a) SHINER spectra of aqueous Rh6G (0.1 mM) over 80 nm Ag NPs, Ag@SiO_2 with 1 nm SiO_2 shell and Ag@TiO_2 with 2 nm TiO_2 shell. **(b**) TEM image of 80 nm Ag core with 2 nm TiO_2 shell. **(c)** TEM image of 80 nm Ag core with 1 nm SiO_2 shell.

SHINs were thus prepared to study the effect of the core material (Figure 6.2). The materials gave comparable Raman signal intensities when excited with 785 nm light, but gave much stronger signals when excited with a 532 nm laser. Shell-isolated Ag structures are therefore a promising tool for probing reactions where a higher sensitivity is required. However, in our research on Ag NPs, we could not obtain the same quality of SiO_2- and TiO_2-coatings as we observed on Au cores. This resulted in more delicate nanostructures that were prone to oxidation and other side-reactions.

Another approach can be found in AuAg alloyed nanorods.[3] Due to the alloying of Au with Ag, they exhibit higher melting temperatures. Moreover, due to the stronger surface plasmon resonances they can be protected with thicker coatings to improve their thermally stability even further.

The relation between catalyst structure and activity is an important study in field of heterogeneous catalysis. With the highly localized sensitivity of SHINERS, the technique seems to be a promising tool for the characterization of such nano-scaled catalysts. Using colloidal synthesis, the size and shape of metal nanoparticles can be tailored to give highly monodisperse solid catalysts. Two projects were therefore started to assemble colloidal catalysts on the exterior surfaces of SHINs to study size, shape and support effects.

The first goal was to study Co/TiO_2 catalysts for Fischer-Tropsch synthesis (FTS). In collaboration with Tom van Deelen (Utrecht University), colloidal Co NPs were assembled over SiO_2- and TiO_2-SHINs (Figure 6.3a) by mixing the two systems in anti-solvents. The polar SHINS and the apolar Co NPs were forced to aggregate in a water/2-propanol/n-hexane mixture. The initial results proved to be very promising, with strong Raman signals of cobalt oxides in air. The system was found to be thermally stable in air or O_2-rich environments in which it could be heated up to 300 °C. SHINERS was successfully applied to study a temperature programmed reduction of the cobalt oxides in H_2-rich conditions up to 300 °C (Figure 6.3b). However, no adsorbed carbonyls were observed in the Raman

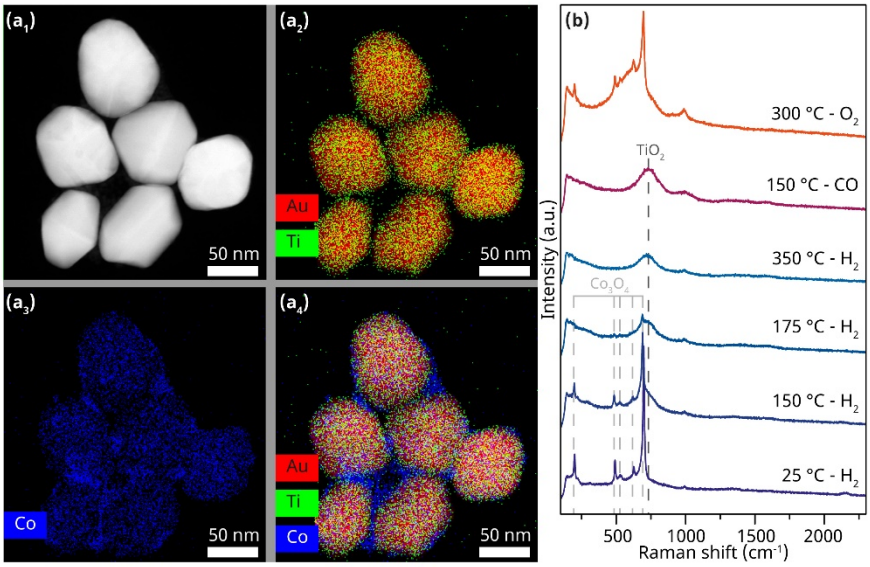

Figure 6.3. STEM-EDX and SHINERS studies of Co/Au@TiO_2. (a1) STEM imaging of Co NPs assembled over Au@TiO_2 NPs. **(a2-4)** STEM-EDX elemental maps of Au (red), Ti (green) and Co (blue). **(b)** temperature-programmed reduction in H_2, followed with *in situ* SHINERS of CoO_x NPs assembled over Au@TiO_2 (blue lines), followed by CO adsorption at 150 °C (red line). Finally, the Co NPs were re-oxidized at 300 °C in O_2 (orange line).

spectra after introducing gaseous CO to the system (Figure 6.3b). The reason of the absence of CO bands in the SHINER spectra remains unknown, and can be related to two causes. First, changes in the nanostructures cause the Co NPs to move out of the probing area. Second, the Co NPs are not fully reduced and thereby not catalytically active. After re-oxidation, Co-O vibrations are observed again, indicating that the SHINs remain intact.

Other colloidal catalysts were prepared and assembled over SHINERS substrates. Colloidal Ru, Rh and Pt catalysts of various sizes and shapes were deposited over Au@SiO_2 SHINs (Figure 6.4). The syntheses were performed with the well-known polyol method, resulting in solid catalysts with a controlled size and shape between 1-10 nm. The 40k M_w polyvinylpyrrolidone (PVP) polymer surfactants were partially removed by washing the NPs in $NOBF_4$ in acetonitrile mixture before anchoring of them to the exterior surface of SiO_2-SHINs (Figure 6.4).[4] Although the TEM images look very promising, these nanostructures were not successful for probing catalyst interfaces. Relatively weak signals were obtained of metal-oxides and after reduction and CO adsorption, there were no clear signals of carbonyls observed. The use of SHINERS for the study of colloidal catalysts therefore remains promising. A better control over the aggregation state and amount of catalyst material should open the possibility of the application of such nanostructures for SHINERS.

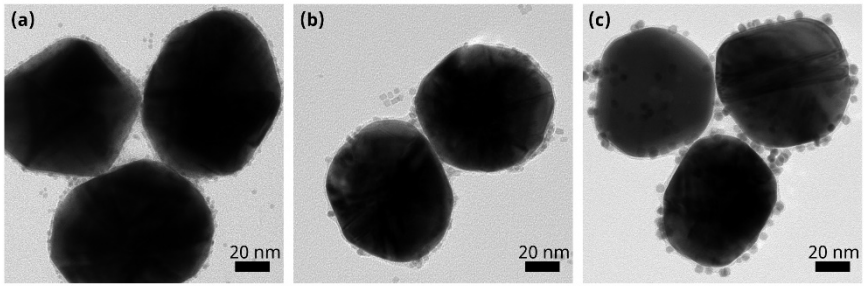

Figure 6.4. TEM images of metal NPs assembled over Au@SiO_2. (a) Ru/Au@SiO_2 **(b)** Rh/Au@SiO_2. **(c)** Pt/Au@SiO_2

In this thesis, we have only focused on the adsorption and hydrogenation of CO, but SHINERS can be applied to virtually any catalytic system. An example of other recent work is based on the CO oxidation over colloidal NPs. In this example, the benefits of SHINERS for exploring the low wavenumber regime (100-1000 cm^{-1}) in combination with the local sensitivity are exploited to find relevant surface species during catalysis.[5]

We have also applied SHINERS to study the NO reduction (Figure 6.5). NO is known to have a wide variety of possible adsorption geometries.[6] SHINERS is therefore an interesting characterization tool, as it can probe the direct interaction between metal and reactant by detecting vibrational bands in the low wavenumber regime. A summary of the results can be found in Figure 6.5. NO was adsorbed at 50 °C and was subsequently desorbed in Ar or reduced under H_2 atmosphere at different temperature with 50 °C interval. After adsorption, we immediately observe Rh-NO stretching (300 cm^{-1}), Rh-O-N-O bending (830 cm^{-1}) and RhN-O_3 stretching (1055 cm^{-1}) vibrations. NO_3^- species seem to be a curious finding during these spectroscopic measurements, but are expectedly related to interactions with SiO_2. By increasing the temperature we see differences arise between the NO desorption and NO reduction experiments. More hydrogen in the feed results in more intense bands at 426, 507 and 610 cm^{-1}, which are all most likely related to hydrogenated nitric oxides, such as Rh-NOH stretching vibrations at around 430 cm^{-1}.

SHINERS is able to probe many different surface species and their interaction with the catalyst. Not all the bands could be assigned, and the RhN-O stretching vibrations around 2200 cm^{-1} seems to be missing. If this is related to the probing are of SHINERS, is yet to be discovered.

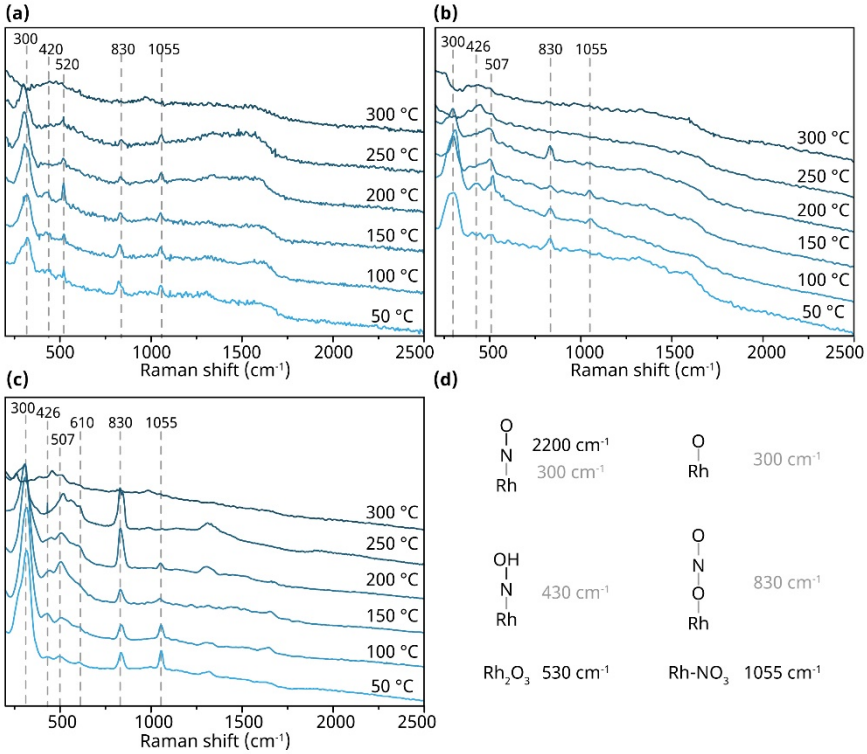

Figure 6.5. Temperature programmed NO desorption and reduction over Rh/Au@SiO_2 as observed with *in situ* SHINERS. (a) NO desorption in Ar at various temperatures with 50 °C interval. **(b)** NO reduction in 1:2 H_2:NO ratio at various temperatures with 50 °C interval. **(c)** NO reduction in 2:1 H_2:NO ratio at various temperatures with 50 °C interval. **(d)** Band assignment, based on previous work on Au@Rh SERS experiments.[7]

Understanding Plasmons

In literature, the most common description of plasmonic hot spots is "the strong increase and spatial localization of the electromagnetic field through coupled resonances at the 'gaps' between metallic nano-objects".[8] It is therefore expected that for the strongest Raman enhancement, the optimal position of catalysts should be in the junction of two plasmonic NPs. Computational methods can help to understand where the strongest signal is obtained and how this will affect the observed spectra. However, they are usually implemented for rather simple systems (e.g. single NPs or dimers) and the calculations will become more sophisticated for modelling the heterogeneous aggregates found in this work. They will consist of many plasmon modes of quasi spherical NPs, and will have to account for the effect of a mix of dielectric materials. Nonetheless, they will contribute to a better understanding of the localized nature of the probing method.

A tool to directly observe localized surface plasmon resonances (LSPRs) on the nanoscale is scanning transmission electron microscopy - electron energy loss spectroscopy (STEM-EELS). For long, the technique was not capable of detecting gap-mode plasmons as STEM-EELS is only sensitive to components of the photonic local density of states (LDOS) parallel to the electron trajectory.[9,10] This restriction was recently lifted with the introduction of tomographic 3D EELS imaging. 3D EELS tomography was capable of fully imaging the gap mode LDOS of a vertically stacked nanotriangle dimer.[11] With this technique and the progress it has made over the last years, it will be made possible to investigate the position and the intensity of a plasmon related to the excitation source to find exactly which (part of the) catalyst NP is under observation.

These trends towards improved understanding of the local sensitivity are already applied in substrate engineering to prepare the most advanced nanostructures. For example, hierarchical SERS substrates can now be prepared to focus light with a large antenna, exhibiting a strong optical response, and couple it to a plasmonic dimer. This hierarchical field concentration approach can be used for single-molecule SERS detection, even when the nanogap between two NPs is as large as 6 nm.[12] Applying such nanostructures for research in heterogeneous catalysis is a large step away from the ease of preparation and the more realistic conditions under which SHINERS can be applied. However, these highly specialized techniques can give us a peek into the active life of individual heterogeneous catalysts.

For operando measurements in realistic catalytic systems, SHINs are the preferred substrates for Raman enhancement. Progress in this area can be made in the controlled aggregation of the colloidal SHINs and catalyst NPs. In Chapter 5, the aggregation of the SHINs was realized by mixing the colloidal solution with aqueous $RhCl_3$. Without aggregating the SHINs beforehand, the SHINERS signal was not sufficient. By controlled aggregation to obtain fixed sizes of aggregates, the plasmon resonance of the substrate can be tailored to match that of the excitation wavelength and the Stokes shift. This will result in better signals with improved reproducibility of the SHINERS experiments.[13]

6.3 Conclusions

In this thesis, SHINERS was developed into a more robust characterization technique for heterogeneous catalysis. Synthesis methods and practical guidelines were advanced to make SHINERS an effective *operando* spectroscopic tool for the characterization of interfacial chemical reactions. Further progress can be made in the preparation of new nanomaterials and the control over the aggregation step will contribute to even stronger signal enhancement and improved thermal stability. This thesis can be considered as a guideline for the application of new SHINERS substrate for heterogeneous catalysis, in which new developments can follow the route laid out in Figure 6.1.

6.4 References

[1] B. Yan, K. Li, P. Gu, Z. Li, C. Tang, F. Liu, P. Zhan, C. Sui, Z. Wang, *J. Raman Spectrosc.* **2018**, *49*, 431–437.

[2] Y. Song, D. Cho, S. Venkateswarlu, M. Yoon, *RSC Adv.* **2017**, *7*, 10592–10600.

[3] W. Albrecht, J. E. S. van der Hoeven, T.-S. Deng, P. E. de Jongh, A. van Blaaderen, *Nanoscale* **2017**, *9*, 2845–2851.

[4] A. Dong, X. Ye, J. Chen, Y. Kang, T. Gordon, J. M. Kikkawa, C. B. Murray, *J. Am. Chem. Soc.* **2011**, *133*, 998–1006.

[5] H. Zhang, C. Wang, H. Sun, G. Fu, S. Chen, Y. Zhang, B. Chen, J. R. Anema, Z. Yang, J. Li, Z. Tian, *Nat. Commun.* **2017**, *8*, 15447.

[6] M. Shelef, G. W. Graham, *Catal. Rev.* **1994**, *36*, 433–457.

[7] C. T. Williams, A. A. Tolia, M. J. Weaver, C. G. Takoudis, *Chem. Eng. Sci.* **1996**, *51*, 1673–1682.

[8] P. G. Etchegoin, E. C. Le Ru, in *Surf. Enhanc. Raman Spectrosc. Anal. Biophys. Life Sci. Appl.* (Ed.: S. Schlücker), Wiley-VCH, Weinheim, **2010**, pp. 1–37.

[9] B. Goris, G. Guzzinati, A. Trügler, U. Hohenester, J. Verbeeck, S. Bals, G. Van Tendeloo, *J. Phys. Chem. C* **2013**, *118*, 15356–15362.

[10] N. Mirsaleh-Kohan, V. Iberi, P. D. Simmons, N. W. Bigelow, A. Vaschillo, M. M. Rowland, M. D. Best, S. J. Pennycook, D. J. Masiello, B. S. Guiton, J. P. Camden, *J. Phys. Chem. Lett.* **2012**, *3*, 2303–2309.

[11] G. Haberfehlner, F. P. Schmidt, G. Schaffernak, A. Hörl, A. Trügler, A. Hohenau, F. Hofer, J. R. Krenn, U. Hohenester, G. Kothleitner, *Nano Lett.* **2017**, *17*, 6773–6777.

[12] S.-Y. Ding, E.-M. You, Z.-Q. Tian, M. Moskovits, *Chem. Soc. Rev.* **2017**, *46*, 4042–4076.

[13] M. Hentschel, D. Dregely, R. Vogelgesang, H. Giessen, N. Liu, *ACS Nano* **2011**, *5*, 2042–2050.

B

Back Matter

Samenvatting

Deze PhD thesis beslaat het werk van vier jaar onderzoek naar *shell-isolated nanoparticle-enhanced Raman spectroscopy* (SHINERS) *for heterogeneous catalysis*, oftewel: verbeterde Raman spectroscopie door schil-geïsoleerde nanodeeltjes voor heterogene katalyse. In de volgende pagina's worden de thema's geïntroduceerd voor een breed publiek zonder achtergrond in de scheikunde. De twee belangrijkste thema's hierin zijn de techniek, SHINERS, en het chemische proces, heterogene katalyse. Daarna volgt een verdieping met een samenvatting van de belangrijkste vindingen per hoofdstuk.

Nanodeeltjes

Een veelgebruikt woord in deze thesis, naast SHINERS en katalyse, is nanodeeltjes (nanoparticles of NPs). In de volksmond kennen we nano als iets heel kleins, zo hebben we ooit de iPod nano gehad, een klein muziekspelertje. De naam nano komt van de Latijnse naam nanus (dwerg) en wordt in de wetenschap gebruikt als voorvoegsel om aan te duiden dat iets 10^{-9}, of 0.000000001 keer zo klein is. Voor de eenheid 'meter' betekent dit dat het zo klein is, dat we het niet met het blote oog kunnen waarnemen, zelfs niet met de beste optische microscoop. Door de kleine afmetingen, kunnen de eigenschappen van nanomaterialen veranderen ten opzichte van materialen met grotere afmetingen: ze reageren bijvoorbeeld anders op licht, hebben een hogere reactiviteit en een lagere smelttemperatuur.

Een nanodeeltje van 100 nm is nog steeds zo klein, dat binnen een halve minuut je haar al meer toegenomen is in lengte. Figuur 1 geeft een idee hoe klein deze nanodeeltjes zijn. In de linkerkant is een haar te zien die ongeveer 300 keer is vergroot. In dezelfde afbeelding is een schil-geïsoleerd nanodeeltje verwerkt van 100 nm groot. Het nanodeeltje is alleen te zien als we hete beeld nog eens 100 keer vergroten. De breedte van een haar is een mooi voorbeeld, omdat het één van de kleinste afmetingen heeft die we met onze blote ogen kunnen waarnemen. De nanodeeltjes in deze thesis zijn zelfs 400 kleiner dan één haar, en kunnen eigenlijk niet waargenomen worden met een vergrootglas (zoals in Figuur 1) en zelfs niet onder een optische microscoop.

We gebruiken in deze thesis nanomaterialen van goud (Au), omdat deze een speciale interactie hebben met zichtbaar licht. Au nanodeeltjes kunnen licht namelijk concentreren op de nanoschaal zodat we heel lokaal met licht kunnen kijken naar materialen en chemische reacties. Deze eigenschap hebben we gebruikt om met licht onderzoek te doen naar katalysatoren die zich in de omgeving bevinden van de Au nanodeeltjes. Dit wordt later verder uitgelegd.

Het blijft fascinerend dat we door middel van scheikunde controle hebben over nanostructuren die we eigenlijk zelf niet waar kunnen nemen. Door middel van het

mengen van chemicaliën en daar vervolgens even op te wachten, kunnen we zelfs de vorm en grootte controleren. Dit klinkt wellicht gemakkelijker dan het is, je moet dit namelijk heel precies doen. Om de juiste structuren te krijgen, moet je de experimenten uitvoeren onder de juiste condities. Daarom wordt aan het eind van elk hoofdstuk beschreven hoe de experimenten zijn uitgevoerd. Als dit goed uitgevoerd wordt, zou overal ter wereld hetzelfde resultaat verkregen moeten worden.

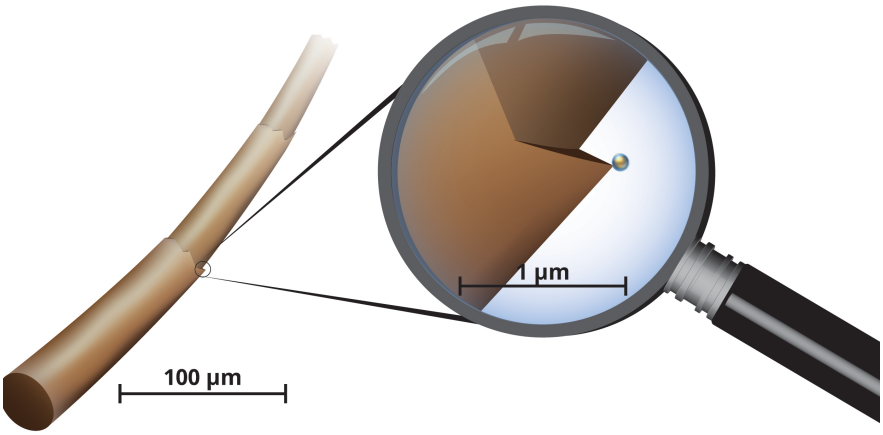

Figuur 1. De nanodeeltjes in deze thesis zijn minimaal 400 keer kleiner dan de dikte van een menselijk haar. Een menselijk haar (ca. 40 µm in de breedte) kunnen we nog maar net waarnemen met onze ogen. De grootste nanodeeltjes uit deze thesis (max 100 nm) zijn dus 400 keer zo klein. Deze nanodeeltjes zijn eigenlijk niet waar te nemen met een normale microscoop en vereisen electronenmicroscopen om gezien te worden.

Katalyse

Katalyse vormt een belangrijk onderdeel van de chemische industrie. Vrijwel alle chemicaliën* die je tegenkomt in het dagelijkse leven zijn ergens in hun productie een katalysator tegengekomen.[1] Een katalysator wordt toegevoegd aan een chemische reactie om deze te versnellen en daarnaast de goede richting in te sturen, of überhaupt plaats te laten vinden. Dit wordt gerealiseerd door de activatie-energie te verlagen van een reactie.[2] Deze activatie-energie kan gezien worden als een barrière, wordt deze niet overkomen, dan zal er geen reactie plaatsvinden. De energie die hiervoor nodig is, kan aangeleverd worden door een hoge temperatuur. Een katalysator verlaagt deze barrière doordat hij werkt als een soort relatiebemiddelaar (Figuur 2). De bemiddelaar/*katalysator* brengt mensen/*moleculen* alvast in een toestand waarin ze aan elkaar kunnen wennen en misschien zelfs een verbinding met elkaar aangaan. Was deze bemiddelaar/*katalysator* er niet, dan was de discussie/*reactie* zo verhit geworden dat er wellicht een stoel door het raam werd

*Chemicaliën zijn niet per se eng, bijna alle materialen om je heen zijn 'chemisch' tot stand gekomen: denk hierbij aan verf (niet Chroom-6! Wel eng), alle plastics evenals heel veel eetwaar (E-nummers).

gesmeten/*ongewenste reactie plaatsvond*. De bemiddelaar is naderhand weer beschikbaar voor een nieuwe koppeling.[3]

Met betere bemiddelaars zullen er een stuk minder stoelen door de ramen vliegen en hebben we dus minder grondstoffen en energie nodig. Ook draagt het bij aan de ontwikkeling van nieuwe reacties zodat we over kunnen stappen naar alternatieve grondstoffen. Dit is de reden dat onderzoek in katalyse zo belangrijk is voor het verduurzamen van de chemische industrie.[4]

In katalyse wordt een onderscheid gemaakt tussen heterogene en homogene katalyse. Een katalysator wordt als homogeen geclassificeerd als de katalysator en de reactanten zich in dezelfde fase bevinden (gas, vloeistof, vast). Meestal wordt homogene katalyse uitgevoerd in de vloeistoffase. Heterogene katalysatoren zijn vaak vaste materialen en zitten niet in dezelfde fase als de reactanten en producten. Dit zorgt ervoor dat heterogene katalysatoren gemakkelijker van de producten te scheiden zijn, en daarmee herbruikbaar zijn. Het gemak van hergebruik draagt eraan bij dat heterogene katalyse de meest gebruikte vorm van katalyse is.

Omdat heterogene katalysatoren vaste stoffen zijn, kan alleen de buitenkant van de katalysator actief deelnemen aan een reactie. Het nadeel van werken in twee of meerdere fases, is dus dat het contactoppervlak tussen de fases moeilijk gemaakt wordt. Dit kan verbeterd worden door het gebruik van nanomaterialen: hoe kleiner de materialen, des te groter de verhouding tussen oppervlak en inhoud.

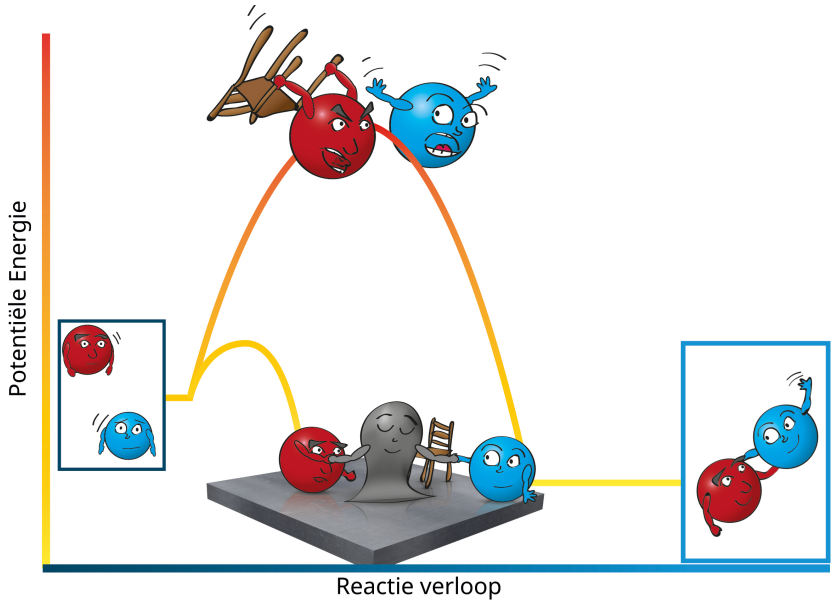

Figuur 2. Een katalysator werkt als een relatiebemiddelaar. De katalysator kan de benodigde energie om twee moleculen te verbinden verlagen. Zo zijn er lagere temperaturen nodig en kunnen ongewenste zijreacties voorkomen worden.

Om de nanodeeltjes stabiel te houden, kunnen ze geankerd worden aan een dragermateriaal zoals silica (SiO_2) en titania (TiO_2). Zo kan er zuiniger gewerkt worden met kostbare materialen; de nanodeeltjes hebben gezamenlijk een groter oppervlak voor een hogere reactiviteit en door het dragermateriaal blijven ze stabiel ondanks de kleine afmetingen.[5]

Een belangrijk onderzoeksgebied in heterogene katalyse bestaat uit het uitvinden van de effecten van de deeltjesgrootte en de invloed van de dragermaterialen. Zoals eerder besproken, zijn nanomaterialen niet simpelweg kleine materialen. Afhankelijk van hun afmetingen kunnen ze zich ook anders gaan gedragen dan 'normale' grotere materialen. Nanodeeltjes kunnen opeens veel actiever worden dan je op basis van de totale oppervlakte zou verwachten. Het tegenovergestelde kan ook plaatsvinden, de nanodeeltjes worden juist veel minder reactief. Vaak is er een optimum te vinden in de relatie tussen nanodeeltjes grootte en katalytische activiteiten. Daarnaast kan de drager een positieve of negatieve invloed hebben op de reactiviteit van de katalysator.[5]

Er zijn dus vele factoren van belang tijdens heterogene katalyse. Het materiaal van de katalysator, de drager, de grootte en zelfs de vorm kunnen effect hebben op de activiteit. Daarnaast zijn de condities van belang: de temperatuur, de druk, en de verhouding tussen de reactanten. In heterogene katalyse wordt daarom gewerkt met veel verschillende meettechnieken die allemaal bijdragen aan het begrijpen van de verscheidene processen die simultaan kunnen lopen.

Bij onderzoek naar katalyse is het belangrijk om de productvorming te meten tijdens een katalytische reactie onder gecontroleerde condities met kennis over de materialen en de structuren van de katalysator. Microscopische technieken kunnen inzicht geven in de (nano)structuur van een katalysator. Het liefst wordt de structuur vooraf en achteraf bestudeerd, zodat bijvoorbeeld ook een verandering in de activiteit gekoppeld wordt aan een verschil in de structuur. Wat nog een stap verder gaat, is om technieken te gebruiken die ingezet kunnen worden tijdens de katalytische reactie. Dit wordt *in situ* genoemd: oftewel, op zijn plaats. Zo kan je onder gecontroleerde condities informatie krijgen over het gedrag van de katalysator. Kan je dit koppelen aan de activiteit van een katalysator, dan wordt dit *operando* genoemd: oftewel, onder werkende condities.[6]

Spectroscopie

Veel methodes voor onderzoek in katalyse zijn spectroscopische technieken: ze bestuderen de interactie van licht met materie. Dit houdt in dat een materiaal beschenen wordt met licht waarvan we de kleur en intensiteit precies weten. Omdat we weten wat de eigenschappen zijn van het licht, kunnen we kleine veranderingen in bijvoorbeeld de kleur gebruiken om meer te weten te komen over het materiaal. Spectroscopie is een breed begrip, alles wat met de studie van licht te maken heeft valt onder deze noemer. Het licht dat wij kunnen zien, maakt slechts een fractie uit van de totale omvang van elektromagnetische straling. In Figuur 3a is een deel van

al het licht gesorteerd op basis van hun golflengte. Alleen de regenboogkleuren kunnen wij waarnemen als zichtbaar licht.

Licht kan op vele manier interactie aangaan met materie. Zo kan het reflecteren om een spiegelbeeld te vormen, of verstrooid raken bij een wolk. Het kan (gedeeltelijk) geabsorbeerd worden waardoor we kleuren waarnemen, maar het kan ook juist vrij komen. Dit zijn vier verschillende verschijnselen die op verscheidene manieren door andere type interacties tot stand kunnen komen. Hierdoor hebben we veel methodes om materialen met licht te bestuderen. Elke methode kan weer een ander inzicht geven. Er zijn daarom meerdere subgroepen bekend binnen de spectroscopie, waarvan vibratiespectroscopie een belangrijke is.

Alle verbindingen tussen atomen hebben een kenmerkende vibratie. Met vibratiespectroscopie kunnen de vibraties gemeten en gekarakteriseerd worden om zo de chemische samenstelling van een materiaal te bepalen. De vibraties tussen de verschillende atomen waaruit een molecuul is opgebouwd zijn sterk afhankelijk van de atoommassa's en de structuur van een molecuul. Zo komt het dat elk molecuul een karakteristieke interactie heeft met licht en zien we als het ware een vingerafdruk van het molecuul. Met behulp van vibratiespectroscopie kunnen we dus achterhalen wat voor structuren aanwezig zijn in de onderzochte materialen.

De frequentie van de vibraties tussen de atomen verschillen, maar vallen allemaal binnen het infrarode (IR) spectrum. Als de frequentie van IR licht precies samenvalt met de frequentie van de moleculaire vibratie, treedt er resonantie op, het molecuul absorbeert het licht en wordt geëxciteerd, en geraakt zo in een hoger energieniveau vanuit de grondtoestand.

In Figuur 3b worden twee vibratietechnieken uitgelegd: IR spectroscopie en Raman spectroscopie. De spectroscopische techniek die in deze thesis veel gebruikt wordt, is Raman spectroscopie. Raman spectroscopie is vernoemd naar de uitvinder Sir Chandrasekhara Venkata Raman in 1928, waar hij in 1930 de Nobelprijs voor de natuurkunde voor ontving. Door slim gebruik van verschillende lenzen en filters, kon Raman aantonen dat een fractie van het zonlicht van kleur verandert nadat het verstrooid wordt door een transparant materiaal. Dit effect is zo klein, dat het meestal ongezien plaatsvindt.

In tegenstelling tot IR spectroscopie, hoeft het licht bij Raman spectroscopie niet precies dezelfde frequentie te hebben als de moleculaire vibratie. UV licht tot IR licht kan gebruikt worden om de molecuul eerst aan te slaan tot een virtuele energietoestand. Een groot deel van de energie in de virtuele toestand valt meteen terug naar de grondtoestand en nemen we waar als Rayleigh verstrooiing: elastisch verstrooid licht, zonder verschil in energie of kleur. Slechts een klein deel zal naar een vibrationeel geëxciteerde toestand vallen. Dit licht nemen we waar als Stokes verstrooiing: inelastisch verstrooid licht dat van kleur is veranderd. Stokes verstrooiing bevat informatie over de chemische samenstelling van de materialen. Vanwege de ontzettend lage sensitiviteit (bij ongeveer 1 op de 10 miljoen fotonen vindt Strokes verstrooiing plaats) was de techniek niet meteen een doorslaand succes voor de analyse van moleculaire structuren. Pas bij de uitvinding van de laser

in de jaren ’60 en veel gevoeligere detectoren werd Raman meer ingezet als karakterisatietechniek van materialen.[7]

Door vooruitgang in de gevoeligheid van detectoren en de versimpeling van de techniek, kan Raman steeds meer ingezet worden als een standaard laboratorium uitrusting. Toch blijft Raman spectroscopie vrij beperkt inzetbaar, en dat komt vooral door de lage opbrengst van Raman verstrooiing. Het signaal is te verbeteren door gebruik van een sterkere laser en door te meten over een langere tijd, maar lage concentraties moleculen blijven altijd verborgen. Terwijl de belangrijkste moleculen voor het begrijpen van een katalytische reactie juist in hele kleine hoeveelheden voorkomen aan het oppervlak van een katalysator. Gelukkig zijn er ook methodes beschikbaar om de Raman verstrooiing van moleculen verder te versterken.

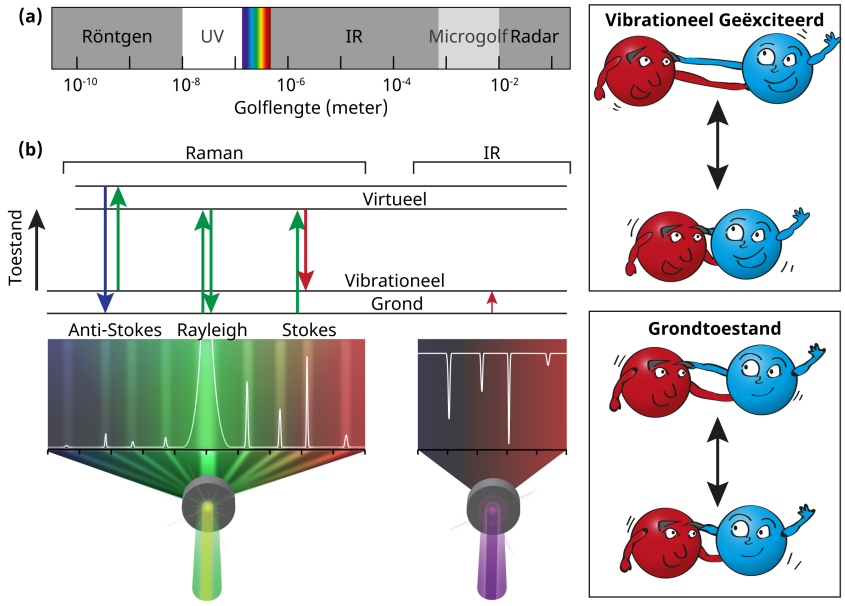

Figuur 3. Spectroscopie in een notendop. (a) Een deel van het electromagnetische spectrum, met daarin het kleine deel van zichtbaar licht in de kleuren van de regenboog. **(b)** Raman en IR spectroscopie zijn vormen van vibratiespectroscopie. De structuur van een molecuul kan bepaald worden aan de hand van de energie die nodig is om een verbinding in een geëxciteerde toestand te krijgen. Bij IR spectroscopie gebeurt dit door middel van directe absorptie van licht met dezelfde frequentie als de specifieke vibratie. Bij Raman spectroscopie kan licht van verschillende golflengtes geabsorbeerd worden, waarna een deel van dat licht gebruikt wordt voor excitatie. De rest, het verschil in energie, wordt weer uitgezonden en wordt waargenomen als verstrooiing van het licht.

Plasmon Versterkte Raman Spectroscopie

Zoals de naam doet vermoeden, is *surface-enhanced Raman spectroscopy* (oppervlakte verbeterde Raman spectroscopie, SERS) een zeer geschikte techniek voor metingen aan oppervlaktes. Er zijn meerdere interessante technieken beschikbaar voor het versterken van het Raman signaal, maar deze bieden niet de lokale sensitiviteit van SERS. SERS is een vorm van plasmon-versterkte Raman spectroscopie (PERS). Hierbij worden nanostructuren ingezet om lokaal het Raman signaal tot wel een miljard keer te versterken. Zo sla je twee vliegen in één klap: je vergroot de sensitiviteit van Raman en daarnaast krijg je een techniek die enkele moleculen aan een oppervlakte kan meten.[8]

De versterking van het licht wordt veroorzaakt door de eigenschappen van nanomaterialen van goud (Au), zilver (Ag) of koper (Cu). Wanneer deze materialen tussen de 10 en 100 nanometer groot zijn, kunnen ze licht opvangen en concentreren op de nanoschaal. Dit gebeurt doordat de elektronen aan de buitenkant van deze metalen kunnen gaan resoneren met de frequentie van zichtbaar licht. Omdat nanomaterialen erg klein zijn, zullen de elektronen niet een golfbeweging maken over het nanodeeltje, maar zijn ze gelimiteerd in hun beweging. Deze lokale oppervlakte plasmon resonantie (LSPR) frequentie creëert een dipool in het nanodeeltje zoals is weergegeven in Figuur 4a. De onderkant van het nanodeeltje is positiever geladen door een gebrek aan elektronen, de bovenkant is juist negatiever geladen door een overschot aan elektronen. De dipool resoneert met de frequentie van het licht en creëert zo een sterk geconcentreerde lichtbron om het nanodeeltje. De versterking van het Raman signaal is daarom het krachtigst vlakbij het oppervlak en neemt sterk af binnen enkele nanometers (Figuur 4b). Door het materiaal, de grootte en de vorm van het nanodeeltje te controleren kan er gezocht worden naar een optimum voor SERS. Op deze manier zijn er materialen gemaakt die zo actief zijn voor SERS dat onderzoekers hiermee de chemische structuur van individuele moleculen kunnen waarnemen, iets wat voorheen onmogelijk was, zeker voor Raman spectroscopie.[9]

Een nadeel van het gebruik van PERS, is dat je voor een groot deel gelimiteerd bent aan de metalen Au, Ag en Cu. In het verleden is hier omheen gewerkt door bijvoorbeeld metalen direct op de bestaande SERS structuren te deponeren.[10] Ook hier kleeft nog steeds een nadeel aan, en dat is dat je niet kan uitsluiten dat de plasmonische nanodeeltjes deelnemen aan de reactie: de resonerende elektronen kunnen zoveel energie hebben dat ze een reactie in gang kunnen zetten. Daarnaast zijn deze nanostructuren vaak niet stabiel onder hoge temperaturen. Daarom zoeken we een manier om de plasmonische eigenschappen van SERS of PERS toe te passen voor het versterken van het Raman signaal, zonder dat de nanodeeltjes interfereren met de katalytische reactie.

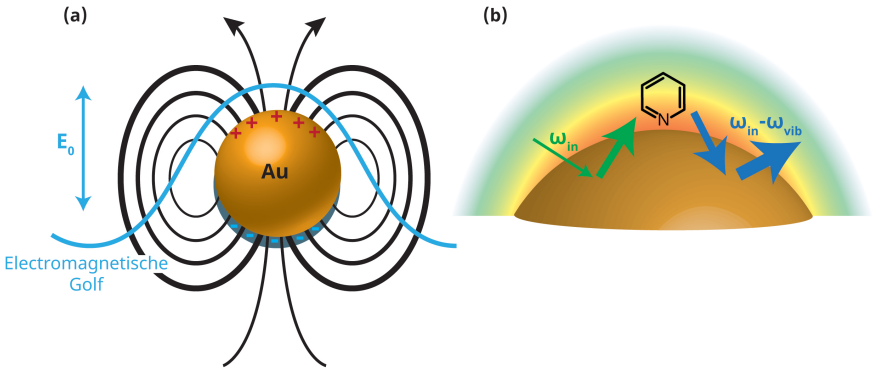

Figuur 4. Bij SERS worden nanodeeltjes van Au of Ag gebruikt om het Raman signaal zeer lokaal te versterken. (a) Het licht, een elektromagnetische golf, induceert een resonerend dipool in een Au nanodeeltje, deze creëert op zijn beurt een sterk lokaal elektromagnetisch rondom het deeltje. **(b)** Het lokale elektromagnetische veld versterkt zowel de frequentie van het inkomende licht (ω_{inc}) en het Raman signaal (ω_{inc}- ω_{vib}) en neemt snel af in sterkte. Zo is na ongeveer 10 nm het effect al verwaarloosbaar.

Doel van de Thesis: SHINERS in heterogene katalyse

SERS kan dus het Raman signaal erg goed versterken, maar de nadelen met betrekking tot de stabiliteit en interferentie zijn groot. Aan het begin van het onderzoek was daarom snel duidelijk dat *shell-isolated nanoparticle-enhanced Raman spectroscopy* (verbeterde Raman spectroscopie door schil-geïsoleerde nanodeeltjes, SHINERS) een belangrijke methode zou zijn om PERS toe te passen voor gebruik in heterogene katalyse. Met SHINERS gebruiken we plasmonische nanodeeltjes zoals Au en Ag als versterkers van het Raman signaal. Deze deeltjes worden geïsoleerd met hele dunne laagjes van een metaaloxide. De verkregen nanomaterialen worden *shell-isolated nanoparticles* (schil-geïsoleerde nanodeeltjes, SHINs) genoemd. We onderzochten verschillende manieren om deze stabiele vorm van PERS toe te passen in de heterogene katalyse. Uiteindelijk was het doel om SHINERS toe te kunnen passen voor onderzoek naar een werkende katalysator. Deze vaste katalysator zou dan in nauw contact gebracht moeten worden met de SHINs. Met SHINERS verwachtten we nieuwe molecuulstructuren waar te nemen aan de oppervlakte van een katalysator.

Samenvatting van de hoofdstukken

Deze thesis gaat over het onderzoek naar SHINERS en het toepassen van deze techniek in heterogene katalyse. De thesis is ingedeeld in vier hoofdstukken die elk een belangrijk deelonderzoek vormen binnen het maken van sensoren die toepasbaar zijn in heterogene katalyse. Na de inleidende bespreking van de

belangrijkste thema's in deze thesis, volgt nu de samenvatting van de onderzoeksbevindingen per hoofdstuk.
In Hoofdstuk 2 onderzochten we methodes om SHINs te maken die stabiel zijn onder verhoogde temperaturen zodat ze gebruikt kunnen worden voor heterogene katalyse. Eerst vonden we dat de optimale grootte van de Au nanodeeltjes voor Raman signaal versterking rond de 80 nm ligt. Ze versterken het Raman signaal dan met een factor 10^5 en hoger. Verder ontwikkelden we methodes om naast goede silica (SiO_2) coatings, ook titania (TiO_2) coatings van slechts 1 tot 4 nm dik te groeien over de Au nanodeeltjes. Deze kern-schil deeltjes worden verder aangeduid als Au@TiO_2 en Au@SiO_2. Coatings van ten minste 2 nm dik konden de plasmonische nanodeeltjes stabiliseren tot 400 °C. Voor coating van maximaal 2.5 nm bleef de Raman signaal versterking boven de 10^4, en leken daarmee erg geschikt voor de toepassing in katalyse.

Deze nanostructuren werden daarom toegepast in Hoofdstuk 3 voor het *in situ* bestuderen van katalysatoren. De katalysatoren werden op Au@SiO_2 en Au@TiO_2 substraten geplaatst door middel van een natte-impregnatie techniek: de nanodeeltjes werden gemengd met een oplossing van rutheniumchloride ($RuCl_3$) in water. Wanneer dit mengsel droogt, worden er aggregaten van SHINs verkregen met daarover kleine $RuCl_3$ deeltjes. Metallisch Ru werd vervolgens verkregen door een reductie onder waterstof (H_2) vanaf 150 °C. Deze complexe nanostructuren, Ru/Au@TiO_2 en Ru/Au@SiO_2, werden vervolgens met succes ingezet om koolstofmonoxide (CO) adsorptie waar te nemen, in tegenstelling tot Ru/SiO_2 zonder plasmonische kern. Zo konden we deze substraten vervolgens toepassen onder katalytisch relevante condities voor de Fischer-Tropsch reactie. Onder verschillende temperaturen met zowel H_2 als CO, bestudeerden we met SHINERS hoe de reactie verliep. Het bleek dat CO bij lagere temperaturen reageerde met H_2 over Ru/Au@TiO_2 dan bij Ru/Au@SiO_2. Zo toonden we aan dat ook bij SHINs het dragermateriaal effect heeft op de katalysator. Hierna toonden we aan dat deze methode universeel toegepast kan worden voor verschillende katalysatoren. Andere katalytisch actieve SHINERS substraten werden verkregen met rhodium (Rh), palladium (Pd) en platina (Pt) op Au@SiO_2. De verschillende manieren van CO adsorptie werd hiermee bestudeerd en de verschillen tussen de katalysatoren konden zo onderzocht worden. Daarnaast werden legeringen van rhodium (Rh) en ijzer (Fe) bestudeerd. Met SHINERS konden we zien dat de verhouding van Rh:Fe in de legeringen de CO adsorptie beïnvloedt: CO bindt meer enkelvoudig met Rh naarmate er meer Fe toegevoegd wordt.

Een nadeel van het gebruik van SHINERS kwam ook aan het licht bij deze eerste toepassingen in de katalyse. Door de sterke signaalversterking en de lokale gevoeligheid is de techniek ook kwetsbaar voor kleine vervuilingen. Dit leidt ertoe dat in het spectrum soms extra signaal verkregen wordt dat niet te herleiden is tot de katalytische reactie. Door deze vervuilingen kan uiteindelijk een groot deel van het spectrum niet gebruikt worden voor het bestuderen van reacties. Bovendien kunnen vervuilingen een effect hebben op de eigenschappen van de katalysator. Er

werd in Hoofdstuk 4 daarom gezocht naar methodes om deze vervuilingen tegen te gaan. De meest succesvolle methodes hebben we vervolgens gepresenteerd als richtlijnen voor het gebruik van SHINERS in heterogene katalyse. Met deze richtlijnen kan SHINERS beter worden toegepast om nuttige resultaten te verkrijgen. Het belangrijkste is om te beginnen met schone materialen. De meest effectieve methode hiervoor vonden we in het verwarmen van de substraten tot 300 °C in een zuurstofrijke omgeving. Ook de gassen moeten schoon zijn, hiervoor is het belangrijk om alle leidingen eerst door te spoelen gedurende minstens 15 minuten en dient een filter geïnstalleerd te worden. Het filter bestaat uit zinkoxide (ZnO), alumina (Al_2O_3) en geactiveerde koolstof om water, carbonylen en organische vervuilingen tegen te gaan. Daarnaast werd onderzocht hoe het laservermogen effect heeft op de uiteindelijke resultaten. Hieruit bleek dat altijd met een gematigd vermogen gewerkt dient te worden, zeker tijdens het bestuderen van reacties. Indien men deze praktische richtlijnen volgt, zullen schone(re) SHINER spectra verkregen worden, met betrouwbaardere en reproduceerbaardere resultaten voor de studie van heterogene katalyse.
De materialen en de kennis van de Hoofdstuk 2 tot 4 werden toegepast om sensoren te maken voor *operando* SHINERS in combinatie met luminescentie thermometrie. In Hoofdstuk 5 ontwikkelden we extrudaten met verschillende nanodeeltjes voor drie functies: 1. Rh nanodeeltjes voor de katalyse van CO hydrogenatie; 2. Au@SiO_2- en Au@TiO_2-nanodeeltjes voor het meten van geadsorbeerde moleculen tijdens katalyse met SHINERS; 3. $NaYF_4$@SiO_2 nanodeeltjes die werken als temperatuur sensors voor het meten van de lokale temperatuur tijdens katalyse.

Deze extrudaat sensor werd toegepast voor de studie van CO hydrogenatie over Rh/SiO_2, Rh/TiO_2 en RhFe/SiO_2 katalysatoren. Met SHINERS namen we verscheidene molecuulstructuren op de Rh katalysator waar tot 350 °C. Het belangrijkste resultaat was dat we met SHINERS molecuulstructuren waarnamen die niet gezien waren met andere technieken, zoals IR spectroscopie. Deze species waren afhankelijk van de katalysator en het dragermateriaal, zoals we konden aantonen met de verschillende katalysatoren. Bovendien kon de temperatuur van de katalysator zelf nauwkeurig in de gaten gehouden worden met luminescentie thermometrie met een afwijking van 0.3 °C bij 300 °C. De temperatuursensor toonde daarnaast aan dat de echte temperatuur van de katalysator sterk kan afwijken van de geprogrammeerde temperatuur. Afhankelijk van de geprogrammeerde temperatuur, de belading van de reactor en de gebruikte gassen, kan de temperatuur tot wel 40 °C afwijken. De belangrijkste oorzaak voor deze afwijking werd toegewezen aan het gebruik van H_2 gas, dit gas kan erg veel warmte op zich nemen. Zulke grote verschillen in temperatuur hebben een belangrijke invloed op de uiteindelijke activiteit en selectiviteit van een katalysator. Luminescentie thermometrie toont dus aan dat het meten van de lokale temperatuur van groot belang is, omdat deze sterk kan afwijken van de

geprogrammeerde temperatuur. Bovendien wijzen de verkregen resultaten in Hoofdstuk 5 erop dat SHINERS een toegevoegde waarde heeft.
De hoofdstukken 2-5 zijn samengevat in Figuur 5, waarbij duidelijk te zien is hoe elk hoofdstuk bijdraagt aan de ontwikkeling van de sensoren in Hoofdstuk 5. We beginnen in het donkere vlak waarbij we nog weinig informatie hebben over SHINERS in heterogene katalyse. Met elk deelonderzoek begrijpen we beter hoe we tot effectieve SHINERS sensoren kunnen komen. Het onderzoek naar SHINERS in heterogene katalyse staat nog in de kinderschoenen, en we verwachten dat er nog veel nieuwe ontwikkelingen zullen plaatsvinden om effectievere materialen en methodes te vinden. Deze thesis zou dan ook gezien kunnen worden als een leidraad voor de ontwikkeling van nieuwe SHINERS materialen, waarbij we met de klok mee Figuur 5 volgen. Eerst willen we weten of de materialen stabiel zijn, om vervolgens te kijken naar hun effectiviteit voor onderzoek naar katalyse. Dan volgt de optimalisatie van de methode zodat we bruikbare sensoren kunnen toepassen in *operando* onderzoek. Dit is een universele methode en is daarom van toepassing op elk materiaal dat ingezet wordt voor SHINERS in heterogene katalyse.

Referenties

[1] J. Hagen, *Industrial Catalysis: A Practical Approach*, Wiley-VCH, Weinheim, **2015**.
[2] G. Ertl, H. Knözinger, F. Schüth, J. Weitkamp, *Handbook of Heterogeneous Catalysis*, Wiley-VCH, Weinheim, **2008**.
[3] H. S. Taylor, *Nature* **1919**, *104*, 94–96.
[4] G. Rothenberg, *Catalysis: Concepts and Green Applications*, Wiley-VCH, Weinheim, **2008**.
[5] B. C. Gates, *Chem. Rev.* **1995**, *95*, 511–522.
[6] B. M. Weckhuysen, *Phys. Chem. Chem. Phys.* **2003**, *5*, 4351–43560.
[7] E. Smith, G. Dent, *Modern Raman Spectroscopy—A Practical Approach*, Wiley, Chichester, **2005**.
[8] P. G. Etchegoin, E. C. Le Ru, in *Surf. Enhanc. Raman Spectrosc. Anal. Biophys. Life Sci. Appl.* (Ed.: S. Schlücker), Wiley-VCH, Weinheim, **2010**, pp. 1–37.
[9] P. G. Etchegoin, E. C. Le Ru, *Phys. Chem. Chem. Phys.* **2008**, *10*, 6079–6089.
[10] Z.-Q. Tian, B. Ren, J.-F. Li, Z.-L. Yang, *Chem. Commun.* **2007**, *34*, 3514–3534.

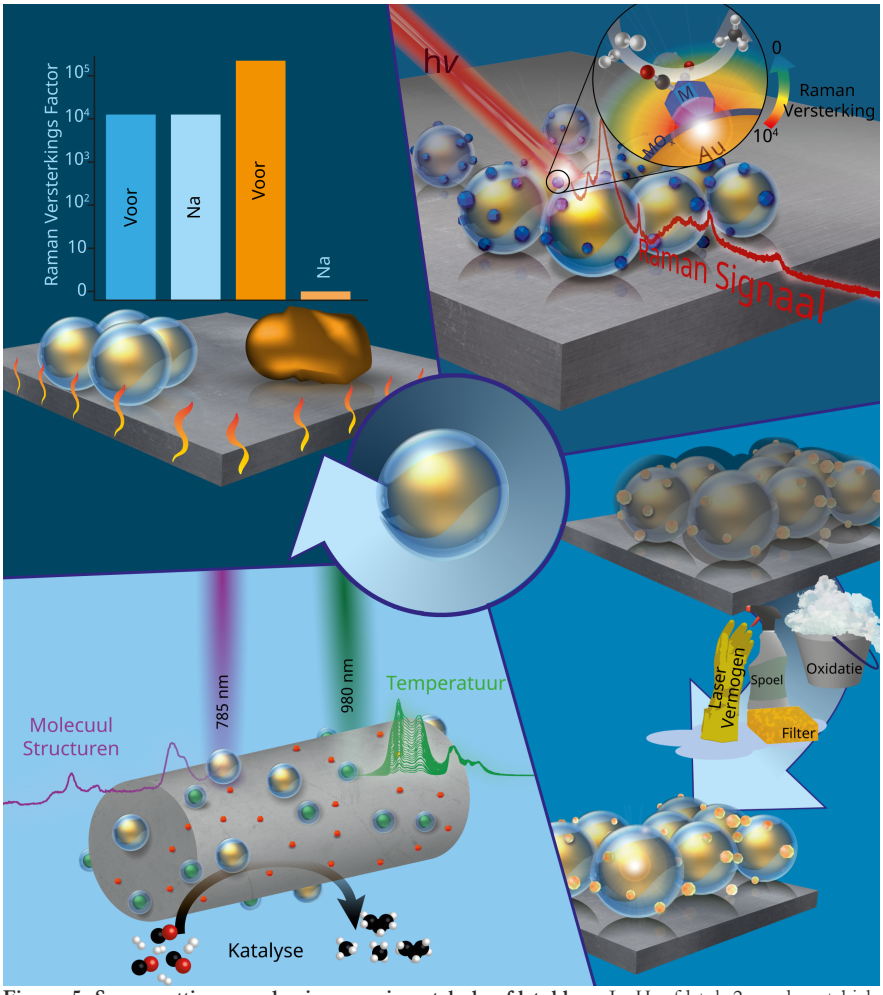

Figuur 5. Samenvatting van de vier experimentele hoofdstukken. In Hoofdstuk 2 werden stabiele schil-geïsoleerde nanodeeltjes gemaakt die goede licht-versterkende eigenschappen hadden voor Raman spectroscopie. In Hoofdstuk 3 werden deze deeltjes toegepast om verschillende katalysatoren te bestuderen. In Hoofdstuk 4 werden enkele problemen opgelost en de techniek geoptimaliseerd zodat er duidelijkere en 'schonere' Raman signalen werden verkregen, zodat in Hoofdstuk 5 sensoren gemaakt konden worden die toegepast konden worden voor *operando* spectroscopie met SHINERS.

Publications and Presentations

List of Publications by the Author

T. Hartman, C.S. Wondergem, N. Kumar, A. van den Berg, B. M. Weckhuysen, Surface- and Tip-Enhanced Raman Spectroscopy in Catalysis*, J. Phys. Chem. Lett.* **2016**, 7, 1570–1584

T. Hartman, B. M. Weckhuysen, Thermally Stable TiO_2- and SiO_2-Shell-Isolated Au Nanoparticles for In Situ Plasmon-Enhanced Raman Spectroscopy of Hydrogenation Catalysts, *Chem. Eur. J.* **2018**, 24, 3733-3741

T. Hartman, C.S. Wondergem, B.M. Weckhuysen, Practical Guidelines for Shell-Isolated Nanoparticle-Enhanced Raman Spectroscopy of Heterogeneous Catalysts, *ChemPhysChem.* **2018**, 19, 2461-2467

T. Hartman, R.G. Geitenbeek, G.T. Whiting, B.M. Weckhuysen, Bifunctional Catalyst Extrudate Sensors for Exploring Reactions using operando SHINERS and Luminescence Thermometry, *in revision for publication*

List of Oral Presentations by the Author

Shell-Isolated Nanoparticle-Enhanced Raman Spectroscopy Substrates for Operando Research in Heterogeneous Catalysis, *12th International Symposium on Heterogeneous Catalysis*, **2018**, Sofia, Bulgaria

Shell-Isolated Nanoparticle-Enhanced Raman Spectroscopy for Heterogeneous Catalysis, *Netherlands' Catalysis and Chemistry Conference*, **2018**, Noordwijkerhout, the Netherlands

SERS and TERS in Heterogeneous Catalysis, *Molecules@Surfaces Winterschool*, **2016**, Bardonecchia, Italy - *Awarded best oral presentation*

List of Poster Presentations by the Author

In Situ Characterization of Supported Rh Catalysts by Shell-Isolated Nanoparticle-Enhanced Raman Spectroscopy, *Netherlands' Catalysis and Chemistry Conference*, **2017**, Noordwijkerhout, the Netherlands

SiO_2- and TiO_2-coated gold nanoparticles as thermally stable SERS substrates, *Netherlands' Catalysis and Chemistry Conference*, **2016**, Noordwijkerhout, the Netherlands

Acknowledgements

Dit was het dan. Vier jaar is voorbijgevlogen. Terugkijkend kan ik concluderen dat dit de mooiste tijd is die ik tot nu toe heb gekend. En ik was hier nooit gekomen zonder de hulp van de volgende personen:

Ten eerste, **Bert**, heel erg bedankt dat je mij door deze mooie vier jaren heen hebt gegidst! Op vele vlakken heb ik van je geleerd. Je *drive* en passie voor het vak zijn zonder grenzen. Het gevoel van vrijheid bij het uitvoeren van het onderzoek was erg fijn, maar het was goed dat je mij af en toe teruggefloten hebt. De mooiste momenten die ik met jou kan herinneren waren in je kantoor, tijdens het bespreken van nieuw werk. Opeens schittert er iets in je ogen en knallen de ideeën eruit, een oneindige stroom aan nieuwe invalshoeken was het gevolg. Hier kon ik dan weer een lange tijd op vooruit. Helaas zijn lang niet alle ideeën tot uitwerking gekomen, maar daar weet jij vast wel raad mee. Bedankt voor alle sportanalogieën, ze blijven altijd goed in je gedachten hangen. Afgelopen vier jaar was een bloedstollende wedstrijd waarin ik veel verschillende trucjes op het veld heb mogen laten zien, om vervolgens vaak stil te blijven staan voor een open doel. Uiteindelijk hebben we toch die winst weten te behalen dankzij het spelinzicht en een aantal strakke assists van aanvoerder Weckhuysen.

Hiernaast wil ik de personen bedanken die wetenschappelijk hebben bijgedragen aan het vormgeven van deze thesis. **Katinka**, mijn directe concullega op het gebied van SHINERS, bedankt voor al je mooie bijdragen. Zowel op het gebied van ons onderzoek en de vriendschap die gegroeid is over de jaren. Na een aantal moeilijke maanden, hoop ik dat je weer de draad op kan pakken. SHINERS, here to stay!* **Robin**, wat hebben we samen een leuk project uitgevoerd! Niet alleen dankzij het onderzoek zelf, maar vooral door de samenwerking met jou, heb ik de laatste maanden nog extra genoten van mijn PhD-leventje. **Naresh Kumar** and **Albert van den Berg**, thank you for your contributions to the first chapter of my thesis, and the first publication of my life! I would also like to thank the students that I supervised: **Adriana Panasewicz**, **Fieke Mulders**, **Jim de Ruiter** and **Tara Bogert**, thank you! The insights we obtained in your projects helped me a lot and shaped this PhD thesis.

Alles was in de soep gelopen zonder de vaste staf van **Inorganic Chemistry and Catalysis**. De motor achter al die mooie boekjes die mij vooraf zijn gegaan: **Belen**, **Dymph**, **Iris**, **Monique**, **Ad[E]**, **Ad**, **Dennie**, **Herrick**, **Jan Willem**, **Pascal** en **Ramon**, heel erg bedankt dat jullie elke dag klaar stonden voor mij, en de vele

*goo.gl/ksnOsz

andere collega's. **Hans**, heel erg bedankt voor alle gezellige TEM-sessies en de mooie hardloopactiviteiten! **Fouad**, bedankt voor alle wijze lessen en de 'assertiviteitstraining'. En natuurlijk alle broodjes tricolore.

Na gezamenlijk een Bachelor en Master studie in de Scheikunde te hebben doorlopen, begonnen we vier jaar geleden ook nog eens tegelijkertijd aan ons promotieonderzoek. **Tom** en **Wouter**, het was mooi jullie aan mijn zijde te hebben de afgelopen jaren en ik ben blij dat we dit samen kunnen afsluiten met jullie als mijn paranimfen.

Kan de boog altijd gespannen blijven? Er was gelukkig ook tijd voor de nodige ontspanning. Mijn dank is groot aan alle collega's die hierbij betrokken waren. Een speciaal plekje in mijn hart heeft het **lunchloopgroepje** ingenomen. Heerlijk was het om even het hoofd te legen buiten de muren van het DDW. Ook de vele koffiepauzes waren genieten met jullie, **Anne-Eva**, **Carolien**, **Joris**, **Marjolein**, **Tom** en **Wouter**! En **Ramon**, als je er op tijd bij was. De **pizzaburgerboys** kan ik natuurlijk niet onbenoemd laten: **Tom**, **Wouter** en **Joris**. Ik hoop dat we gezamenlijk nog vele culinaire hoogstandjes kunnen blijven produceren.

So many more colleagues I am grateful for, with many different stories. **Carlos**, thank you for waving back at me for almost 4 years. You were the best overbuurman I can think of. Sometimes it felt as if we could speak telepathically; words were not necessary as your facial expressions said enough. That brings me to all the colleagues that worked near me on the 4th floor: **Ana**, **Bea**, **Carolien**, **Charlotte**, **Donglong**, **Egor**, **Iris**, **Jelle** Perenboom, **Joris**, **Katarina**, **Katinka**, **Khaled**, **Lennart**, **Lisette**, **Maarten**, **Marjolein**, **Max**, **Miguel**, **Sophie**, **Suzanne**, **Thijs**, **Tom**, **Sander**, **Stanislav** and **Wouter**mans. Thanks for the great (working) atmosphere: the fun times, the help and interest in each other's work and life. Never a dull moment, thanks to you!

Aan alle vrienden buiten mijn onderzoek: bedankt! Jullie hebben zeker bijgedragen aan mijn geestelijke gezondheid (meestal positief) en me zo geholpen om hier te komen. De **Maennies** wil ik allereerst bedanken. Deze vriendschap gaat ver terug en zal hopelijk altijd blijven bestaan. **Roy**boy, de avonturier, doe een beetje rustig aan, aan de andere kant van de wereld, maar verander nooit! **Tim**mie, met jou heb ik kunnen lachen sinds de kleuterschool en ik verwacht dat dat nooit zal stoppen. Okay, je was soms onuitstaanbaar, maar op de goede manier! **Wouter**tje, ik weet nog goed dat ik je leerde kennen tijdens de scheikundeles in de vierde klas van de middelbare school. De stoere boy met een klein hartje. We hebben zeker een mooie vriendschap opgebouwd over de jaren!

Peter, ik ben blij dat we, als indirecte collega's, elkaar weer tegen zijn gekomen op de Uithof. Samen rondjes hardlopen vanuit werk, gevolgd door curries eten in het educatorium, het was elke keer weer genieten!

Villa Regina, met **Ruben** in het speciaal, bedankt dat ik zo'n gezellig thuis had met jullie in de eerste twee jaar van mijn PhD!

Het kamerplantencollectief, **Bodo** en **Riccardo**, bedankt voor alle gezellige avonden, de loopjes en de goede discussies over planten!

Luister goed familie, want dit soort dingen zeg ik niet vaak (genoeg). **Pap** en **Mam**, jullie zijn geweldig. De 'onverantwoordelijke' liefde en ondersteuning om mij te laten doen wat ik graag wil, is erg belangrijk voor mij geweest. Ik ben helaas geen Olympisch kampioen geworden, maar ik denk dat een doctorstitel ook voor wat telt, nietwaar? Mijn broers en zus: **Steven**, **Marieke** en **Joost**, jullie ook heel erg bedankt voor jullie liefde, steun en de fantastische voorbeelden in het leven. Ik heb kunnen afkijken van de besten.

Daarnaast wil ik de **familie La Grouw** bedanken voor alle gezelligheid!

Lieve **Yvonne**, wat heb ik een geluk met jou, mijn skettie. Naast alle leuke tijd samen heb je me ook door de moeilijkere dagen heen gesleurd en weer opgebeurd. We begrijpen elkaars onderzoek misschien amper, maar dat maken we meer dan goed met het begrip voor elkaar. Dat de afgelopen vier jaar dan ook vallen in de mooiste zeven jaar die ik ken, is niet toevallig. Sinds ik jou ken, wordt alles alleen maar leuker. Hoe blij jij mij maakt, is ongelooflijk! Ik houd van jou!

Curriculum Vitae

Thomas Hartman was born on the 11th of May 1991 in Woerden, the Netherlands. After obtaining his high school diploma in 2009, he enrolled in an undergraduate study in chemistry at Utrecht University. In 2012 he graduated with a Bachelor of Science degree after writing his bachelor thesis on the synthesis of magnetite nanocubes. In September 2012, Thomas started his Master's studies in *Nanomaterials: Chemistry and Physics* at Utrecht University and began his Master's research on zeolitic imidazolate frameworks for heterogeneous catalysis under the supervision of Prof. dr. ir. Bert Weckhuysen. He finished the research and Master's studies in August 2014. Thomas continued to work under the supervision of Prof. Weckhuysen as a PhD candidate in the Inorganic Chemistry and Catalysis group. The main results of this project are described within this thesis and in the published articles in scientific journals. During his PhD research, Thomas developed an interest in designing scientific illustrations. He is committed to making science approachable via the power of images. When not working on scientific research, Thomas enjoys making music on the piano.